Multi-Constellation GNSS Scintillation at Mid-Latitudes

Marc Henri Jean

Thesis submitted to the faculty of the Virginia Polytechnic Institute and State University in partial fulfillment of the requirements for the degree of

Master of Science
In
Electrical Engineering

Wayne A. Scales
Scott M. Bailey
Dennis G. Sweeney

11/22/2016
Blacksburg, VA

Keywords: Mid-Latitude scintillation, amplitude scintillation, phase scintillation, Novatel GP6-Station receiver, Novatel Connect, spectral index, histogram distribution, GPS L1, GPS L2, GPS L5, GLONASS G1, GLONASS G2, Galileo E1, Galileo E5A, Galileo E5B, SPIRENT GPS Simulator

Multi-Constellation GNSS Scintillation at Mid-Latitudes

Marc Henri Jean

Abstract

Scintillation of Global Positioning Systems (GPS) signals have been extensively studied at low and high latitude regions of the Earth. It has been shown in past studies that amplitude scintillation is severe at low latitudes and phase scintillation is severe at high latitudes. Unlike low and high latitude regions, mid-latitude scintillation has not been extensively studied. Further, it has been suggested that mid-latitude scintillation is negligible. The purpose of this research is to challenge this belief.

A multi-constellation and multi-frequency receiver, that tracks American, Russian, and European satellites, was used to monitor scintillation activity at the Virginia Tech Space Center. Analysis was performed on collected data from various days and compared to past research done at high, mid, and low latitudes. The results are discussed in this thesis.

Multi-Constellation GNSS Scintillation at Mid-Latitudes

Marc Henri Jean

General Audience Abstract

Earth's atmosphere disrupts signals transmitted by Global Navigation Satellite Systems (GNSS). In certain regions of the Earth, these signals can be severely degraded. Not much research has been done on what could potentially happen to GNSS signals at mid-latitude regions of the Earth. It is important to gain a better understanding of the impacts mid-latitude regions can have on GNSS signals, in preparation for potential future outages across the system.

The United States and Russia have had Global Positioning Systems (GPS) technology for decades. Today, China and Europe are expanding their global positioning systems. In the future there may be up to one hundred or more satellites available for public usage. This study was done to determine if outages could potentially occur at mid-latitudes, and to gain more knowledge on which of these satellite constellations have the best service.

Acknowledgements

I would like to thank Dr. Wayne Scales for providing his support and wisdom. I would also like to thank my lab mates Augustine Yellu and Yuxiang (Phillip) Peng for giving me good advice. Finally, I would like to thank James Conroy for giving me tips on how to code MATLAB more effectively.

Dedication

I would like to dedicate my research to my sisters Lody, Paola, and my grandmother Jeannette Jean for their support.

Table of Contents

List of Figures

List of Tables

Chapter 1

Introduction

The purpose of this study is to analyze ionospheric scintillation on Global Navigation Systems (GNSS) signals at mid-latitudes in the northern hemisphere, which are regions that are between 30 degrees to 60 degrees latitude. It has been shown from previous studies, which were done at high and low latitudes, that ionospheric turbulence disrupts GNSS signals, which operate in the L band frequency range [1]. The goal of this study is to compare scintillation characteristics at mid-latitudes to previous studies done at high latitudes, which are regions typically between 60 degrees to 90 degrees latitude in the northern hemisphere and at low latitudes, which are regions typically between 0 degrees latitude to 30 degrees latitude in the northern hemisphere. The corresponding definitions of latitudinal regions hold true in the southern hemisphere as well.

Scintillation at mid-latitude regions has been considered to be negligible in the past, compared to high and low latitude regions. According to [1, p1] "In mid-latitude regions, both amplitude and phase scintillation are negligible". It can certainly be argued that scintillations at mid-latitudes should be much weaker than at high and low latitudes. However, few studies have been done on scintillation at mid-latitude regions and part of this study is to challenge the belief that mid-latitude scintillation effects are unimportant.

New space science measurement facilities have shown that the physics of ionospheric irregularities are much more complex than have been thought in the past [2]. Both the Global Navigation Satellite System (GNSS) and SuperDARN space weather high frequency (HF) radar facilities are used in this study to investigate scintillation at mid-latitude. A multi-constellation and multi-frequency GNSS receiver, which tracks

GPS frequency bands L1 (1.575 GHz), L2 (1.227 GHz), and L5 (1.176 GHz), GLONASS frequency bands G1 (1.5980625 – 1.6093125) and G2 (1.2429375 – 1.2516875 GHz), and Galileo frequency bands E1 (1.575), E5A (1.176 GHz), and E5B (1.207 GHz), was used to monitor scintillation activity [3], [4], [5]. This is one of the first studies of its kind.

SuperDARN radar data were used to observe and further interpret Ionospheric conditions. SuperDARN collects data using a chain of high frequency (HF) radars to monitor ionospheric conditions at high and mid latitudes [2]. The chain of radars has 16 to 24 beams that scan at rate of 1 to 2 minutes. SuperDARN radars are pulse radars that transmit pulses that have a length of 300 microseconds. The radars measure back scatter from ionospheric structure in the E and F regions, typically resulting from plasma irregularities [2], [6]. The SuperDARN radar ionosphere scatter plots provide the signal to noise (SNR) in decibels (dB), which is the ratio of power caused by the back scatter from the ionosphere and noise power interference.

Figure 1 shows the Total Electron Content TEC (left) and SNR from the back scatter of the of the ionosphere (right). The data was collected during a geomagnetic storm on February 16th, 2016. The TEC shows levels of electron content as high as 10 total electron content units (TECU) and the back scatter plot shows a signal to noise ratio (SNR) ranging from 10 to 20 dB in mid-latitude regions above North America. The TEC and backscatter are used to interpret the ionospheric conditions during the time the scintillation data is collected. The TEC and backscatter characterize ionospheric disturbances that produce GNSS scintillation.

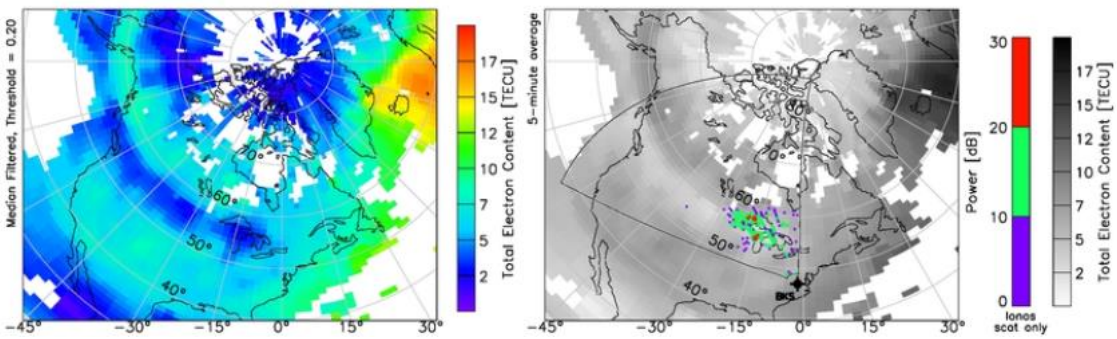

Figure 1: SuperDARN plots of TEC and radar back scatter of storm which occurred on February, 16th 2016 [7]

The study of mid-latitude scintillation is very important because not much is known about how these regions of ionospheric disturbances can affect GNSS signals. For example, research done in low latitude regions near the equator show that GNSS signals can be faded during large ionospheric disturbances. However, few detailed investigations of what could potentially happen to GNSS signals, under the same circumstances at mid-latitudes, have been undertaken. Since a large percentage of the earth's population live in mid-latitude regions of the Earth and are dependent on GNSS technology, it is important to be prepared for potential GNSS blackouts that may be caused by a severe space weather event.

Objective of this Study

This research focuses on analyzing the effects that scintillation may have on the different frequency bands on GPS, Galileo, and GLONASS satellite systems. The frequency bands analyzed in this research include GPS L1, L2, L5, GLONASS G1, G2, and Galileo E1, E5A, E5B. These frequency bands are compared to determine which is degraded less and has the best overall performance relative to mid-latitude scintillations. The results are compared to previous research done at low latitudes and high latitudes. Another goal of this research is to analyze the power spectral density of both phase and

amplitude scintillation at mid-latitudes. The results are also compared to previous research done at mid-latitudes and high latitudes. Such studies may ultimately provide insight into the ionospheric plasma processes causing the turbulence [8]. Finally, the last part of this research involves simulating scintillation models using a radio frequency (RF) hardware GPS simulator. The GPS hardware simulator has a built-in virtual scintillation model, which may allow useful comparisons to the data. The purpose of this study is to see if mid-latitude scintillation conditions can be replicated using the hardware simulations across GPS frequency bands L1, L2, and L5.

Chapter 2 Technical Background

2.1 GNSS basics

Global Navigation Satellite Systems (GNSS) are widely used for civilian, military, and scientific applications. The United States (US) has a total of thirty-two Global Positioning System (GPS) satellites in its constellation [9]. A minimum of twenty-four of the satellites are needed for global tracking, with four satellites in six orbital planes [9]. Aside from the United States, Russia, China, and the European Union (EU) have operable GNSS constellations. The Russian GLONASS constellation has 24 active satellites [4]. The Chinese Beidou Constellation has 21 satellites in orbit, and the EU Galileo constellation currently has 12 satellites [10], [11], [12]. Unlike the other three GNSS constellations, Galileo is still in early stages of development and is expected to be completed by 2020 [5]**.** In the near future, Galileo will have a full fleet of 30 satellites and Beidou will have 35 [10], [11]. The US GPS satellites have near circular orbits, which means that the eccentricity of these satellites is nearly zero [9]. The satellites are located roughly 26,000 km from the center of the Earth, at 55 degree inclinations [9]. By

the time all the GNSS constellations are complete, there may be up to 121 available GNSS satellites available for civilian usage. Having a GNSS receiver will allow users to track multiple constellations across multiple frequency bands, which will improve position accuracy and receiver performance.

GNSS transmit signals in the L band range from 1 to 2 GHz. In the L band frequency range, wavelengths can measure anywhere from 20 cm to 30 cm in length. For example, GPS satellites transmit wavelengths anywhere from 19 cm to 25 cm. Each of these constellations have frequency bands that are available for civilian usage. GPS has three frequency bands, L1, L2, and L5, that are available for civilian usage [3]. GLONASS has two frequency bands available for civilian usage: G1 and G2 [4]. Galileo has three frequency bands available for civilian usage: E1, E5A, and E5B [5].

GNSS also have different multiple accessing schemes. GPS and Galileo use code division multiple accessing (CDMA) [3], [5]. In CDMA systems, the same frequency bands are transmitted across all users, but satellites are identified by pseudo random codes [13]. Each of the satellites are identified by a unique code. Unlike GPS and Galileo, GLONASS uses frequency division multiple accessing scheme (FDMA) [4]. In an FDMA system, frequency is divided within the available spectrum. As a result, each of the GLONASS satellites in view of a receiver has to transmit a different frequency band to avoid interference. The 24 GLONASS satellites use a range of 12 different frequencies. GLONASS satellites can transmit the same frequency for different users only if the receivers are located 180 degrees apart to avoid interference.

GPS have three important segments shown in **Figure 2**. The segments include the control segment, the space segment, and the user segment [9]. The control segment

monitors the location of the GPS satellites from Earth. Once the control segment determines the location of the satellites, it transmits parameters referred to as the ephemeris, used for determination of the satellite position, back to the GPS satellites in space, which in turn then transmit the ephemerides to the user segment. The user segment includes the GPS receivers monitoring the satellites. The ephemerides are used by the user segment to determine the satellite locations, which are ultimately used in the navigation solution.

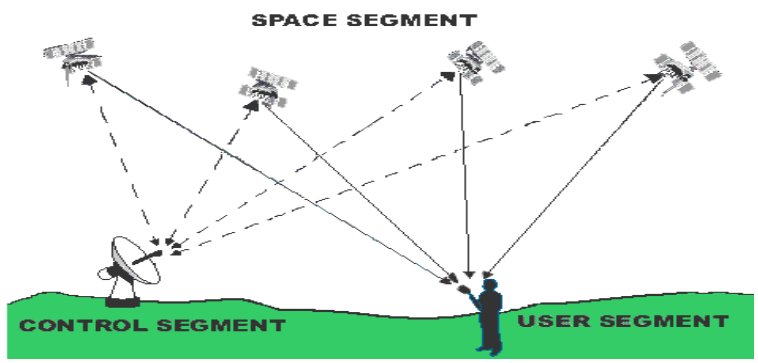

Figure 2: Control, space, and user segments of a GPS system [14]

In order to determine the navigation solution, the user segment needs to be locked into at least four GPS satellites [9]. Three satellites are needed to determine the unknown values of *X*, *Y*, *Z* of the user position. The fourth satellite is used to determine the GPS receiver clock offset. Since there are four unknown variables, four equations are required to solve the system of four unknown values. Tracking more than four satellites provides a more accurate solution.

The system of unknown equations is built around an important parameter referred to as the pseudorange. The pseudorange is the measured distance between the GPS receiver and satellite, which includes satellite and receiver clock offset errors [9]. In **equation (1)**, the pseudorange for satellite *j* is represented by variable P^j.

$$P^j = \rho^j + c\delta^j - c\delta_R \ (\mathbf{1})$$

The actual distance from the GPS receiver to the satellite, the range, is represented by variable ρ^j**.** From **equation (1)** it is seen that the pseudorange is equal to the actual range added to the satellite and receiver clock offsets, $\delta^j$and δ_R, which are multiplied by the speed of light *c*.

Using the **equation (1)**, the actual distance or range ρ^j is set to the vector magnitude distance from the satellite to the receiver, which is shown in **equation (2)** [9]**.**

$$\rho^j = \sqrt{(X^j - x)^2 + (Y^j - y)^2 + (Z^j - z)^2} \ (\mathbf{2})$$

The values $X^j, Y^j,$ and Z^j are known satellite coordinates, *x*, *y*, and *z* are the unknown user coordinates in the Earth Centered Earth Fixed ECEF coordinate system. Since the magnitude vector of the range ρ^j is a non-linear equation, the Newton Raphson method is used to solve for the unknown variables in the system of four equations.

2.2 Basics of GNSS signal propagation in the Ionosphere

The Earth's atmosphere is divided into multiple layers that can be distinguished by the temperature variation and charged particle density**.** As altitude increases, temperature varies in each of the atmospheric layers**.** At high atmospheric altitudes above 70 km is a region known as the ionosphere, which is partially ionized due to intense radiation from the sun [15].

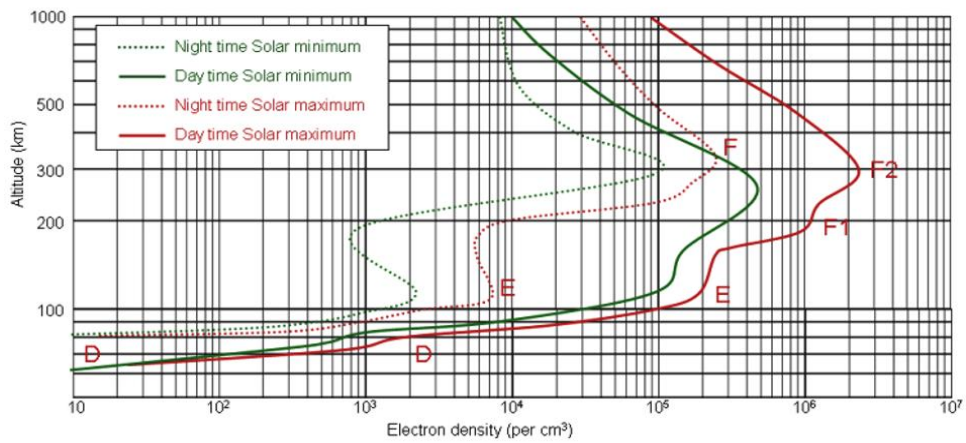

Figure 3: Ionospheric D, E, and F layers during the day and night time hours. This plot presents the electron density of each of layer vs. altitude [15]

The ionosphere is divided into three distinct regions, referred to as the D, E, F regions. These regions are divided according to electron density variations (dominantly produced by photo-ionization), shown in **Figure 3** [15]. The D region spans from 50 – 90 km and has the lowest electron density in the order of $10^8 - 10^{10} e/m^3$ during the day. The D region has ionized Nitric Oxide (NO) molecules. At night, the D layer disappears, except in high altitude regions. The E region spans from 90 – 140 km and reaches a maximum electron density of $10^{11} e/m^3$, during the day. The E region has ionized Oxygen (O_2) molecules. During the night, the E region disappears. Out of the three regions, the F regions has the highest electron density. The F1 region spans form 140 – 200 km and has an electron density of $3 \times 10^{11} e/m^3$. The ionized molecules in this region are Oxygen (O) molecules. The F2 regions spans above 200 km and has a maximum electron density of roughly $2 \times 10^{12} e/m^3$. The ionized molecules in this region are Nitrogen (N) and Oxygen (O) molecules.

The electron content in the ionosphere impacts RF waves. When the free roaming electrons interact with an incoming RF wave, they cause the wave to refract, attenuate, or

disperse [16]. RF waves that operate at frequencies above roughly 10 MHz can penetrate and travel through the electron density present in the ionosphere [9]. That is, the RF frequency must be larger than the so-called ionospheric plasma frequency defined as $f_p = 8.98\sqrt{N_e}$, which varies based on electron density N_e. RF waves that operate roughly below the plasma frequency will reflect or refract from the ionosphere. **Figure 4** presents a visual of how waves may reflect and penetrate the ionospheric layer.

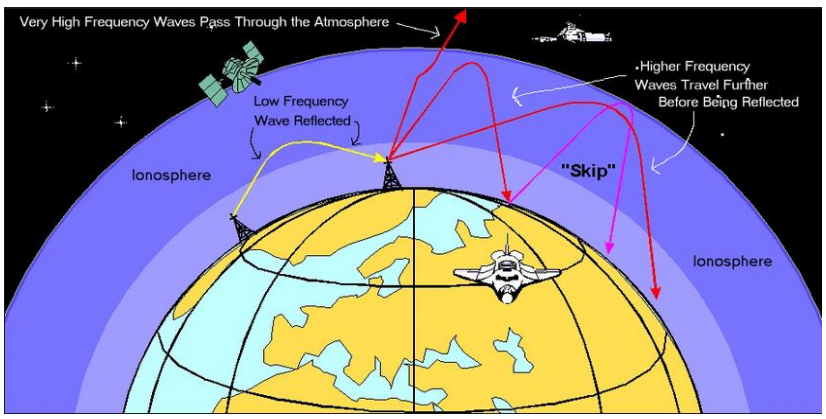

Figure 4: Lower RF reflecting from the ionosphere and higher RF penetrating the ionosphere [17]

Since GNSS satellites operate well above the plasma frequency, they are able to penetrate and travel through the ionosphere [9]. However, the phase velocity V_{ph} of the waves traveling at L band frequency ranges is reduced due to the impact of the electron density on the refractive index. The index of refraction is described with respect to speed of light C and phase velocity V_{ph} in **equation (3)** [18].

$$n_{ph} = \frac{C}{V_{ph}} \quad (3)$$

Substituting the expression of phase velocity V_{ph} presented in **equation (4)** into the denominator of **equation(3)** gives

$$V_{ph} = \frac{c}{\sqrt{1 - \left(\frac{fp}{f}\right)^2}} \quad (\mathbf{4})$$

This leads to the expression presented in **equation (5),** where the index of refraction is presented with respect to the plasma frequency fp and the frequency of the transmitted wave f [18].

$$n_{ph} = \sqrt{1 - \left(\frac{fp}{f}\right)^2} \quad (\mathbf{5})$$

As previously mentioned since GNSS signals operate at L band frequencies much larger than the plasma frequency, the expression for index of refraction can be approximated and rewritten as shown in **equation (6)** [18]**.**

$$n_{ph} \approx 1 - 0.5\left(\frac{fp}{f}\right)^2 \quad (\mathbf{6})$$

Substituting the plasma frequency defined as $fp = 8.98\sqrt{N_e}$ into **equation (6)** leads to the expression presented in **equation (7)**, where index of refraction is related directly to electron density N_e [18].

$$n_{ph} = 1 - \frac{40.3}{f^2} N_e \quad (\mathbf{7})$$

Ultimately, the expression presented in **equation (7)** can be used to calculate the signal delay by integration with respect to distance *dl***.** The delay time is

$$\Delta t = -\frac{40.3}{f^2} \int N_e \, dl \quad (\mathbf{8})$$

Here *dl* is the infinitesimal Euclidean distance from the satellite to the receiver, which describes a path through the electron content in the ionosphere [18]. Integrating the electron density N_e along the signal path results in the slant total electron content (*STEC*) presented in **equation (9)** [18]**.**

$$STEC = \int N_e \, dl \quad (\mathbf{9})$$

The total electron content in the Ionosphere can cause GNSS signals to be delayed by 10's of nano-seconds (ns) as they travels to the receiver [9]. Ionospheric delay in the signal causes errors in pseudorange, which results in navigational solution errors. Currently ionospheric delay is the largest source of GNSS positioning error**.**

The errors involved with the time delay can be almost eliminated by using multiple frequencies in GNSS receivers. The time delay can also be calculated using pseudorange values from dual frequency bands. **Equation (10)** describes the difference in time delay between L1 and L2 frequency bands as shown

$$\Delta t = \frac{PL2 - PL1}{C} \quad \mathbf{(10)}$$

obtained by taking the difference of the Pseudoranges on each frequency band ($PL2 - PL1$) and dividing by the speed of light *C*. The time delay can be used to correct the error in the Pseudorange. Note for simplicity for the discussion here **equation (10)** does not incorporate error sources associated with the pseudorange measurements [9].

The time delay can be substituted into **equation (11)**, to solve for the total electron content (TEC) [9]. The TEC is dependent on the time delay Δt, speed of light *C*, and the dual frequencies as shown

$$TEC = \frac{\Delta t * C * f_{L1}{}^2 * f_{L2}{}^2}{40.3 * (f_{L1}{}^2 - f_{L2}{}^2)} \quad \mathbf{(11)}$$

TEC is usually scaled with respect to total electron units (TECU), where 1 TECU = $10^{16}\ e/m^2$ [18].

2.3 Basic Concept of GNSS Scintillations

Scintillation describes the fluctuations in signal amplitude and phase of the RF signals traveling through ionospheric disturbances often called ionospheric irregularities [2], [19]. The amplitude scintillation equation is presented in **equation (12).**

$$S_4 = \sqrt{\frac{<I^2> - <I>^2}{<I>^2}} \quad \textbf{(12)}$$

In the equation, I is defined as the signal intensity [2]. The operation $<*>$ is the ensemble average, therefore $< I^2 >$ is the variance of the signal intensity and $< I >^2$ is the mean square. S_4 is the index describing the amplitude scintillation, which is the standard deviation of the signal intensity, divided by the average of the signal intensity. An S_4 value of 0 means that there is no scintillation. An amplitude scintillation value ranging from 0.1 to 0.3 usually indicates low signal fade, while amplitude scintillation of values of 0.4 and greater usually indicate that there is a high fade in the received signal [19]. S_4 is usually computed over 60 second intervals of data.

A fade in received signal means that the RF signal has experienced loss in intensity and the signal amplitude has been reduced significantly at the receiver. Carrier to noise ratio density (C/No) is used to indicate how much a signal has faded**.** The carrier to noise ratio density is presented in **equation (13)**. It is the ratio of power received divided by the system noise power, where the noise bandwidth of the receiver is set to 1 Hz. The C/No is represented in dB-Hz.

$$C/No = 10log10\left(\frac{Pr}{No}\right) = 10log10(Pr) - 10log10(No) \quad (\mathbf{13})$$

The power received P_r can be calculated using the Friss transmission equation presented in **equation (14)**.

$$\mathrm{Pr} = \frac{PtGrGt\lambda^2}{(4\pi R)^2 Ls} \ (\mathbf{14})$$

The power received is related to antenna gains (*Gt*, *Gr)*, transmit power (*Pt)*, RF wave length (λ), range distance between the antenna links (*R)*, and losses (*Ls)* that could be associated with the system. The system noise power, which is presented in **equation (15)** relates the system noise temperature *(Tn)* and the Boltzmann's constant (*K)*.

$$No = KTn \ (\mathbf{15})$$

The phase of the signal that passes through the ionosphere can be measured using the expression presented in **equation (16)**.

$$\varphi = \frac{40.3}{Cf} TEC \ (\mathbf{16})$$

In the expression, *TEC* is the total electron content, *C* is the speed of light, and *f* is the frequency of the transmitted wave [2]. Phase scintillation is computed by taking the standard deviation of the phase in radians. Scintillation monitoring devices detrend the phase over a period of time.

Power spectral density of both amplitude and phase can also be used to determine scintillation intensity in the frequency domain. This is done via fast Fourier transform, usually for 60 seconds of high rate data for either amplitude or phase and plotted on a log-log scale. The power spectral density characterizes the signal energy with respect to frequency, as the signal passes through the ionospheric medium. The expression presented in **equation (17)** is used to determine the power spectral density of phase scintillation.

$$S\emptyset(f) = \frac{\mathrm{T}}{f^p} \ (\mathbf{17})$$

T represents the power density of the signal at 1 Hz and variable f represents the desired frequency range [2], [19]**.** The phase power spectral density slope is greatly reduced at a lower cut off frequency [19]. Everything past the lower cut off is referred to as the noise floor [2], [19]. For the power spectral density of the phase, the lower cut off frequency is dependent on the GNSS receiver phase lock loop bandwidth, which is usually set to 10 Hz [19]. Anything past the bandwidth of the receivers phase lock look bandwidth is considered to be the noise. The variable p represents the slope of the line, which is approximated from a linear fit curve in the power region. The power region is between the low cut off frequency and noise floor cut off frequency of the power spectral density plot [2], [19]. **Figure 5** is an example of the power spectral density of phase. Linear fits are used to approximate spectral index p over a desired range of frequency f. The linear fit curves are drawn from the low cut off region to the noise floor. The slopes in the power region determine the intensity of the scintillation event. Based on the scintillation index library, very high scintillation usually generates values of p that are as high as -2.6 [19].

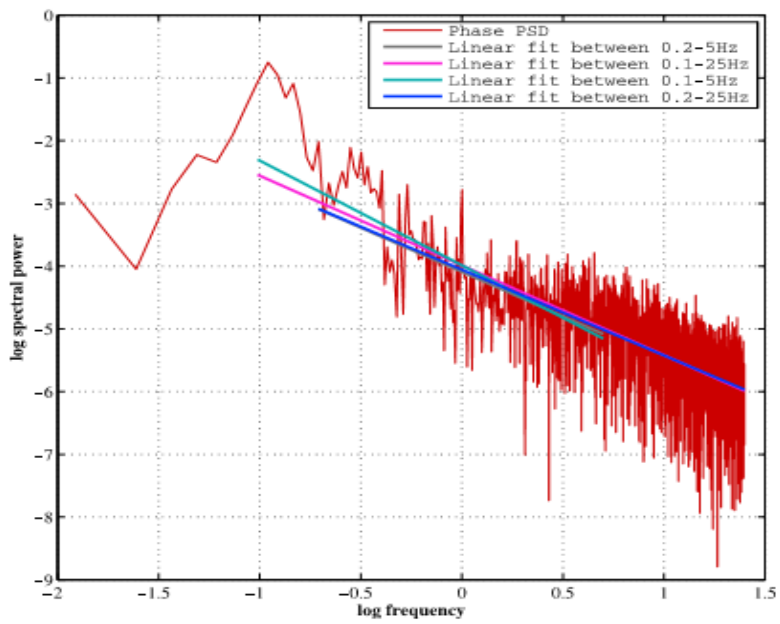

Figure 5: Power spectral density of phase. Linear fit curves are drawn in the power region between the low cut off region and high cut off region over desired frequency range *f*. The spectral index *p* is approximated from the linear fit [1**]**

The amplitude intensity and phase power spectral densities are similar in that they both have cut off frequencies at the noise floor [2]. The main difference between the power spectral density of the amplitude and the phase is that the amplitude power spectral density has a cut off frequency, referred to as the Fresnel frequency. Fresnel zones describe the constructive and destructive interference boundaries of signals transmitted to a receiver [16]. Transmitted signals can travel by line of sight (LOS) and also reflect or diffract off surfaces. The total distance that the wave travels, which is the LOS distance with the reflected or diffracted distance, can cause both constructive and destructive interference. The expression presented in **equation (18)** describes the radii for each Fresnel zone.

$$hn = \sqrt{\frac{nd1d2}{d1+d2}} \quad \textbf{(18)}$$

In the equation *d1* is the distance from the transmitter to point of reflection or diffraction and *d2* is the distance from point of reflection or diffraction to the receiver. The variable *n* are integer values that can either be even or odd. Odd values of *n* define destructive Fresnel frequency zones, while even values define constructive interference zones. Since ionospheric disturbances cause GNSS signals to refract and bend, this can cause destructive and constructive interference at the GNSS receiver.

As shown in **Figure 10**, the Fresnel frequency is defined by the cut off at which the signal intensity begins to roll off and vary [2]**.** Fresnel frequency can be defined by **equation (19)**.

$$F_f = \frac{\mathrm{Vr}}{\sqrt{2}\,\lambda r} \quad (\mathbf{19})$$

It is related to the relative velocity between the satellite and ionospheric irregularities and the wavelength of the signal. Lower case *r* in the equation is the distance between the irregularities and GPS receiver [2].

To approximate spectral index *p* from the power spectral density of amplitude a linear fit has to be drawn in the power region, which is between the Fresnel cut off frequency and noise floor cut off frequency. **Figure 10** is an example of a linear fit done on the power spectral density of amplitude. A curve is drawn in the power region, which is between the Fresnel frequency and noise floor.

It has been shown from past research that at low latitudes, amplitude scintillation is more severe than phase scintillation, and at high latitudes, phase scintillation is more severe than the amplitude scintillation [1]. One of the goals of this investigation is to determine the severity of amplitude and phase scintillation at mid-latitude.

2.4 Past Scintillation Investigations

2.4.1 Low Latitudes

Studies have been done on GPS scintillation at low latitudes by a number of researchers [20]. GPS scintillation data has been collected in Brazil near the equator. Scintillation data collected in Cachoeira Paulista, Brazil, can be seen in **Figure 6**. The top portion of the graph is the C/No carrier to noise ratio density in dB-Hz, which describes the signal strength with respect to system noise. The bottom portion of the graph is the scintillation data S_4, which is the normalized standard deviation of signal intensity.

It can be shown from the graph in **Figure 6** that at low S_4 values of roughly 0.1, the carrier to noise ratio density maintains stability at roughly 40 dB-Hz [20]. However, as soon as S_4 values begin to increase to 0.4 and higher, the carrier to noise ratio begins to decrease by as much as 20 dB-Hz. The S_4 values in the graph below are very high because ionospheric irregularity activity at the equator is very intense compared to other regions of the earth. S_4 has values as high as 0.90 and slightly above 1. At high scintillation values of 0.90 and greater, the received GPS signal experiences extreme degradation.

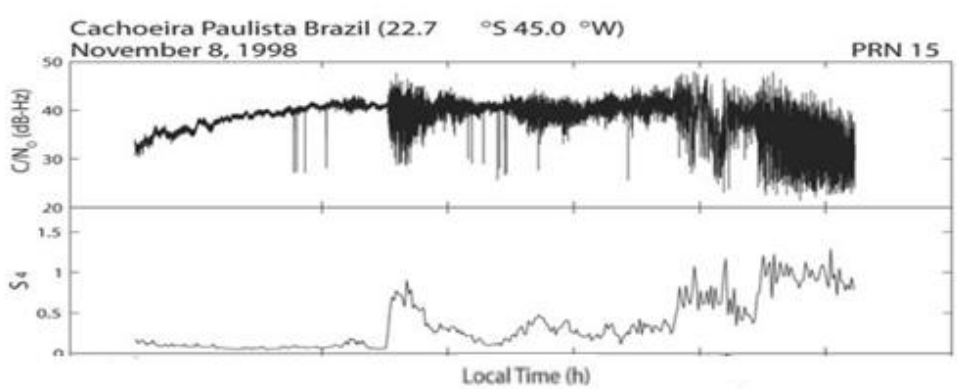

Figure 6: Scintillation data collected in at Cachoeira Paulista, Brazil [20]

Previous research done at low latitudes have shown that lower frequencies tend to fade more than higher frequencies [21], [22]**.** Data showing such characteristics has also been collected in Brazil [21], [22]. Based on the study, the GPS receivers lost lock more often for signals operating at L2 and L5 frequency bands, than L1 [21]. The receivers used for the study are Septentrio PolaRxS, which collected data for 45 days and a Novatel GP station receiver which collected data for 11 days. Histogram distributions shown in **Figure 7** were used to plot the scintillation density for frequency bands L1, L2, and L5.

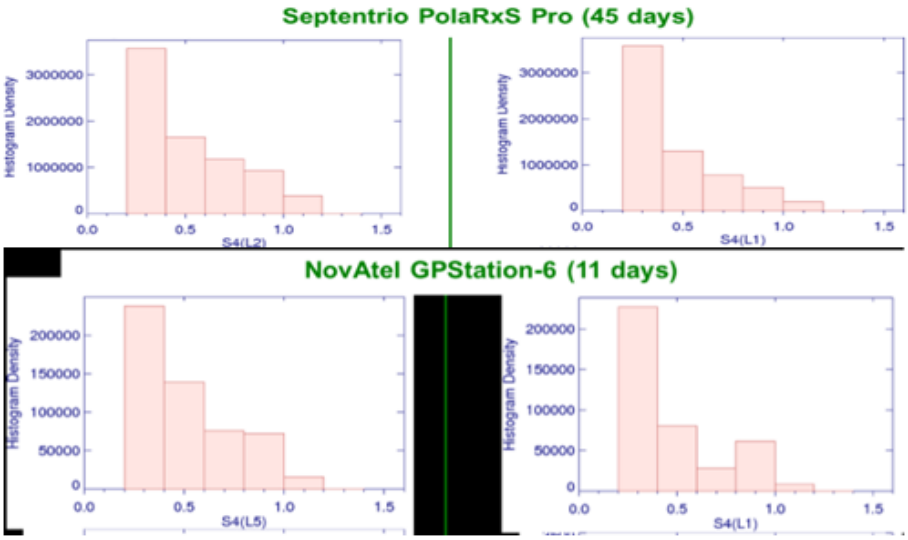

Figure 7: Histogram distribution of scintillation of L1 and L2 bands collected using Septentrio PolaRxS Pro (top) and histogram distribution of scintillation L1 and L5 collected using Novatel GPStation-6 (bottom) [21]

The PolaRxS was used to compare frequency bands L1 and L2 [21]. As shown in **Figure 7**, scintillation of 0.5 and higher occurred more often for frequency band L2 than on L1. The Novatel GPStation-6 receiver was used to compare frequency bands L1 and L5. It can also be seen from **Figure 7** that scintillation values of 0.5 and higher occurred more often for frequency band L5 than on L1. Overall, the conclusion of the study showed that frequency band L1 scintillates less than both L2 and L5. It is important to

note that when this study was done back in 2012, only three satellites transmitted frequency band L5 and ten satellites transmitted frequency band L2.

2.4.2 High Latitudes

Studies have been done on scintillation at high latitude regions in Lonyearbyen, Norway [1]. For this study, both phase and amplitude power spectral densities were analyzed in the frequency domain. The power spectral density of the phase is used to determine spectral index *p*, since phase scintillation is considered to be more severe at high latitudes and the power spectral density is used to determine the Fresnel frequency.

Figure 8 is an example of the power spectral density graph of both the phase in green and the amplitude in blue, collected in Lonyearbyen, Norway [1]. As shown in the figure, the phase and the amplitude power spectral densities have a similar frequency power spectral variation. **Figure 9** is a plot of spectral index *p* varying with respect to time. The spectral index *p* was determined by linear interpolating the power spectral density of the phase. As shown on the plot, *p* can vary from values less than 1 to values as high as 3.5.

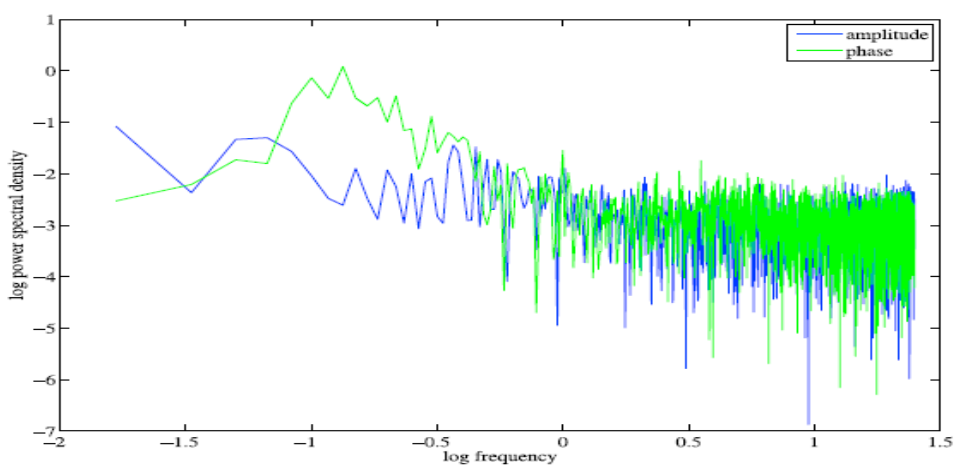

Figure 8: Power spectral density of amplitude and phase scintillation, green representing phase and blue representing amplitude. Both data sets were collected at Lonyearbyen, Norway [1]

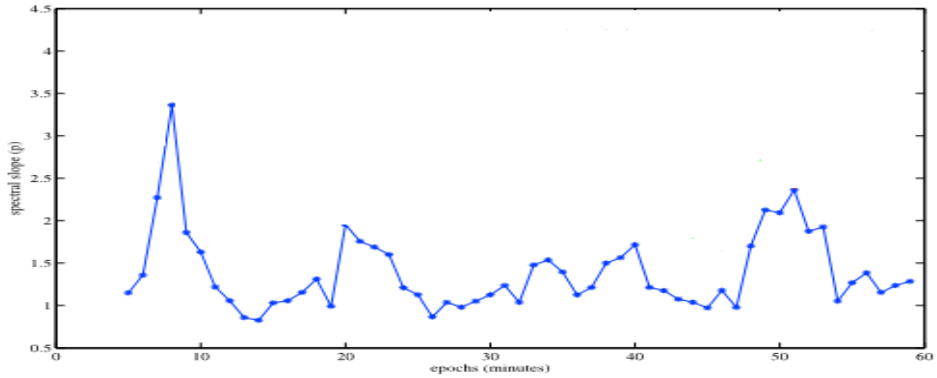

Figure 9: Linear interpolation of spectral index p over time. As shown on the plot above, *p* can vary from values less than 1 to values as high as 3.5 [1]

2.4.3 Mid Latitudes

Few scintillation studies have been done at mid latitude regions. It is believed that mid-latitude scintillation is negligible [1]. Some recent studies were performed at mid-latitudes at the GPS laboratory at Virginia Tech in Blacksburg, VA [2]. Based on the studies done, it was shown that at mid-latitude regions severe amplitude scintillation can occur. **Figure 10** is the observed amplitude power spectral density with a linear interpolation from the roll off Fresnel frequency to the noise floor, which is used to estimate the spectral index *p*.

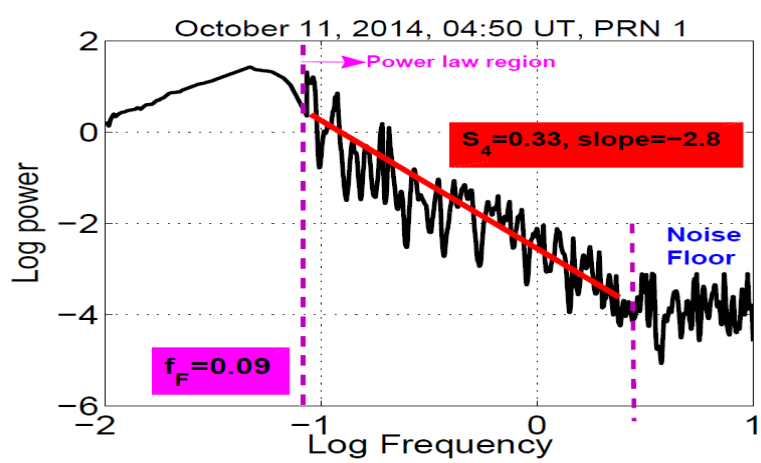

Figure 10: Power spectral density plot of amplitude generated from data collected at mid-latitude [2]

At an S_4 value of 0.33, the power spectral density resulted in a roll off Fresnel frequency of roughly 0.09 Hz [2]. The line was interpolated from the Fresnel cut off to

the noise floor cut off. The slope of the line was estimated to be -2.8. Based on these findings it is shown that significant scintillation may occur at mid latitudes.

2.4.4 Summary

Based on the previous studies mentioned, it is clear that phase scintillation can be severe reaching spectral index *p* values of up to 3.5, as shown in **Figure 9** [1]. The severity of amplitude scintillation at low-latitude during the scintillation event can be seen in **Figure 6**. During this event, amplitude scintillation reached levels of 0.90 and greater, which severely degraded the receiver carrier to noise ratio density [20]. It is shown from **Figure 10**, from the power spectral density of amplitude, that scintillation can be significant at mid-latitudes, with a spectral index *p* of -2.8 [2].

Based on the histogram distributions shown in **Figure 7**, it can be seen that L1 typically has lower S_4 values compared to L2 and L5 at low latitudes. One of the main motivations for this research is to determine which is more effected at mid-latitude, phase or amplitude scintillation. Another goal is to determine which GNSS frequency bands are likely to have lower amplitude and phase scintillation at mid-latitudes.

Chapter 3 Experimental Approach

3.1 GNSS Receiver

The scintillation data for this research was collected using a Novatel GP-6 GPS receiver. Novatel GP-6 is capable of computing scintillation, carrier to noise ratio, and phase of all the GPS satellite signals that it tracks. The Novatel GP-6 system used for experimental observations in this work has ability to track signals from three GNSS constellations. These constellations include GPS, GLONASS, and Galileo. The Novatel GP-6 station is shown in **Figure 11**.

Figure 11: Current GP-6 station used at the Virginia Tech GPS lab [23]

The GP-6 station receiver can collect both high rate and low rate data. Both the high rate and low rate data are collected at 50 Hz sampling rate or 50 samples per second [23]. The low rate data includes computed amplitude scintillation, phase scintillation in radians, carrier to noise ratio density in dB-Hz, and satellite elevation and azimuth angles for each tracked satellite. The amplitude and phase scintillation are reduced and detrended over 60 seconds of data, which corresponds to 3,000 data points. The phase is first detrended using a 6th order Butterworth high pass filter. The statistics of the residuals of the previous 60 seconds worth of data (3,000 data points) are computed over periods of 1 second, 3 seconds, 10 seconds, 30 seconds, and 60 seconds of phase sigma. The amplitude is detrended by normalization over 60 seconds, or 3,000 data points.

High rate data generated by the receiver includes the measured power that is relative to the base power, and is computed from the I and Q channels of the receiver [23]. Since the measured power is relative to the base power it is unitless. The phase is computed using Accumulated Doppler Range (ADR) data for every 0.02 seconds of data, which corresponds to 50 Hz sampling rate. The high rate data provides the phase in mili cycles.

Novatel GNSS receivers have a software interface called Novatel Connect. Novatel Connect is used to communicate with the receiver, using a windows computer

through USB port connection. Once the software connects to a Novatel receiver, Novatel Connect will load the screen displayed in **Figure 12**.

The window includes an elevation and azimuth plot of all the GNSS satellites locked onto the receiver, carrier to noise ratio of all locked satellites, user position, carrier to noise ratio of different satellite frequency bands, dilution of precision of tracked satellites, and a command window. String commands are typed into the command window and sent to the receiver to collect data. This gives the user the ability to log data, such as GPS time, pseudorange, Doppler frequency, carrier phase, etc.

Figure 12: Novatel connect window, which displays user position, carrier to noise ratio, satellite elevation and azimuth plot, etc. [24]

Two string commands are used to collect both low and high rate data from the GP-6 station receiver. The command "LOG ISMREDOBSB ONNEW" is used to collect the low rate data and "LOG ISMRAWOBSB ONNEW" is used to collect the high rate data [23]. Both commands can be inputted to collect both high rate and low rate data at the same time. Once the receiver begins to collect data, the data file can be saved as a .GPS file extension.

Novatel provides C code that can be used to convert the GPS file to excel data files in .CSV format. The code itself can be initiated using a windows command prompt. Two commands are used to convert the GPS files, one is called PARSERAW and the other one is called PARSEREDUCED [23]. The PARSERAW command is used to convert high rate data GPS files and PARSEREDUCED is used to convert low rate data .GPS files. The .CSV files for low rate and high rate data are generated differently for the tracked satellites. Low rate data files include data for every single tracked satellite in one .CSV file, while high rate data generates individual .CSV files for each of the tracked satellites. As a result, different coding schemes were used to process the high rate and low rate data.

3.2 High Rate and Low Rate Data File Format

Both high rate and low rate files provide different sets of data, which required different coding schemes for processing the data. Low rate data files include a total of seventeen columns of data as shown in **Table 1**. The columns that were used in the data processing are the following: GPS time, satellite PRN number, frequency band (SigType), satellite elevation and azimuth angles, carrier to noise ratio density (CNo) in dB-Hz, amplitude scintillation index S_4, and phase (60 SecSigma).

Table 1: The figure above is an example of the low rate .CSV file and the columns of data that are included in it

19	GPS TOW	PRN	Freq	SigType	Az	Elv	CNo	Lock Time	CMC Avg	CMC Std	S4	S4 Cor	1SecSigm	3SecSigm	10SecSigr	30SecSigr	60SecSigr
20	348060	18	0	1	264.66	21.02	41.48	3157.1	-6.473	0.224	0.102719	0.084448	0.073521	0.076589	0.079344	0.079332	0.079343
21	348060	29	0	1	227.93	57.36	49.78	12477.23	-6.26	0.033	0.09911	0.032427	0.045757	0.051727	0.05416	0.054146	0.054149
22	348060	29	0	5	227.93	57.36	47.43	12472.83	-10.084	0.062	0.114236	0.042503	0.048341	0.05191	0.053488	0.053466	0.053462

An example of a high rate data file is presented in **Table 2.** The high rate data file has the constellation type and PRN number listed at the header. For the particular case shown in **Table 2**, the system constellation is GPS and satellite number is nine. Raw

.CSV files have four data columns. The columns that were used in data processing are the GPS time, phase in mili cycles, and relative power which is computed from the receiver I and Q channels and is unitless.

Table 2: An example of the high rate .CSV file and the columns of data that are included in it

1	Raw phase and amplitude data				
2					
3	GPS Signa	4 = L2Y	5 = L2C	6 = L2P	7 = L5Q
4					
5					
6	Week Nur	GPS PRN# 9			
7					
8	GPS TOW	Freq	Signal Typ	ADR	Power
9	249921	0	1	-1.1E+07	2.4E+09
10	249921	0	1	-1.1E+07	1.84E+09
11	249921	0	1	-1.1E+07	1.48E+09

3.3 Software Design

MATLAB was used to develop software to process both the high rate and low rate data files. The software requests the user for the following inputs: .CSV file name to be processed, option to graph data for a single satellite or all satellites, month, day, and GPS week number. The GPS week number along with the GPS time in seconds are used to calculate UTC time, which includes the month, day, hour, and seconds that the data was collected. The user input for month and day are compared with the calculated UTC month and day to make sure that the data selected is for the proper time frame.

There are a number of ways to access excel files in MATLAB. The two commands that were considered are *xlsread* and *fopen*. The *xlsread* command can be used to load excel data files into MATLAB. However, the issue with *xlsread* is that it may take excessive time to load large data files. As a result, *xlsread* proved to be very

inefficient. Unlike *xlsread*, *fopen* doesn't load the excel file data, but rather opens the file, which saves time. As a result, this made accessing large amounts of data faster.

A number of steps had to be taken to access and store the data. For example, the header information at the top of the .CSV file does not need to be stored, so a method had to be implemented to skip over the header characters. A *while* loop and the *fgetl* command were used to skip over the header characters. The MATLAB command *fgetl* is used grab consecutive lines in a file that has been opened. As shown in **Appendix 1**, the while loop had to be incremented nineteen times to skip over the header characters at the top of the .CSV file. Since the header characters take up nineteen lines of space, the loop had to be incremented nineteen times to reach the data.

The next step taken in the coding procedure was to determine the length of the data file. When working with data files it is crucial to determine the length of the file in order to identify the total number of lines of data in the file. This number is used to set a limit on a looping method, used to process the whole data file. Shown in **Appendix 1** is the coding scheme used to determine the total number of lines in the .CSV file.

A while true loop is used to continuously loop through the file and *fgetl* is used to grab the lines of data. The *if* condition in this code is used to identify the end of the file, which doesn't include any characters. As long as *fgetl* grabs a line which contains characters, the variable size will continue to increment. Once the *if* condition is true for no characters found at the end of the file, a break is used to break out of the while true loop. The variable size will contain the total number of lines of data in the .CSV file.

The MATLAB command *strread* shown in **Appendix 1** was used to scan and store data for each row in the .CSV file. *Strread* can store a variety of data types, such as

floating numbers, decimal numbers, etc. Since the low rate data file has seventeen columns of data, seventeen variables were used to store data for each scanned row. For low rate data the variables that were stored are the following: GPS time in seconds, satellite PRN number, frequency band of operation, azimuth and elevation satellite angles, carrier to noise ratio density, scintillation index S_4, and phase scintillation in radians.

For high rate data, the *textscan* function shown in **Appendix 1** was used to store the GPS time in seconds, frequency band of operation, phase, and signal power. The *textscan* function was used over *strread* because it was more efficient in processing larger data files. The signal power is stored in sixty second intervals and used to compute scintillation index S_4, within that time frame. Phase is stored in mili cycle units and converted to cycles. The format of *strread* command used to store the high rate data files is presented in **Appendix 1**.

Chapter 4 Experimental Results

4.1 Introduction

For this study data is collected at mid-latitude from a GNSS receiver located in Blacksburg, VA at 37.205 degrees latitude north and 80.417 degrees longitude west. Observations were made on GNSS frequency bands L1, L2, L5, G1, G2, E1, E5A, and E5B to conclude which band had better overall performance. The GNSS frequency band observations are qualitatively compared to typical observations made at low latitudes in Brazil [20], [21], [22]. Power spectral density of both amplitude and phase were used to determine scintillation intensity by linear interpolation of slope *p*. The slope *p* values are compared to previous mid-latitude observations from Blacksburg, VA and with *p* values

obtained from observations at high latitudes made in Lonyearbyen, Norway [1]. These comparisons were made to investigate how mid-latitude scintillation characteristics in general compare to those at low and high latitudes.

Three sets of data were collected on multiple days during severe and moderate space weather conditions. The space weather was tracked by the space weather prediction center, which uses magnetometers to make space weather predictions [25]. The space weather prediction center provides daily Kp index values, which determine storm activity over three hour intervals. A Kp index value which falls within a range of 4 to 9 indicates that a geomagnetic storm is occurring. A Kp index value less than 4 is an indication of moderate conditions. SuperDARN TEC and radar backscatter data, along with Kp index, are used to show the conditions of the upper atmosphere while the data sets were collected.

4.2 Data Set 1 Presentation

The first data set analyzed was collected on August 15th and 16th of 2015. During this period of time a storm was tracked using the space weather prediction center. **Figure 13** is a Kp index plot of the storm which occurred on August 15th and 16th of 2015. The storm begins at 12:00 PM UTC time and continues through the 16th of August. As shown on the plot, the Kp index value is as high as 7 and 6 when the storm begins and reduces to a Kp value of 4 as it fades out on August the 16th.

Figure 14 is a TECU and radar backscatter plot generated by SuperDARN. As shown, the TEC content varies from 7 to 12 TECU above Blacksburg, Virginia, where the data was collected. The radar backscatter plot shows a SNR ranging from 10 to 20 dB, above Virginia.

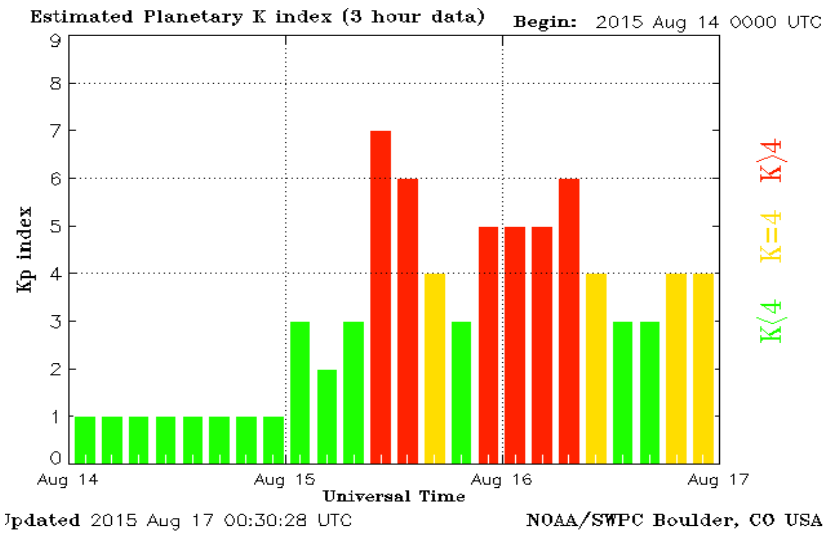

Figure 13: Kp index plot of a small geomagnetic storm that occurred on August the 15th and lasted until August the 16th [25]

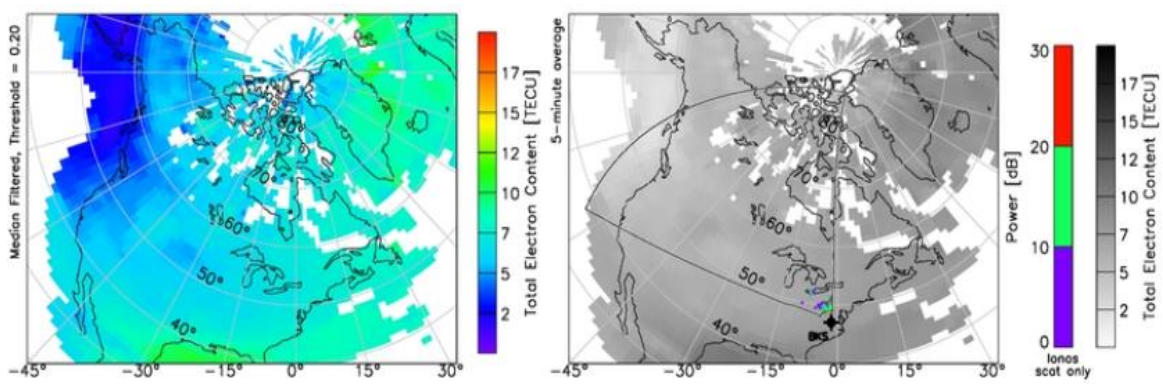

Figure 14: Total electron and radar backscatter plots at 13:18:00 UTC of the geomagnetic storm that occurred on August the 16th [7]

4.2.1 Scintillation Analysis

Low rate data was collected for data set 1. The scintillation index S_4, carrier to noise ratio density in dB-Hz, and phase in radians are presented for satellites from the GPS, GLONASS, and Galileo constellations. The scintillation conditions were compared across GPS frequency bands L1, L5, GLONASS G1, G2, and Galileo E1, E5A, and E5B.

It is important to note that the Galileo constellation is not completely filled at this time. This is expected by 2020. During the time this data was taken in 2015, the receiver could track at most four Galileo satellites which limited the Galileo data observations.

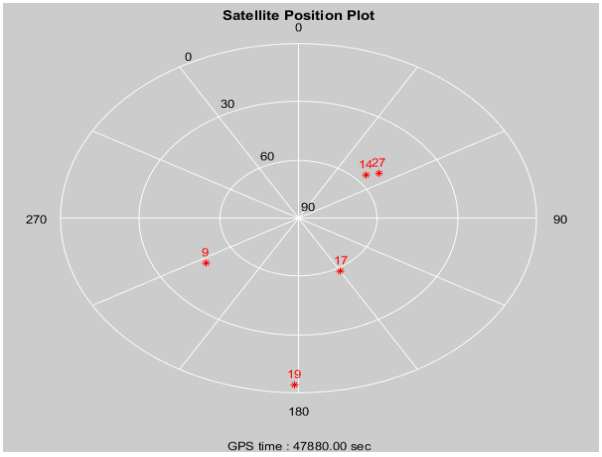

Figure 15: Elevation and azimuth plot of satellites analyzed during a turbulent event. The satellites are represented, by red stars. GPS satellites 9, 27, GLONASS 14, 17, and Galileo 19 are shown on the plots [26]

Figure 15 is an elevation and azimuth plot of the GNSS satellites analyzed during the August the 16th storm. These are the locations of the satellites during the event which occurred at 13:18:00 UTC time. This plot is meant to give a visual of the satellite locations during the event. GPS satellites 9 and 27 and GLONASS 14 and 7 are fairly close to one another. Galileo satellite 19 has a very low elevation angles compared to the other observed satellites and is the farthest away. As a result, it is important to note that Galileo satellite 19 may not have been effected by the turbulent events like the other satellites, but may have been experiencing high amplitude scintillation at lower elevation angles since there is a longer line of site (LOS). Since the GPS and GLONASS satellites are relatively close to one another, this could have been the reason why all these satellites experience severe amplitude and moderate phase scintillation at the same time frame. The scintillation analysis is further discussed in this section.

Table 3 lists the satellite numbers, frequency bands, maximum amplitude scintillation index S_4, maximum phase scintillation, frequency bands, and satellite location during the period of maximum scintillation. The majority of the observed satellites are all above 15 degrees elevation angle to mitigate multipath effects. These observations indicate that at mid-latitudes, scintillation can potentially be severe just as low and high latitude regions. However, since this storm only lasted a short period of time, the scintillation wasn't prolonged.

Table 3: Data from August the 16th storm. S4, frequency bands, carrier to noise ratio, and change in carrier to noise ratio, displayed below

Sat Type	Sat No	Freq Band	Max Amplitude Index ($S4$)	Max Phase φ (radians)	Azimuth Angle At Max (S4)	Elevation Angle At Max (S4)
GPS	9	L1	0.8139	0.354	236.56	47.93
GPS	9	L5	0.6528	0.262	236.56	47.93
GPS	27	L1	0.8425	0.350	52.81	51.84
GPS	27	L5	0.6350	0.260	52.81	51.84
GLONASS	14	G1	0.6098	0.374	48.88	56.25
GLONASS	14	G2	0.4598	0.289	48.88	56.25
GLONASS	17	G1	0.9142	0.373	150.00	58.29
GLONASS	17	G2	0.4236	0.307	150.00	58.29
Galileo	19	E1	0.3876	0.358	214.37	14.08
Galileo	19	E5A	0.5450	0.267	211.35	9.64
Galileo	19	E5B	0.5661	0.274	211.56	9.93

The satellites listed in **Table 3**, excluding Galileo satellite number 19, resulted in severe scintillation at 13:18:00 UTC time. All the satellites listed in **Table 3** experienced maximum phase scintillation at 12:22:00 UTC time during a period in which amplitude scintillation is low. GPS satellite numbers 9 and 27 at L1 frequency band and GLONASS satellite number 17 at G1 frequency band resulted the highest amplitude scintillation values of 0.8139, 0.8425, and 0.9142 for short periods of time. These values are comparable to the low latitude scintillation values collected, by [20]. The highest phase scintillation occurred on frequency bands L1, G1, and E1 across GPS, GLONASS, and Galileo. The values were fairly close at 0.354 and 0.350 radians on GPS L1, 0.374 and 0.373 radians on GLONASS G1, and 0.358 radians on Galileo E1. The lowest scintillation values occurred across bands GPS L5, GLONASS G2, and Galileo E5A, E5B. These values are also relatively close**.** The max phase scintillation across L5 are 0.262 and 0.260 radians, 0.289 and 0.307 radians on GLONASS G2, and 0.267 and 0.274 on Galileo E5A and E5B.

The upper atmospheric disturbance that occurred at 13:18:00 UTC degraded signals operating at the L1 and G1 frequency bands more severely than frequencies transmitted at L2, G2, and L5. GPS satellites 9 and 27 had maximum amplitude scintillation at L1 of 0.8139 and 0.8425, but had less amplitude scintillation at L5 of 0.6528 and 0.6350. GLONASS satellites 14 and 17 had maximum amplitude scintillation at G1 of 0.6098 and 0.9142, but had less amplitude scintillation at G2 of 0.4598 and 0.4236. It is important to note that frequency band G2 had less amplitude scintillation than L1, L5, and G1 during the time of the disturbance.

Unlike the other satellites, Galileo satellite number 19 had maximum scintillation at E1, E5A, and E5B at different periods of time, but the time difference is relatively small and it could be argued that the same atmospheric disturbance degraded the satellite signal strength. Galileo satellite 19 had maximum amplitude scintillation of 0.3876 at 12:52:00 UTC for frequency band E1, 0.5450 at 13:07:00 UTC for frequency band E5A, and 0.5661 at 13:06:00 UTC for frequency band E5B. These severe scintillation values were collected at different elevation angles less than 15 degrees. As a result, multipath errors could have likely contributed to the signal degradation.

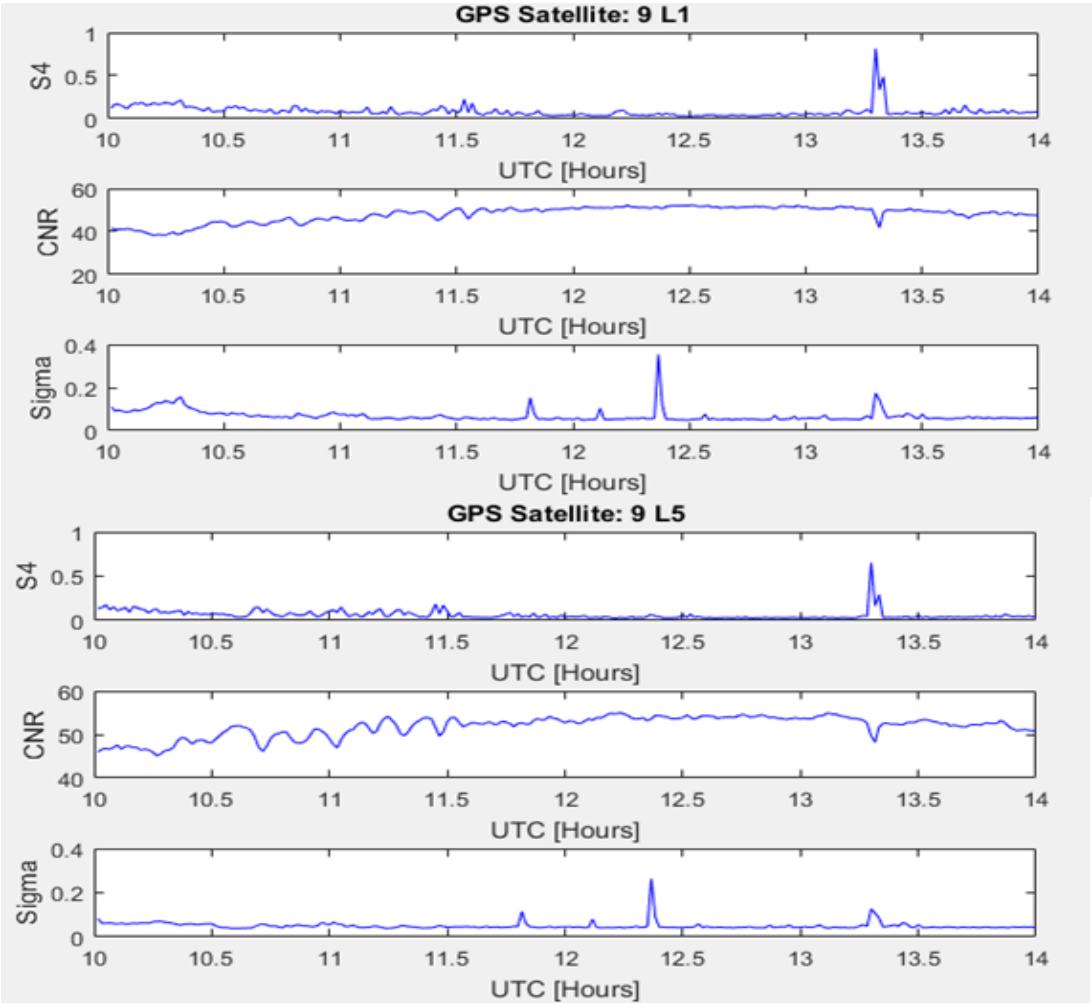

Figure 16: Scintillation, carrier to noise ratio, and phase of GPS satellite PRN number 9, at frequency L1

Figure 16 includes scintillation index S_4, carrier to noise ratio density in dB-Hz, and phase in radians of GPS satellite 9, for both L1 and L5 frequency bands. Low rate data was graphed for a duration of four hours during the geomagnetic storm which occurred on August 16th 2015. As shown in the figures, scintillation remains very low, close to the value 0, for both frequency bands and peaks at 13:18:00 UTC during an upper atmospheric disturbance event. It can also be shown from the figures that phase scintillation changes by 0.1733 radians of phase scintillation for frequency band L1 and 0.1269 radians of phase scintillation for frequency band L5. The carrier to noise ratio density of the signal is also effected on both frequency bands. L1 is reduced from roughly 50 dB-Hz to 41.85 dB-Hz and L5 is reduced from roughly 55 dB-Hz to 48.16 dB-Hz. L5 frequency band has a higher carrier to noise ratio density than L1 frequency band, which resulted in better overall performance, during the disturbance. Based on the change of phase scintillation during the turbulence L5 has less of a phase change than L1.

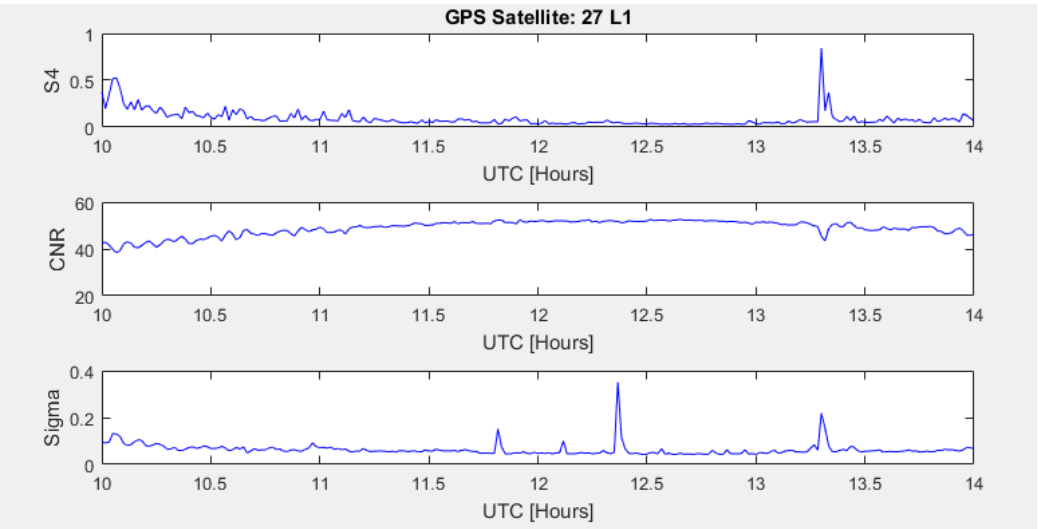

Figure 17: Scintillation, carrier to noise ratio, and phase of GPS satellite PRN number 27, at frequency L1

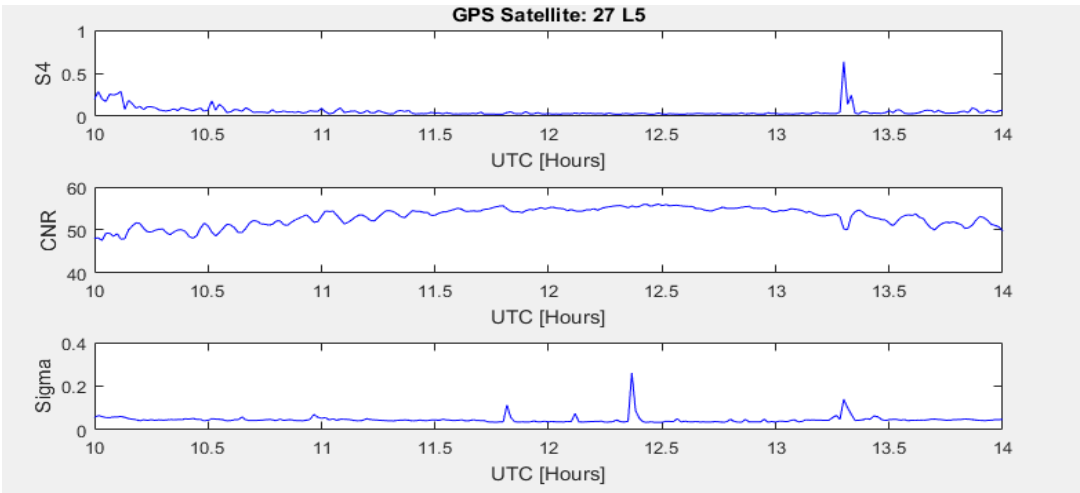

Figure 18: Scintillation, carrier to noise ratio, and phase of GPS satellite PRN number 27, at frequency L5

Figure 17 and **Figure 18** show scintillation index S_4, carrier to noise ratio density in dB-Hz, and phase scintillation in radians of GPS satellite 27, for both L1 and L5 frequency bands. Low rate data was graphed for a duration of four hours during the geomagnetic storm which occurred on August 16th 2015. Like GPS satellite 9, the L1 and L5 frequency bands transmitted by satellite 27 maintained low amplitude scintillation values of roughly 0 and peaked at 13:18:00 UTC during the upper atmospheric disturbance event. The carrier to noise ratio density of L1 is reduced from roughly 50 dB-Hz to 43.43 dB-Hz and L5 is reduced from roughly 55 dB-Hz to 50 dB-Hz. Like the previous results from GPS satellite 9, data from GPS satellite 27 shows that L5 has a better overall performance than L1. The phase scintillation during the turbulence at L1 was 0.2185 radians, while L5 was 0.1395 radians. Like the data from GPS satellite 9, this data from satellite 27 also shows that the L5 signal phase was less effected by the turbulence compared to the phase at L1.

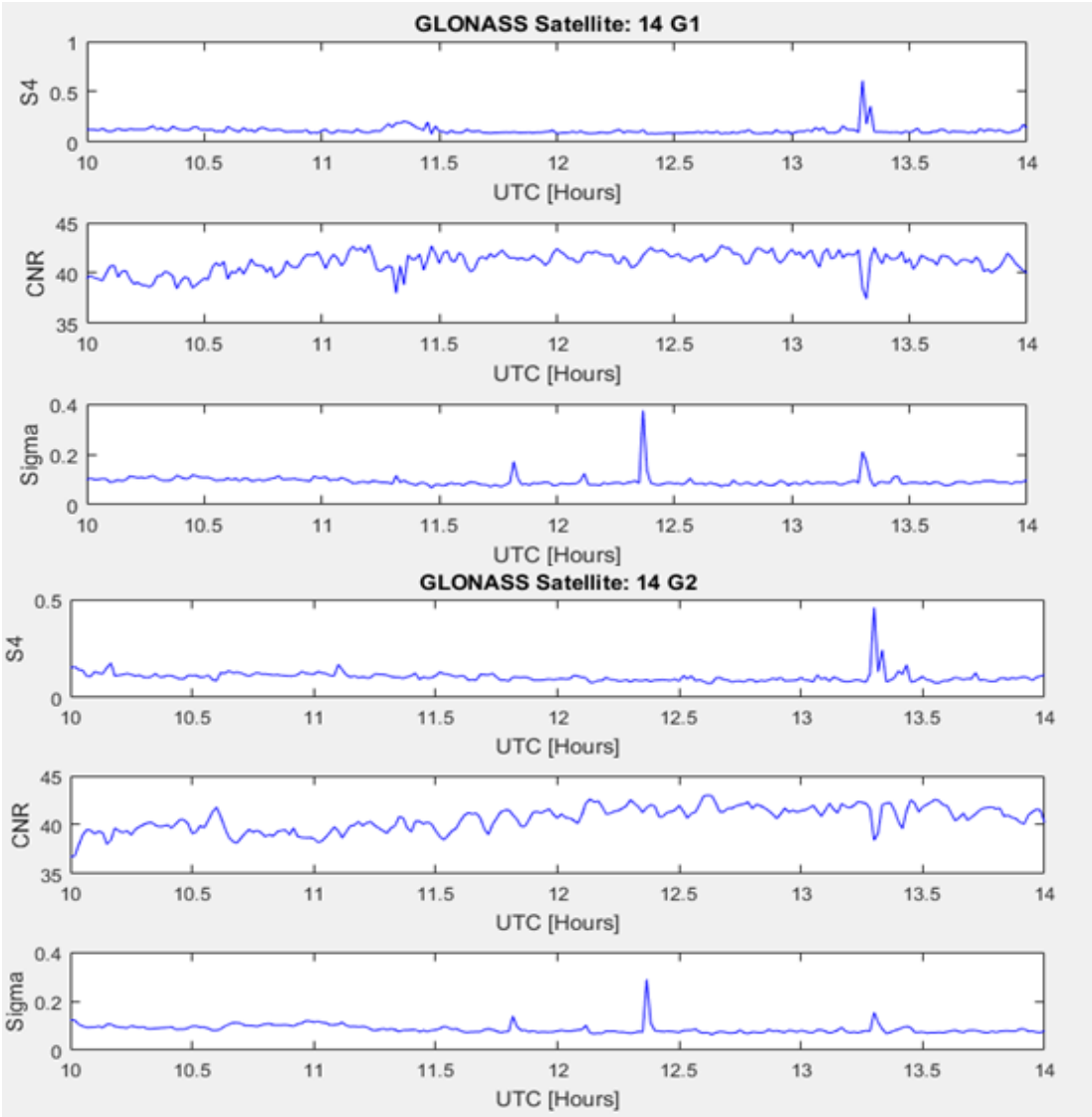

Figure 19: Scintillation, carrier to noise ratio, and phase of GLONASS satellite PRN number 14, at frequency G1

Figure 19 depicts graphs of scintillation index S_4, carrier to noise ratio in dB-Hz, and phase in radians of GLONASS satellite 14, for both G1 and G2 frequency bands. Low rate data for this satellite was graphed for a duration of four hours. Like GPS satellite number 9 and 27, GLONASS satellite 14 was effected by the disturbance at 13:18:00 UTC. As shown in the above figures, the amplitude scintillation peaks at 13:18:00 UTC. Frequency band G1 scintillates more than G2. For both frequency bands

the carrier to noise ratio density peaks at roughly 40 dB-Hz and the degradation of performance is almost equivalent. The carrier to noise ratio density of G1 degrades to 37.46 dB-Hz, while G2 degrades to 38.42 dB-Hz. However, the change in phase scintillation of G2 at 0.1537 radians is less than G1 at 0.2104 radians. As a result, the overall performance of G2 is better than G1 during the turbulence.

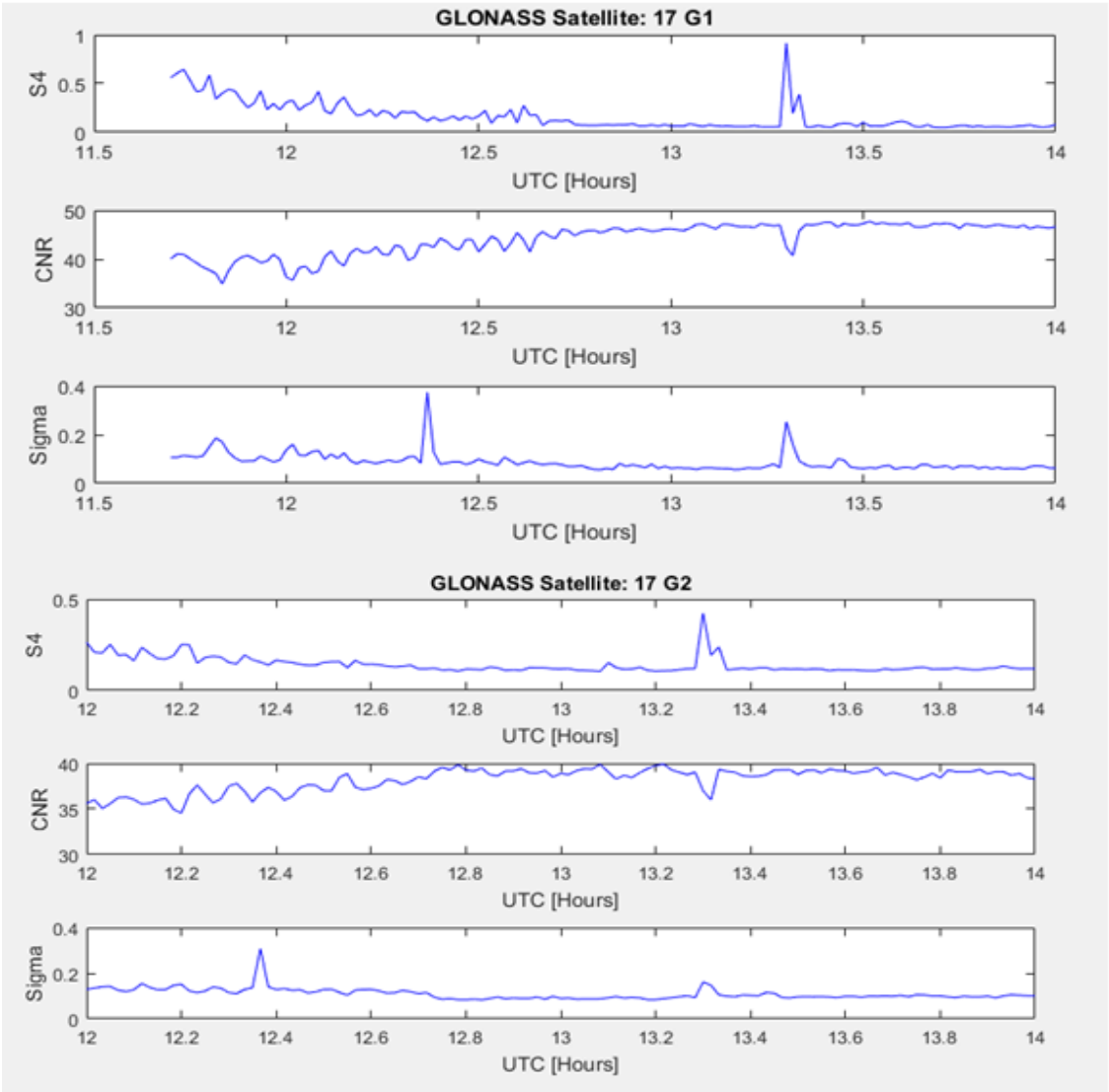

Figure 20: Scintillation, carrier to noise ratio, and phase of GLONASS satellite PRN number 17, at frequency G2

Figure 20 depicts graphs of scintillation index S_4, carrier to noise ratio in dB-Hz, and phase in radians of GLONASS satellite 17, for both G1 and G2 frequency bands. Low

rate data for GLONASS satellites were graphed for a duration of two hours, since GLONASS satellite 17 was tracked a little over an hour after the other satellites were tracked during the disturbance. This was done to keep the time consistent between both GLONASS satellite plots. Like all previous satellites, GLONASS satellite 17 was effected by the disturbance at 13:18:00 UTC. Like the data from GLONASS satellite number 14, G1 frequency band experiences higher amplitude scintillation than G2 during the disturbance. The carrier to noise ratio density of G1 degrades from roughly 45 dB-Hz to 40.7 dB-Hz, while G2 degrades from 40 dB-Hz to 36.02 dB-Hz. Although G1 maintains a larger carrier to noise ratio density, the degradation between G1 and G2 is about the same. However, the change in phase scintillation of G1 at 0.2528 radians is higher than G2 at 0.1617 radians. As a result, the performance of G2 is better than G1 during the time of turbulence.

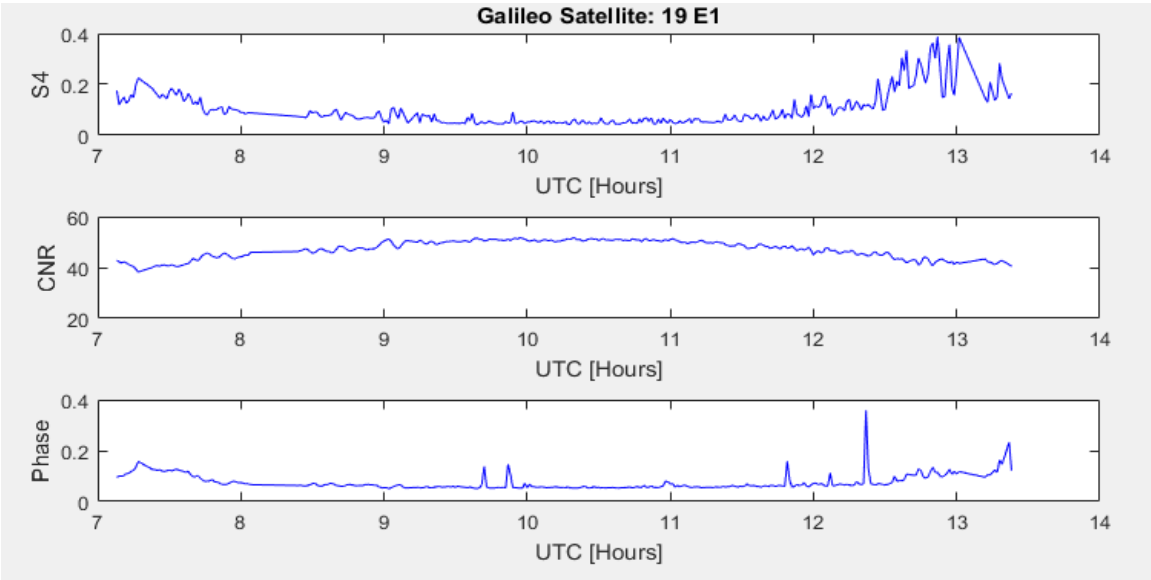

Figure 21: Scintillation, carrier to noise ratio, and phase of Galileo satellite PRN number 19, at frequency E1

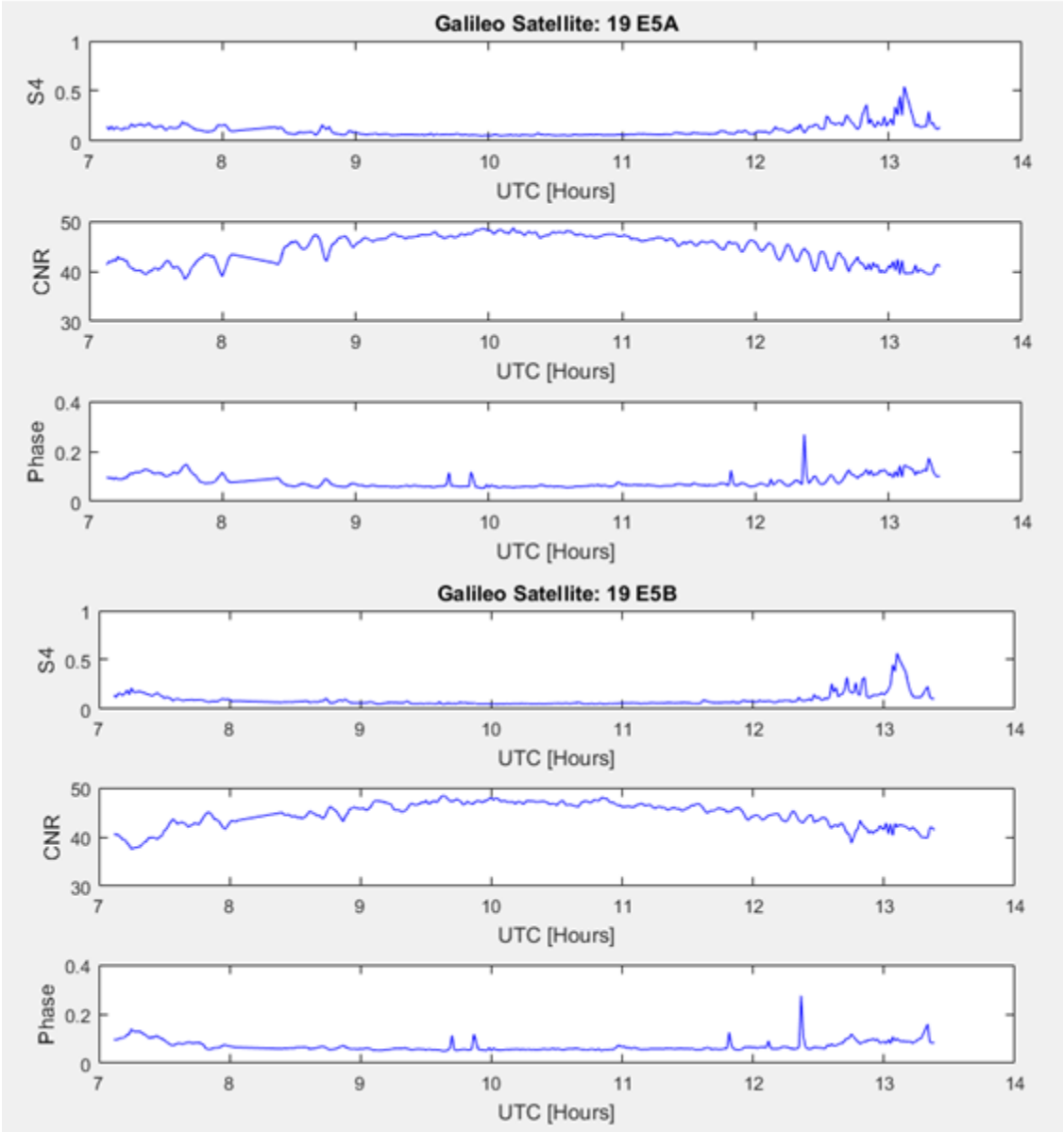

Figure 22: Scintillation, carrier to noise ratio, and phase of Galileo satellite PRN number 19, at frequency E5A and E5B

Figure 21 and **Figure 22** are graphs of scintillation index S_4, carrier to noise ratio in dB-Hz, and phase in radians of Galileo satellite 19 at E1, E5A, and E5B. Galileo satellite 19 experiences signal degradation from 12:00:00 UTC to around 13:06:00 UTC. Within that time range, frequency band E1 experiences greater scintillation fluctuations compared to frequency bands E5A and E5B. The carrier to noise ratio density of the

frequency bands diminish from 12:00:00 UTC to 13:06:00 UTC. The carrier to noise ratio density of E1 degrades from 50 dB-Hz to 42.62 dB-Hz, while E5A from roughly 48 dB-Hz to 42.2 dB-Hz, and E5B from 48 dB-Hz to 42.01 dB-Hz. The carrier to noise ratio density reduction is fairly the same across all three of these frequency bands during this turbulent event caused by the geomagnetic storm or from a longer line of site (LOS). At 12:22:00 UTC time all three frequency bands experience a change of phase. E5A has a change of phase of 0.2676 radians and E5B of 0.2747 radians, which is less than both E1 and E5B. During the disturbance, E1 had the worst performance of the three frequency bands. E5A and E5B resulted in similar carrier to noise ratio density degradation and change in phase scintillation. However, E5A had slightly better performance.

4.2.2 Summary

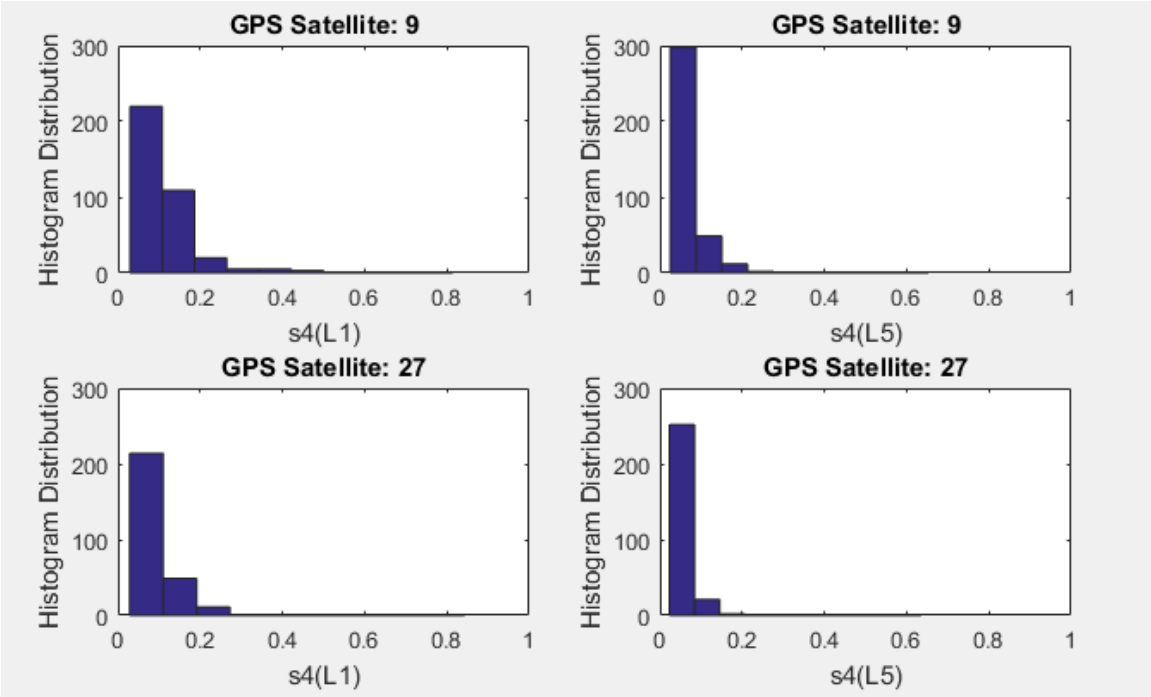

Figure 23: Histogram distribution of GPS satellite PRN 9 (L1, L5) and GPS satellite PRN 27 (L1, L5) scintillation above 15 degrees elevation angle

Figure 23 are histogram distributions of all amplitude scintillation data, above 15 degrees elevation angle, collected for GPS satellites 9 and 27 during the geomantic storm from August the 15th to August the 16th, 2015. The histogram distributions show that signals transmitted at L1 for both GPS satellites 9 and 27 have higher scintillation occurrence, compared to frequency band L5. This validates the previous analysis done on **Figure 16** through **Figure 18**, which shows that signals transmitted on L5 experienced less amplitude scintillation. These results are not in alignment with other observations which indicate that L1 scintillated less than L5 [21]. However, the data analyzed for this research is collected at mid-latitudes unlike the data collected at low latitudes, by [21]. The difference in upper atmospheric region could possibly be why L5 outperforms L1 and L2 at mid-latitude, but L1 outperforms L2 and L5 in low latitude regions [21].

For this data set, L5 maintains a greater carrier to noise ratio density than L1, so it can be inferred that signals transmitted on L5 have greater received power than signals transmitted on L1. It is shown that L5 increases to a maximum carrier to noise ratio density of roughly 55 dB-Hz, while L1 increase to a maximum carrier to noise ratio density of roughly 50 dB-Hz. In this case, L5 has 5 dB-Hz greater maximum carrier to noise ratio density than L1. One of the factors that contributes to L5 having greater carrier to noise ratio density is the fact that signals transmitted on L5 have 3 dB more signal power than signals transmitted on L1 [27]. Having a greater transmit power may reduce both amplitude and phase scintillation which leads to better overall carrier to noise ratio performance. However, it is important to note that transmit power isn't the only factor in calculating the overall carrier to noise ratio density, other variables shown above in **equation (14)**, includes signal wave length, distance the signal traveled from transmitter to receiver, and losses caused by the atmosphere. Since this data is collected at mid-latitudes, the atmospheric losses are different from high and low latitudes. As a result, the scintillation across the observed frequency bands will be affected differently. Further observations will be discussed in Section 4.3 and Section 4.4**.**

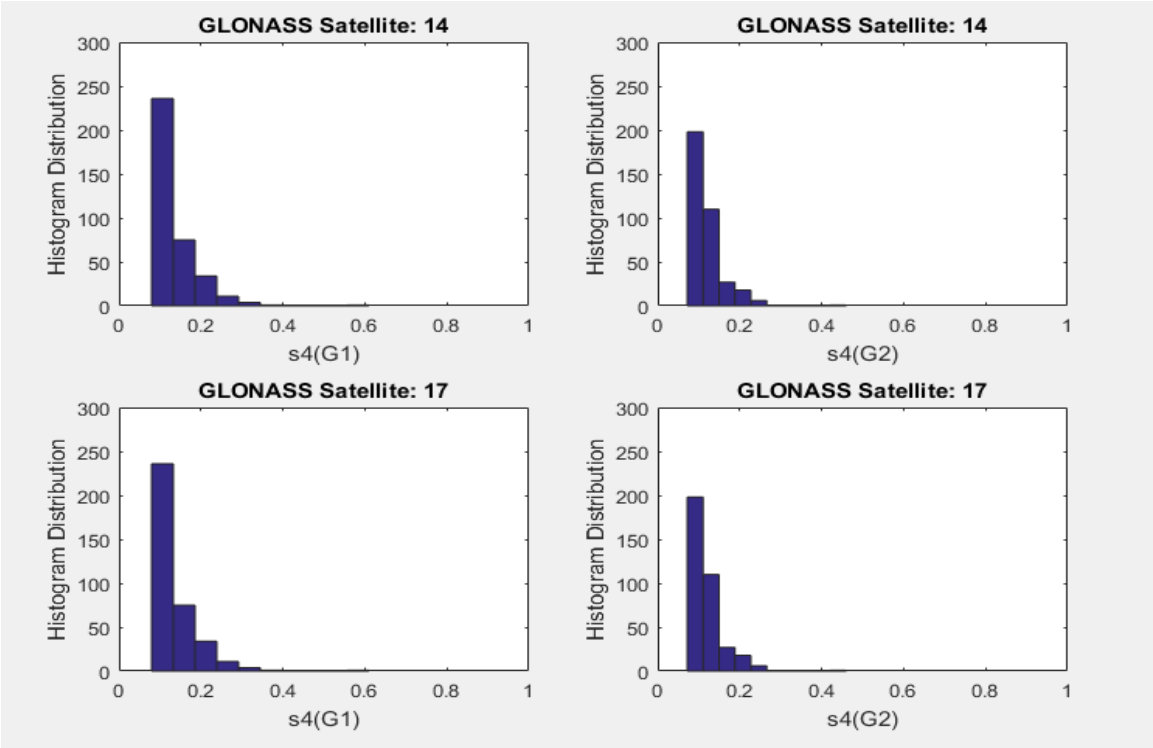

Figure 24: Histogram distribution of GLONASS satellite (G1, G2) and GLONASS satellite 27 (G1, G2) scintillation above 15 degrees elevation angle

During the disturbed upper atmospheric conditions at 13:18:00 UTC, it is shown from the analysis done on **Figure 20**, that G2 performs better than G1. However, the histogram distribution of scintillation density in **Figure 24**, shows discrepancies between GLONASS satellite 14 and 17. For Satellite 14, G2 scintillates less than G1 and for satellite 17 G1 scintillates less than G2. The difference in scintillation could be due to FDMA, which GLONASS uses. Since GLONASS is an FDMA system, each satellite in view uses a different frequency band, to avoid interference with other neighboring satellites. Since each frequency band is different, the scintillation may vary across each band. As a result, variation in scintillation for G1 for satellite 14 is different for satellite 17 and the same can be said for G2. As a result, this makes GLONASS more difficult to carefully analyze.

Other histogram plots that show the same discrepancies across GLONASS G1 and G2 are discussed in data set 3. GLONASS G1 and G2 do share a similar resemblance in distribution. In data set 3, it is shown that G1 and G2 have similar amplitude and phase scintillation. The correlation characteristics of both amplitude and phase scintillation across G1 and G2 are further discussed in data set 3.

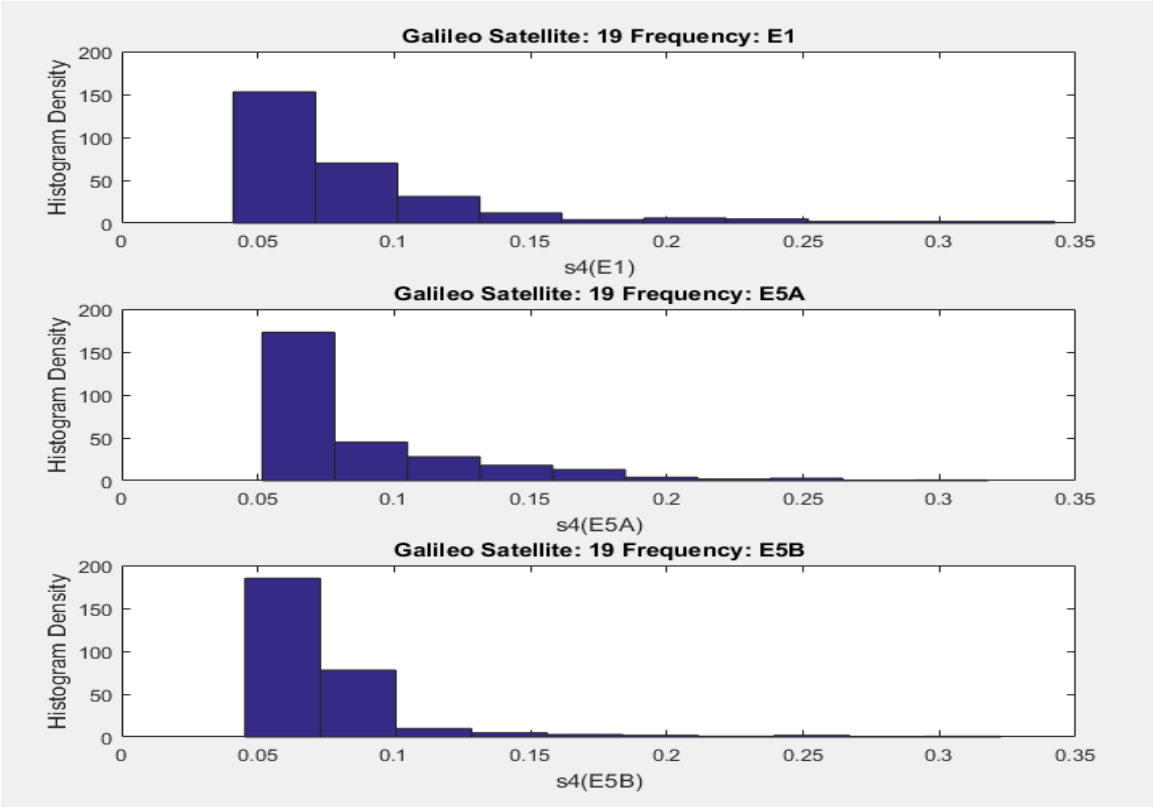

Figure 25: Histogram distribution of Galileo satellite 19 (E1, E5A, E5B) scintillation above 15 degrees elevation angle

Figure 25 is the scintillation distribution for Galileo satellite 19. Based on the distribution E5A has a higher scintillation distribution compared to higher frequencies of E1 and E5B. E1 and E5B both have similar distributions. However, E1 experiences slightly less scintillation than E5B and less scintillation than E5A. E1 may have had less scintillation than the other frequency bands, due to higher carrier to noise ratio density. As shown in **Figure 21** and **Figure 22**, E1 had a maximum carrier to noise ratio density

of roughly 50 dB-Hz, while E5A and E5B had a maximum carrier to noise ratio density of 48 dB-Hz.

Based on the values listed in **Table 3**, the magnitude of amplitude scintillation is higher than the magnitude of phase scintillation. The highest amplitude scintillation was 0.9142 and the highest phase scintillation was 0.373 radians. From these values it appears that amplitude scintillation is more severe at mid-latitudes than phase scintillation.

4.3 Data Set 2 Presentation

The second set of data was taken during a geomagnetic storm, on February 16th, 2016. As shown in **Figure 26**, the storm begins at 12:00:00 PM UTC and lasts up till February 17th 3:00:00 AM UTC. The storm maintains a Kp index of 5 and peeks at an index of 6 at 18:00:00 UTC. Like the storm from data set 1, data set 2 shows electron content ranging from 7 to 12 TECU, shown in **Figure 27**. Unlike the back scatter from data set 1, the back scatter of data set 2 is not as strong above Virginia, shown in **Figure 27**. The small concentration of scatter resulted in a SNR ranging from 10 to 20 dB.

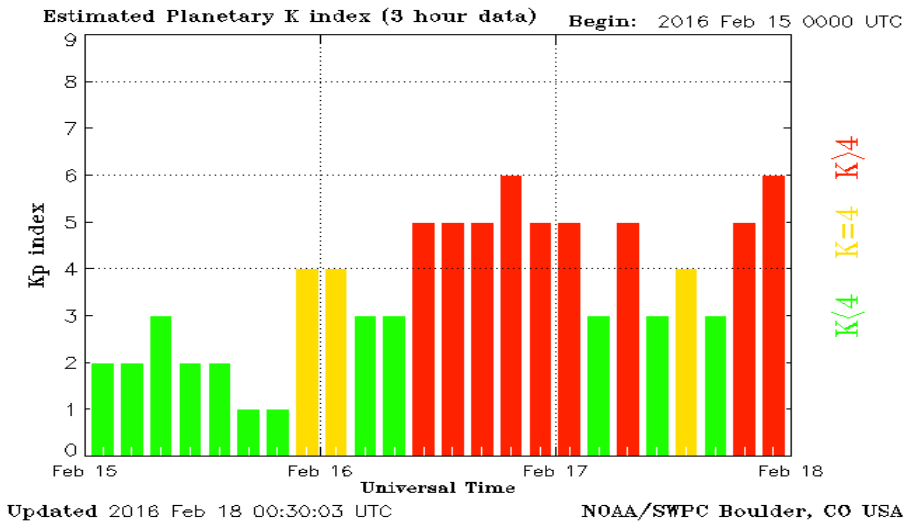

Figure 26: Kp index plot of a small geomagnetic storm that occurred on February the 16th and lasted until February the 17th [25]

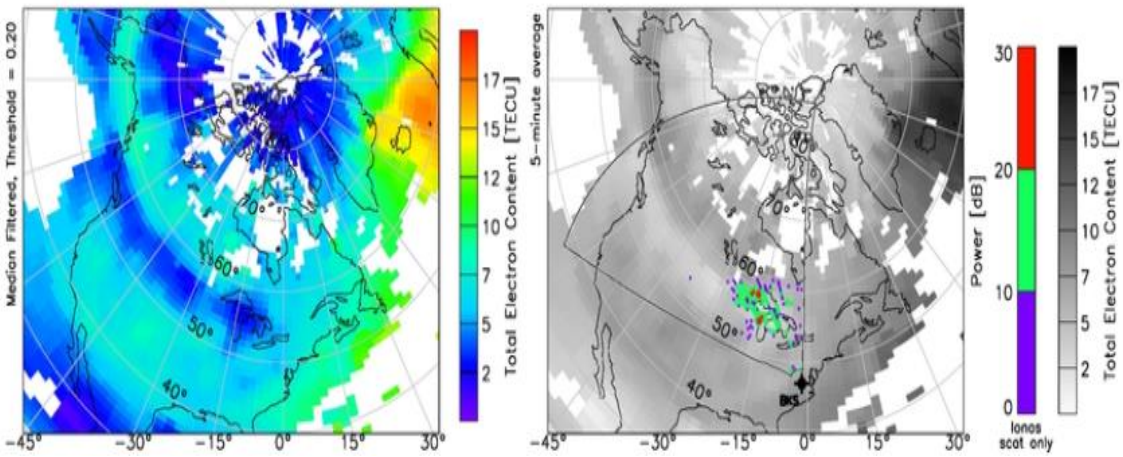

Figure 27: Total electron and radar backscatter plots at 12:00:00 UTC of the geomagnetic storm that occurred on February the 16th [5]

4.3.1 Scintillation Analysis

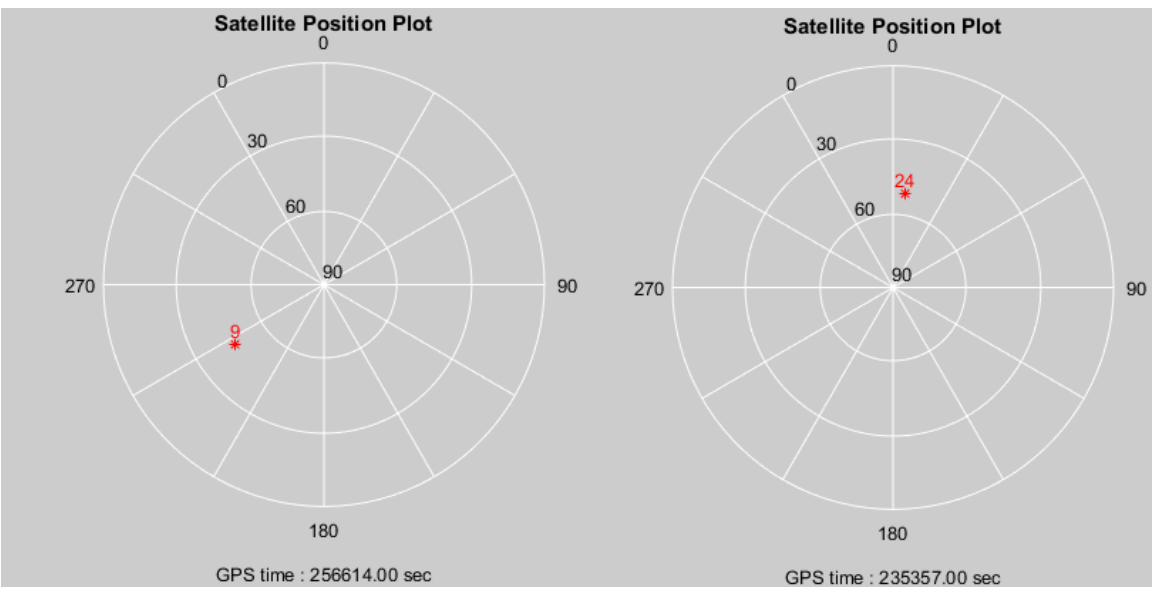

Figure 28: Location of GPS satellite 9 and 24 during the storm on February the 16th [26]

Figure 28 are the locations of GPS satellite 9 and 24 during the ionospheric disturbance, which occurred during the storm on February the 16th. Both these satellites were selected because they both experienced abrupt amplitude scintillation events, due to the ionospheric turbulence at fairly similar GPS times. Satellite 9 experienced an abrupt

scintillation at GPS time of 256614 seconds and satellite 24 at 235357 seconds. These two satellites are used to further validate abrupt amplitude scintillation events at mid-latitude. Since high rate data doesn't include the satellite elevation and azimuth angles, STK software tool [28] was used to determine the location of these satellites during the turbulent event. Both satellites had elevation angles above 15 degrees during the event. Satellite 9 had an elevation angle of 46.43 degrees and satellite 24 had an elevation angle of 51.722 degrees.

High rate data was collected for data set 2. The high rate 50 Hz data includes the signal power, which is computed from the I and Q channels and is unitless, since it is relative to the base power. The signal power is plotted on a logarithmic scale defined by $Signal\ \ Power = 10 * log10(I^2 + Q^2)$. The phase of the high rate data is in units of millicycles. The high rate signal power is graphed for GPS L1, L2, L5, GLONASS G1, G2, and Galileo E1, E5A, E5B to determine which frequency bands are more prone to fading.

High rate data is used to compute spectral index *p* using the amplitude signal power, since it is shown in data set 1 that amplitude scintillation is more severe than phase scintillation. Only a few satellites were selected from each constellation to determine spectral index *p* during maximum amplitude scintillation events. These results were found to be representative of the larger group of satellites tracked. Nonetheless, it is important to note that more studies need to be done in the future to further investigate spectral index *p* and to further observe the variations of signal power across the frequency bands analyzed in this study.

GPS satellite numbers 1, 3, 8, 9, 24, 25, 26, 27 are satellites that track L1, L2, and L5 frequency bands. The signal amplitude intensity for each of the frequency bands is plotted in decibels versus samples and compared across all nine satellites, in order to determine which frequency bands have the best overall performance. Power spectral index *p* across L1, L2, and L5, are used to determine scintillation intensity.

Figure 29 includes signal power plots for GPS satellites 1, 3, 8, 9, 24, 25, 26, and 27. The signal power are plotted across frequency bands L1 colored in red, L2 colored in black and L5 colored in blue. For every single one of these tracked satellites, frequency band L5 maintains an average power intensity of 106.48 dB. Signals transmitted at L1 and L2 maintain average signal intensities of 100.93 dB and 100.54 dB respectively. Although L1 does maintain slightly higher signal power compared to L2, there are moments in time when both frequency bands have the same signal power. The average signal power of both L1 and L2 are very similar at roughly 100.93 dB and 100.54 dB.

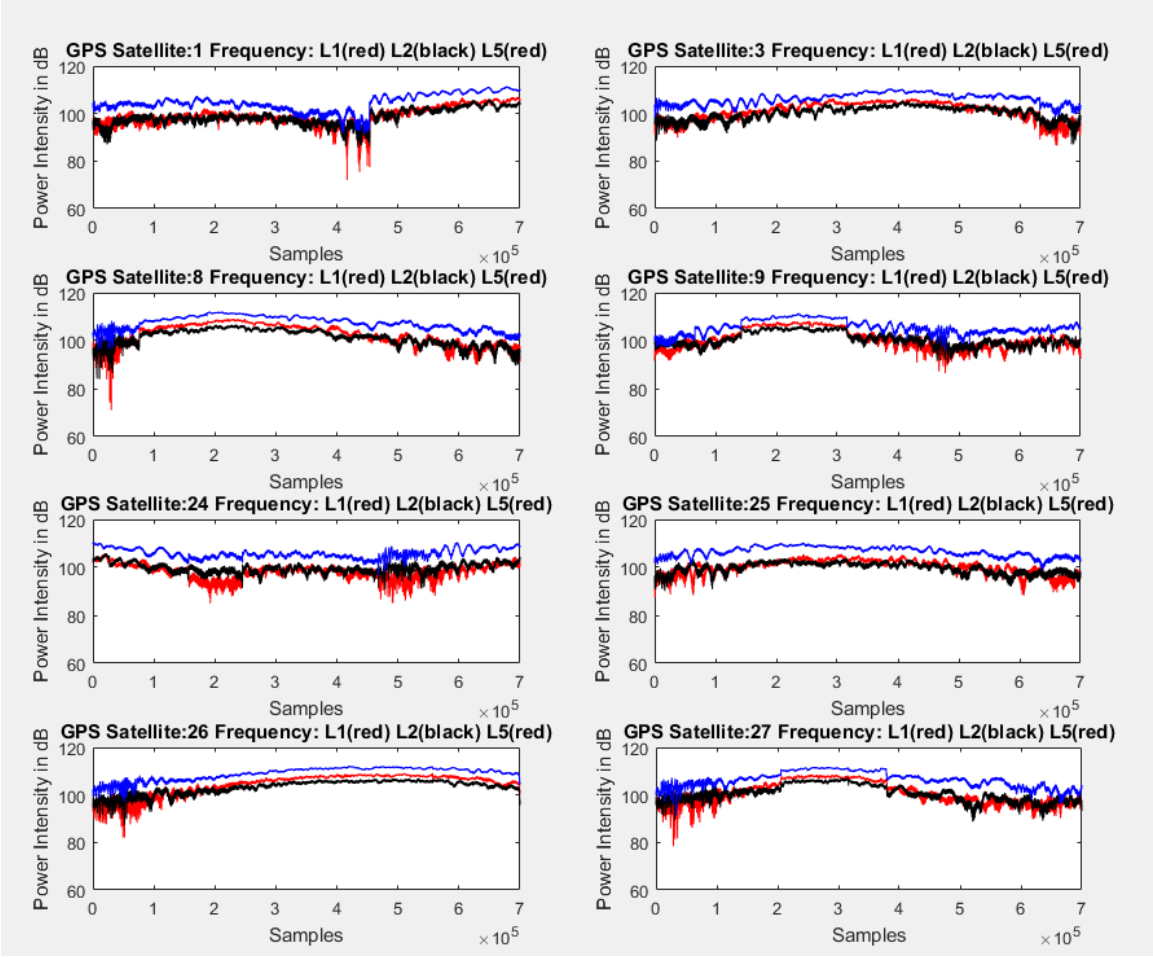

Figure 29: Signal power in dB for GPS satellites 1, 3, 8, 9, 24, 25, 26, 27, L1(red), L2(black), L5(blue)

Table 4 includes the satellite PRN number, frequency band, Fresnel frequency (Ff), and spectral index *p* for GPS satellites 1, 3, 8, and 9. The power spectral density of amplitude was determined by taking the fast Fourier transform of the signal power for 60 seconds at 50 Hz sampling rate and was used to determine spectral index *p* on a log-log scale for GPS satellites 1, 3, 8, 9, 24, 25, 26, and 27. **Figure 30** is an example of the power spectral density of amplitude on a log-log scale, for GPS satellite 9. Linear interpolation from the roll off Fresnel frequency to the low cut off frequency, at the noise floor, was used to determine slope spectral index *p*.

Table 4: GPS Satellite Numbers 1, 3, 8, 9, Frequency Bands, Fresnel Frequency (F_f), and Spectral Index *p*

Satellite PRN Number	Frequency Band	F_f (Hz)	Spectral Index *p*	Max Scintillation
1	L1	0.066	-2.02	0.4437
1	L2C	0.08	-1.393	0.2993
1	L5	0.10	-1.644	0.2937
3	L1	0.15	-2.621	0.848
3	L2C	0.10	-1.699	0.429
3	L5	0.15	-2.08	0.547
8	L1	0.066	-1.93	0.605
8	L2C	0.05	-2.00	0.564
8	L5	0.066	-2.047	0.606
9	L1	0.066	-1.303	0.342
9	L2C	0.066	-1.913	0.368
9	L5	0.066	-1.911	0.350

Table 5 includes the satellite numbers, frequency band, Fresnel frequency (F_f), and spectral index *p* for GPS satellites 24, 25, 26, and 27. The spectral index *p* vary between values from -1.179 to -2.621. The average spectral index *p* across L1, L2C, and L5 from **Table 4** and **Table 5** is -1.922.

Table 5: GPS Satellite Numbers 24, 25, 26, 27, Frequency Bands, Fresnel Frequency (F_f), and Spectral Index *p*

Satellite PRN Number	Frequency Band	F_f (Hz)	Spectral Index *p*	Max Scintillation
24	L1	0.083	-1.936	0.521
24	L2C	0.083	-1.701	0.378
24	L5	0.050	-1.704	0.251
25	L1	0.183	-1.721	0.444
25	L2C	0.116	-1.179	0.312
25	L5	0.166	-1.447	0.202
26	L1	0.100	-2.380	0.592
26	L2C	0.116	-2.214	0.562
26	L5	0.150	-2.142	0.496
27	L1	0.083	-2.187	0.807
27	L2C	0.083	-2.562	0.668
27	L5	0.100	-2.403	0.535

A spectral index value of -2.6 is considered intense scintillation [19]. Severe scintillation that occurred across L1, L2C, and L5 resulted in spectral index *p* values above -2.0. For example, GPS satellite 27 experienced severe scintillation across frequency bands L1, L2C, and L5 of 0.807, 0.668, and 0.535. The corresponding spectral index values for these scintillation events are -2.187, -2.562, and -2.403. These characteristics can also be seen on GPS satellite 3, which experiences the highest maximum scintillation of 0.848 on frequency band L1, which corresponds to a spectral index value of -2.621.

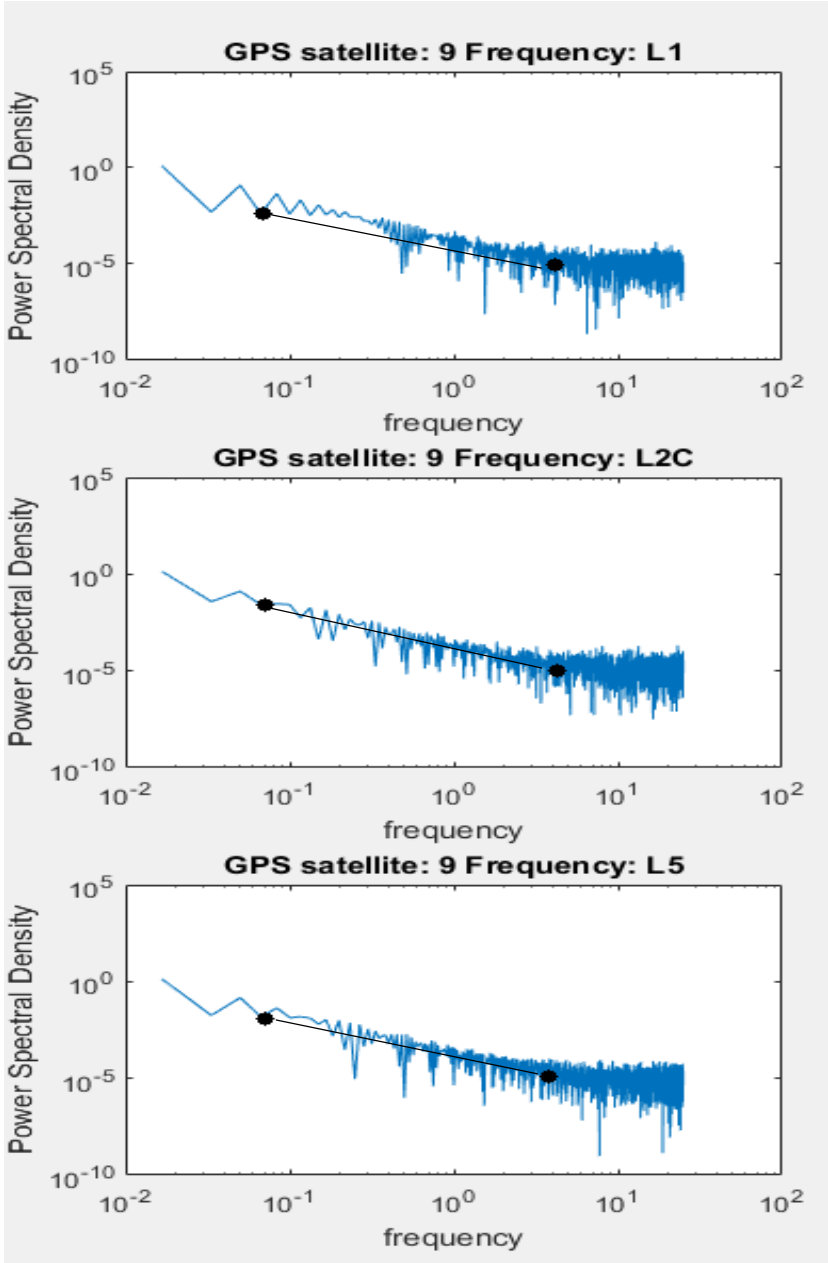

Figure 30: Power spectral density graph amplitude in (blue) for frequency L1, L2C, L5

The power spectral density of amplitude for GPS satellite 9 is shown in **Figure 30**. The Fresnel frequency is estimated at the roll off, which is indicated by the upper point in the graph. The second point is the point where the signal beings to degrade, at the noise floor. A line is drawn from the Fresnel frequency to the low cut of frequency, at the

start of the noise floor. A linear interpolation is used to estimate spectral index *p* of the lines for each frequency band L1, L2C, and L5.

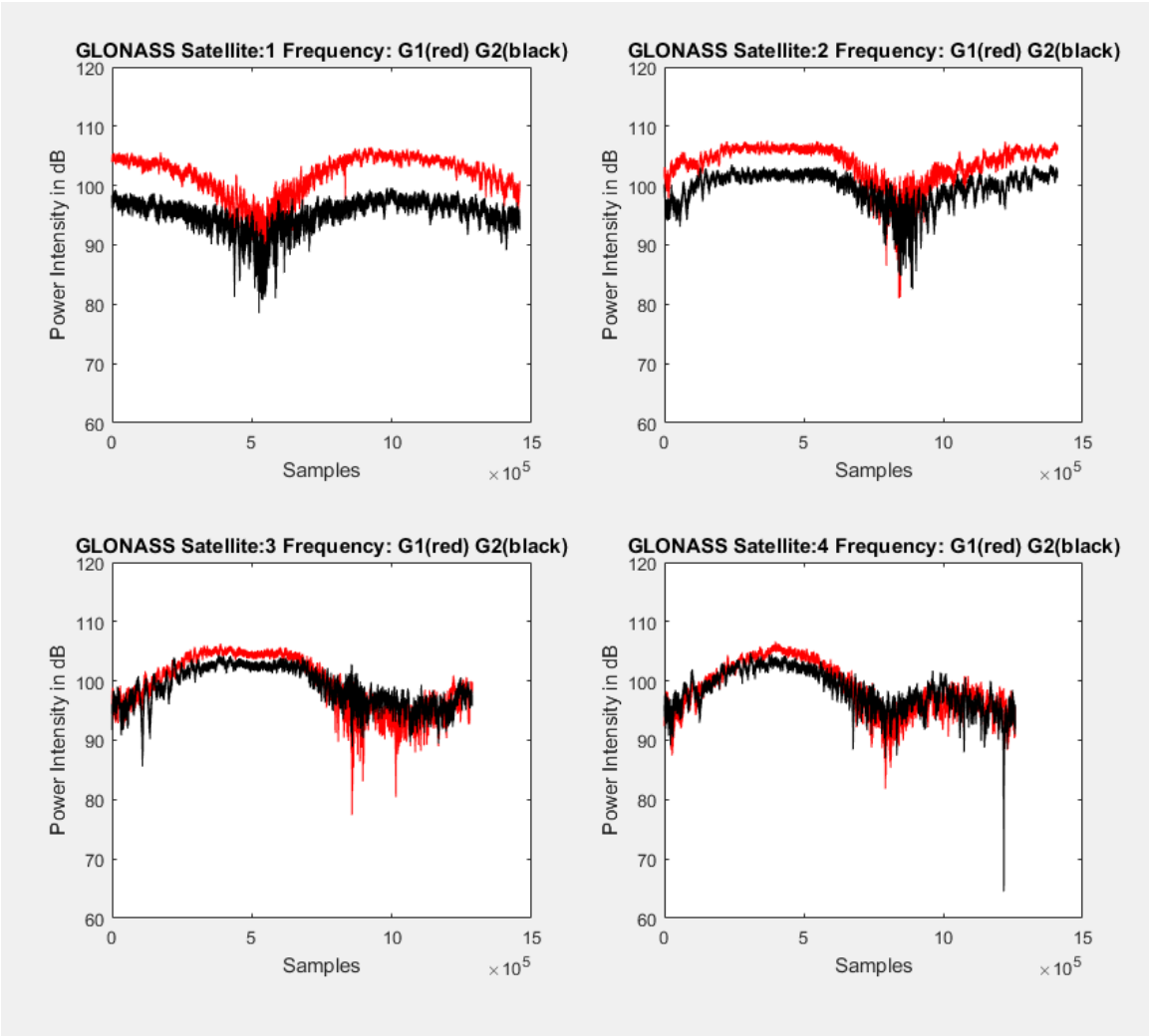

Figure 31: Signal power in dB for GLONASS satellites 1, 2, 3, and 4 G1 (Red) and G2 (Black)

GLONASS satellites 1, 2, 3, 4 are used to compare the signal power transmitted on frequency bands G1 and G2. For the GLONASS plots, G1 is colored in red and G2 is colored in black. Power spectral density of amplitude is used to compute spectral index *p* across G1 and G2, to determine scintillation intensity. As shown in **Figure 31**, G1 tends to fade less than G2. G1 maintains an average intensity of 100.95 dB and G2 maintains average intensity levels of 98.11 dB. Like GPS L1 and L2, GLONASS G1 and G2 have

similar signal intensities. As shown in **Figure 31**, for GLONASS satellites 3 and 4 the signal intensities of G1 and G2 have similar amplitudes. This can potentially be the reason for the variation of scintillation across G1 and G2 shown in data set 1**,** for GLONASS satellites 14 and 17**.**

Table 6: GLONASS Satellite Numbers 1, 2, 3, 4, 6, 8, 10 Frequency Bands, Fresnel Frequency (F_f), and Spectral Index *p*

Satellite PRN Number	Frequency Band	F_f (Hz)	Spectral Index *p*	Max Scintillation
1	G1	0.166	-1.534	0.459
1	G2	0.083	-1.079	0.459
2	G1	0.066	-1.916	0.718
2	G2	0.100	-2.008	0.575
3	G1	0.083	-1.510	0.603
3	G2	0.100	-1.756	0.545
4	G1	0.116	-2.299	0.485
4	G2	0.100	-1.505	0.413
5	G1	0.050	-0.819	0.262
5	G2	0.066	-1.432	0.309
6	G1	0.15	-1.466	0.278
6	G2	0.050	-2.092	0.444
8	G1	0.066	-1.369	0.399
8	G2	0.066	-2.154	0.437
10	G1	0.083	-1.635	0.355
10	G2	0.05	-1.955	0.285

Table 6 includes the satellite numbers, frequency band, Fresnel frequency (F_f), and spectral index *p* for GLONASS satellites 1, 2, 3, 4, 5, 6, 8, and 10. Like the results from **Tables 4** and **5**, the power spectral density of amplitude was used to estimate spectral index *p*. **Figure 32** is a graph of the power spectral density of amplitude for GLONASS satellite 8, for G1 and G2 frequency bands. A line is drawn from the approximated Fresnel frequency to the low cut of frequency, near the noise floor. Linear interpolation is used to estimate the spectral slope *p*. The spectral index *p* values vary from -0.891 and the highest spectral index value of -2.299. The average spectral index *p* across all the GLONASS satellites is -1.658.

Unlike the spectral index values of the observed GPS satellites, none of the GLONASS satellites in **Table 6**, have a spectral index above -2.6. However, some GLONASS satellites like satellite number 4 did result in a spectral index of -2.299 from a maximum amplitude scintillation event of 0.485. Which indicates severe scintillation, but not as severe as GPS satellite 3, which resulted in a spectral index of -2.621. Like GPS, GLONASS spectral index values fall within a similar range, from values close to -1 and above -2. As a result, the average across G1 and G2 of -1.658 is close in proximity to the average across L1, L2C, and L5 of -1.922.

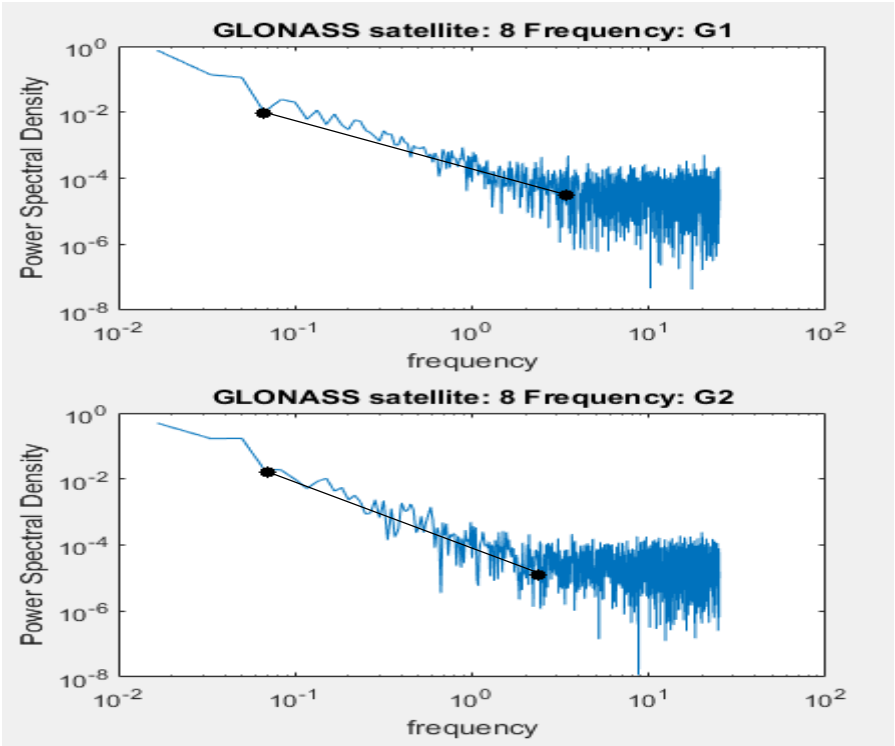

Figure 32: Power spectral density graph of amplitude in (blue) for frequency band G1 and G2

Figure 33 includes plots of signal power for Galileo satellites 11, 12, and 22 frequency bands E1 (red), E5A (black), E5B (blue). E5B maintains a higher signal power than signals transmitted on E1 and E5A. E5B has an average signal power of 111 dB. Frequency bands E1 and E5A have an average signal power of 102.82 and 101.84 dB. Frequency band E1 is slightly higher than E5A for both satellites 11 and 22, but the signal power does intersect and fluctuate between them. Like GPS L1, L2, and GLONASS G1, G2, Galileo E1 and E5A have similar signal strength. As shown in **Figure 33**, the signal strength of E1 and E5A are similar for Galileo satellite 12, in which they overlap.

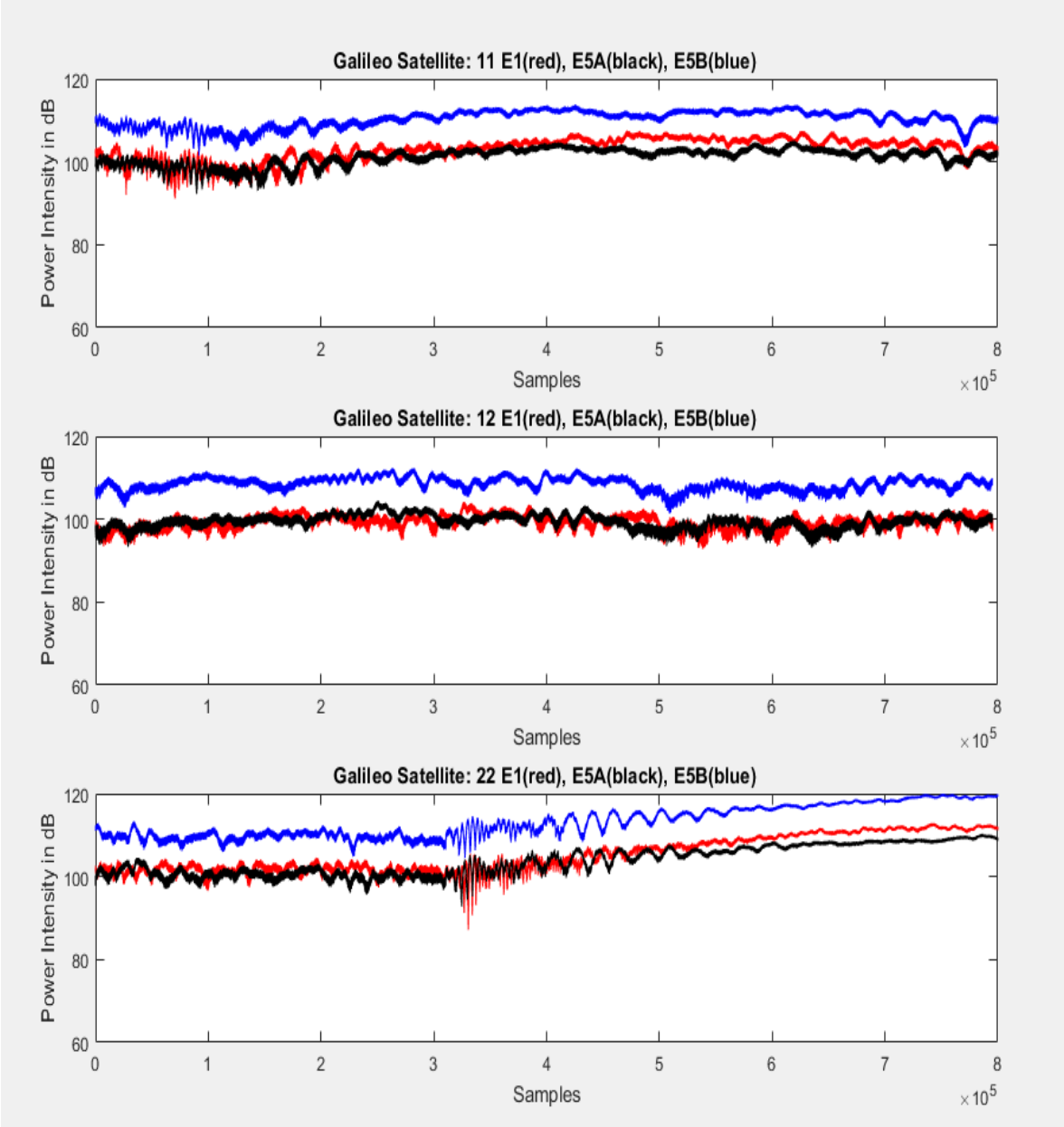

Figure 33: Signal power dB for Galileo satellite 11, E1 (Red), E5A (Black), and E5B

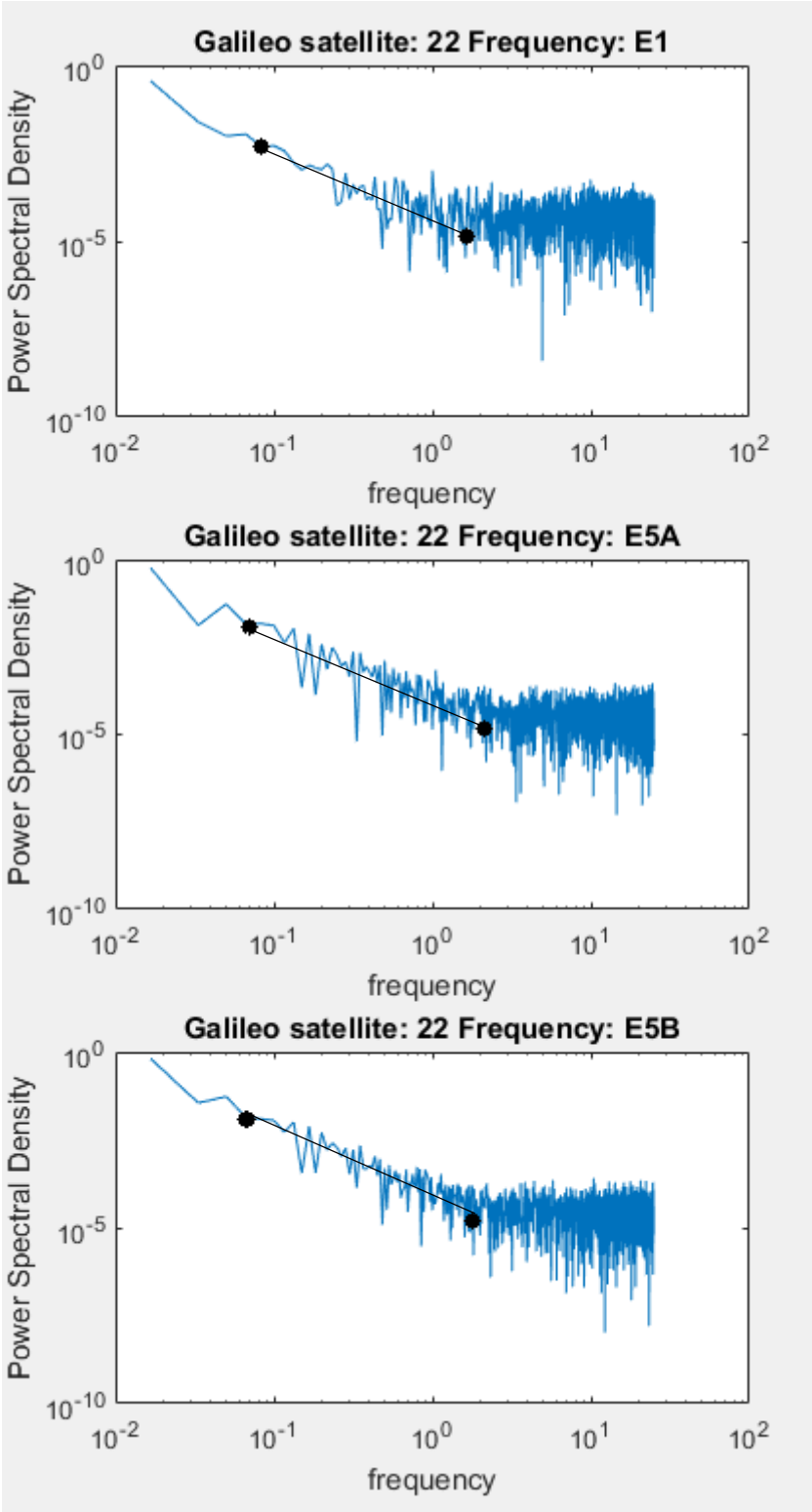

Figure 34: Power spectral density graph of amplitude in (blue) for frequency bands E1, E5A, and E5B

Table 7: Galileo Satellite Numbers 11, 12, 22, 24 Frequency Bands, Fresnel Frequency (F_f), and Spectral Index *p*

Satellite PRN Number	Frequency Band	F_f (Hz)	Spectral Index *p*	Max Scintillation
11	E1	0.083	-1.326	0.440
11	E5A	0.100	-1.545	0.427
11	E5B	0.100	-1.820	0.384
12	E1	0.116	-1.448	0.182
12	E5A	0.100	-0.716	0.158
12	E5B	0.133	-1.767	0.175
22	E1	0.083	-1.539	0.225
22	E5A	0.066	-2.109	0.285
22	E5B	0.066	-1.834	0.293
24	E1	0.100	-2.027	0.782
24	E5A	0.100	-1.214	0.502
24	E5B	0.083	-1.755	0.491

Table 7 includes the satellite numbers, frequency band, Fresnel frequency (F_f), and spectral index *p* for Galileo satellites 11, 12, 22, 24, across frequency bands E1, E5A, and E5B. The power spectral density of the amplitude was used to determine the spectral index *p*. **Figure 34** is an example of the power spectral density of amplitude, for Galileo satellite number 22. A line is drawn from the Fresnel frequency to the low cut off frequency, near the noise floor. Linear interpolation is used to estimate spectral slope *p*. Like the spectral index *p* from both GPS and GLONASS satellites, data from Galileo satellites resulted in fairly low spectral index *p* values. The spectral index values vary

from -0.710 to as high as -2.109. The average spectral index across the Galileo satellites is -1.575.

Like GPS and GLONASS, Galileo spectral index *p* values are close to -1 and -2. The highest spectral index value of -2.109 was experienced by satellite 22 on frequency band E5A. The average spectral index across E1, E5A, and E5B is -1.575, which is close in proximity to the averages of GPS -1.922 and GLONASS -1.658. The average across these constellations aren't near a spectral index *p* of -2.6, which indicates that the scintillation events are fairly moderate.

4.3.2 Summary

The signal power graphs for GPS indicate that L5 fades less than both L1 and L2. This also shows that the received signal strength of L5 is stronger than both L1 and L2. This validates the previous results from data set 1, where L5 scintillated less than L1 and L2. Previous studies at low latitudes indicates that lower frequency bands tend to fade more than higher frequency bands [21], [22]. Results from this research indicate that at mid-latitudes lower frequency band L5 fades less than higher frequency bands L1 and L2. However, like the previous research, L1 did fade less than L2 [21].

G1 fades less than G2, but there are periods of time in which G2 fades less than G1, since both frequency bands have similar intensities. E5B has an average signal power of 111 dB, which is higher than the average signal power of E1 at 102.82 dB and E5A at 101.84 dB. As a result, E5B faded less than both E1 and E5A. Like G1 and G2, E1 and E5A have similar signal intensities, which causes a variation in fade across both frequency bands. Sometimes E1 may fade less than E5A, but other times E5A may fade less than E1.

Although the power spectral density of amplitude was used to determine spectral index *p*. There are rare occasions in which the power spectral density characteristics of amplitude and phase are highly correlated. This occurred during abrupt scintillation events, which can be seen across satellite 9 and 24 in **Figure 35**. The high correlation between amplitude and phase can be seen in the power spectral density plots in **Figure 36** across frequency bands L1, L2C, and L5 for GPS satellite 9. In the case of these events, the power spectral density of both phase and amplitude are similar, which leads to the same spectral index *p*, since the interpolated lines are parallel. As a result, either phase or amplitude could potentially be used to estimate spectral slope *p*.

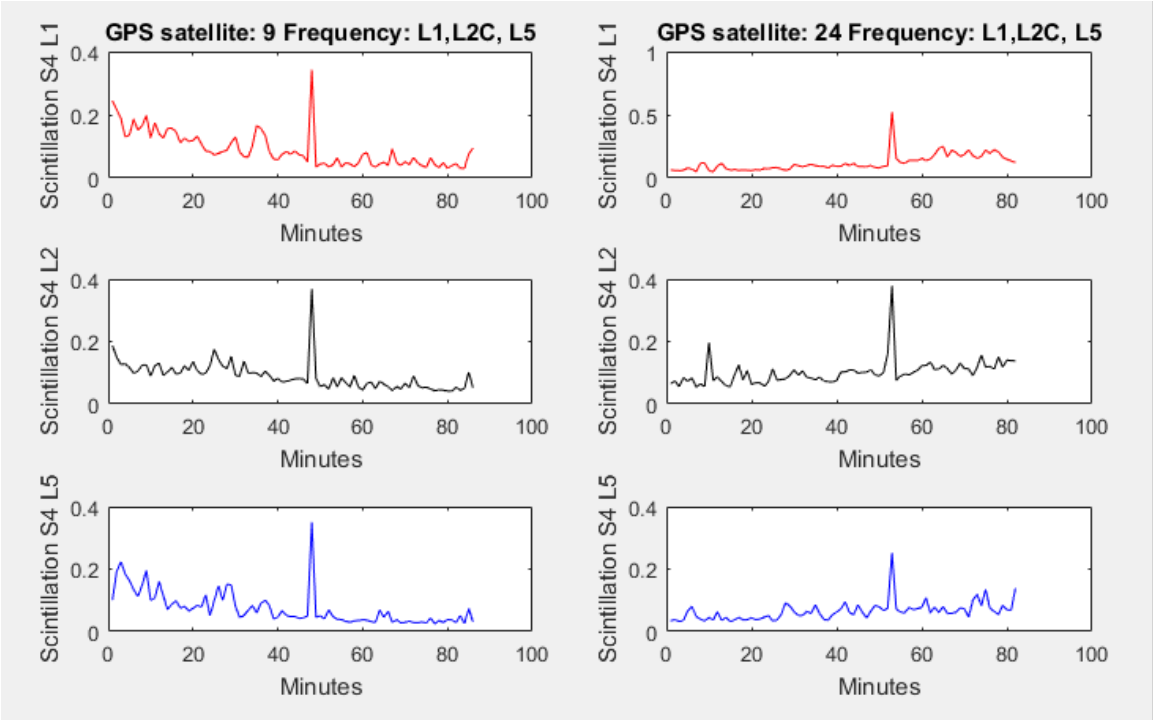

Figure 35: High rate amplitude scintillation data for GPS satellite 9 and 24 at L1, L2C, and L5. Abrupt scintillation occurs at 48 minutes for GPS satellite 9 and 53 minutes for satellite 24

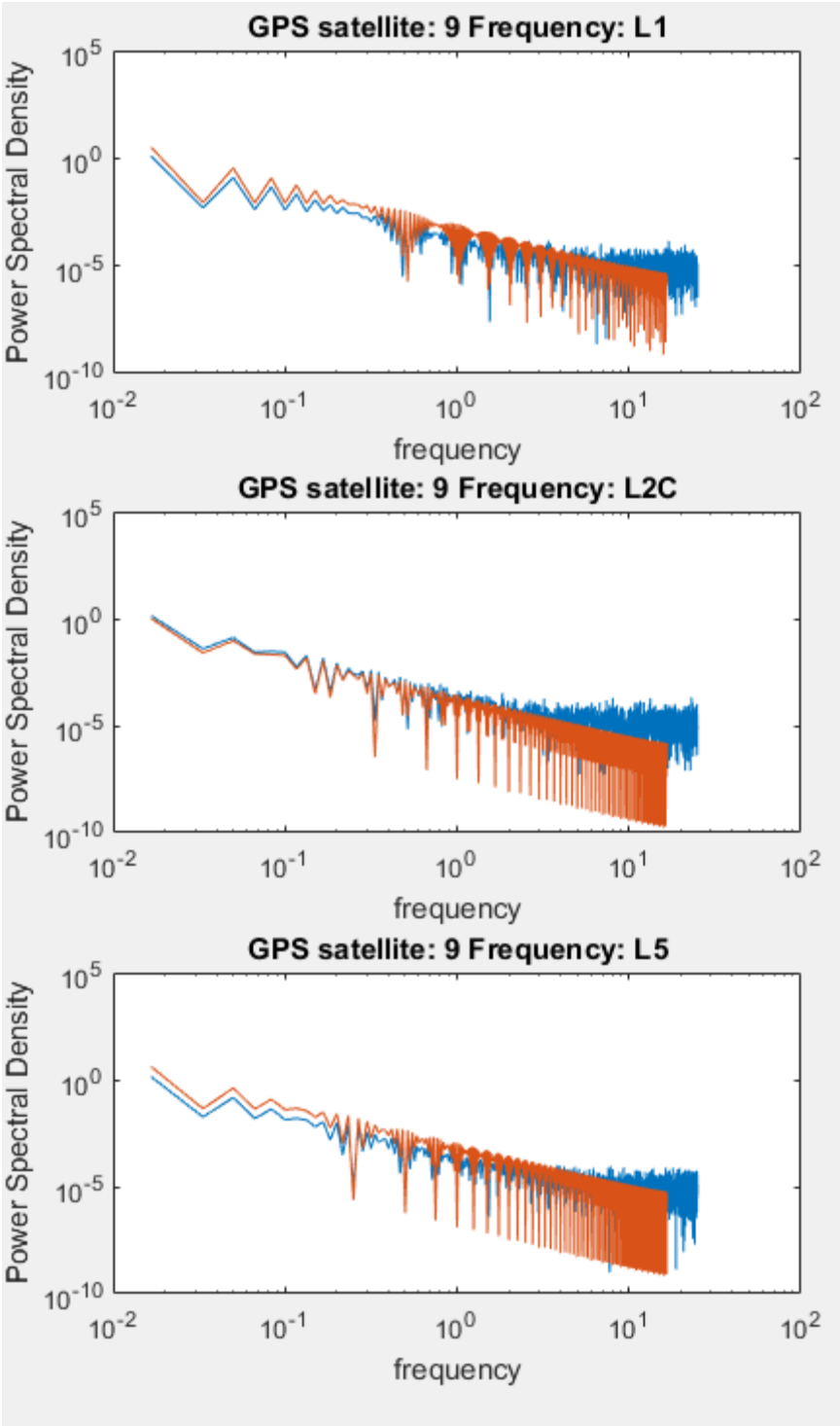

Figure 36: Power spectral density graph of amplitude in (blue) and phase in (orange) of GPS satellites 9 and 24

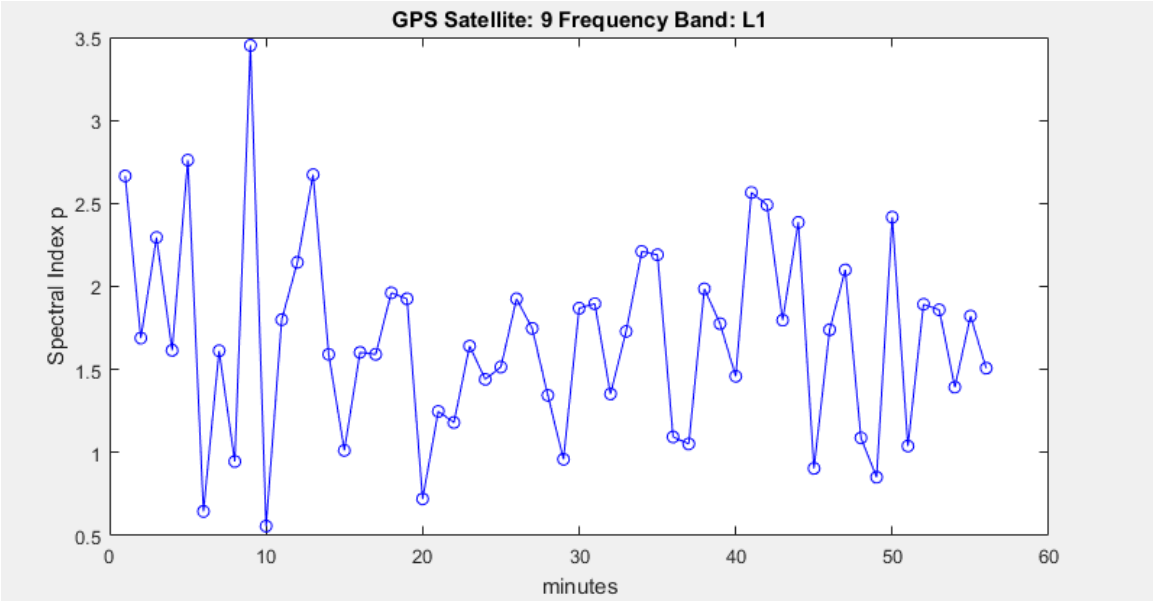

Figure 37: Power spectral index p for GPS satellite 9 over 60 minutes

The approximated Fresnel frequency and spectral index *p*, are within the range of 0.09 Hz and -2.8 estimated from previous research done at mid-latitude, shown in **Figure 10** [2]. The average Fresnel frequency for the GPS satellites from **Table 4** and **Table 5** is approximately 0.0966 Hz, which is very close in proximity to 0.09 Hz [2]. The highest spectral index *p* is -2.621, which is comparable to -2.8 [2]. Both these values are fairly close to -2.6, which is an indication of a severe scintillation event.

Figure 37 is a plot of the spectral slope *p* for GPS satellite 9 L1 frequency band over the course of 60 minutes of tracking. The spectral index *p* was estimated from the power spectral density of amplitude. Like the results at high latitudes presented in **Figure 9,** the mid-latitude spectral slope varies to values less than 1 and has a maximum value of 3.5. The average spectral index *p* is roughly 1.69 for the course of 60 minutes of tracking. Since the overall average spectral index is less than 2, this is an indication that the scintillation is fairly moderate. These results validate that spectral index *p* at mid-latitudes may fall within the same range as high latitude regions.

The average spectral index across L1, L2C, L5, G1, G2, E1, E5A, and E5B frequency bands is roughly -1.764 and the average. Since the average of the power spectral density across all the satellites isn't near the value of -2.6, it can be interpreted that scintillation is fairly moderate for these observations.

4.4 Data Set 3 Presentation

Data set 3 was collected for 11 days, from August 4th to August 15th, 2016 This data set was used to test if previous assumptions would hold true for longer periods of time. Data set 3 was collected during moderate space weather conditions with low Kp index values. The Kp index values shown in **Figure 38**, maintain values from 2 to 4, which indicate moderate activity.

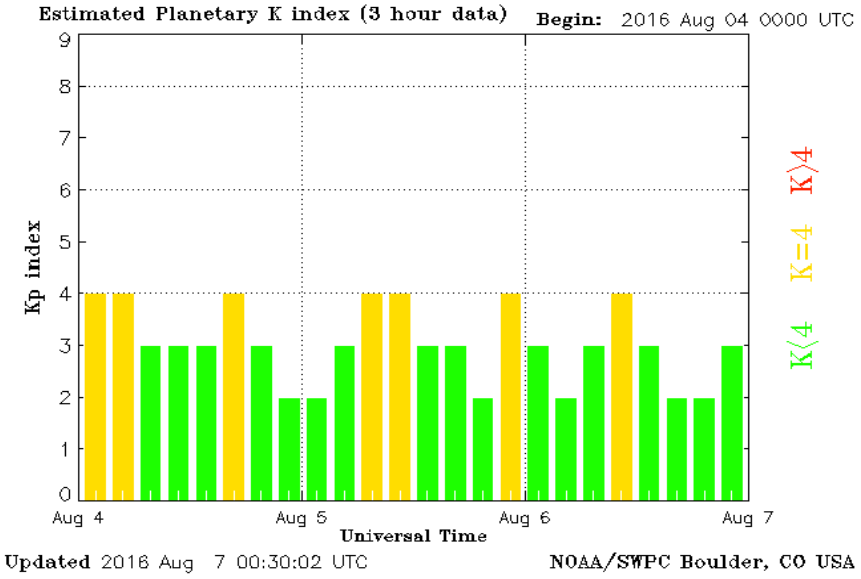

Figure 38: Range of Kp index values for data set 3, which range from Kp of 2 to 4 [25]

Low rate scintillation was collected for data set 3. Histogram distributions of scintillation density are plotted across GPS L1, L2, L5, GLONASS, G1, G2, and Galileo E1, E5A, E5B, in order to determine which frequency bands had the best overall

performance, over the 11-day period. Since data is collected over a longer period of time, it can better validate results from data set 1 and data set 2.

4.4.1 Scintillation Analysis

The eight GPS satellites that transmit L1, L2, and L5 are used to compare the performance of L1, L2, and L5. Again, the scintillation data is plotted for satellites above 15 degrees, in order to mitigate multipath effects. Histogram distributions were plotted for GPS satellites 6, 8, 9, 26, 27, and 30. It can be seen from **Figure 39** and **Figure 40**, that L5 scintillated less than both L1 and L2 for the 11-day period. Signals transmitted on frequency band L1 scintillated less than L2, over the 11-day period. Compared to L1 and L5, L2 had the worst performance. These results validate the previous assumptions made, that at mid-latitudes L5 performs better than L1 and L2, from data set 1 and 2.

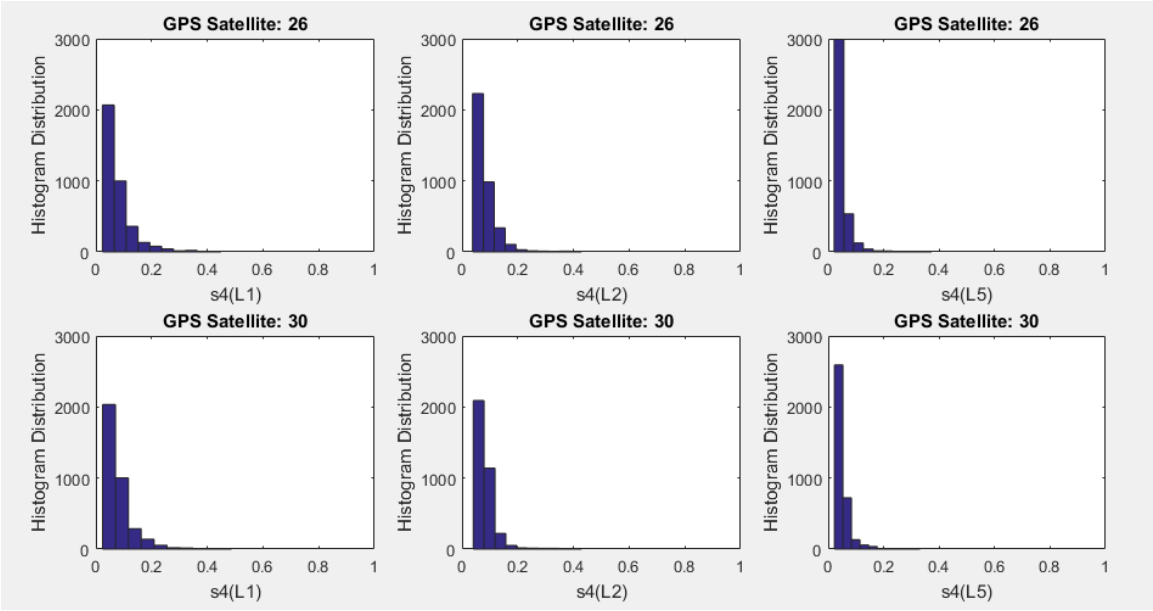

Figure 39: Histogram distribution of GPS satellites 26 (top) and 30 (bottom) L1, L2, L5 over 11-day period

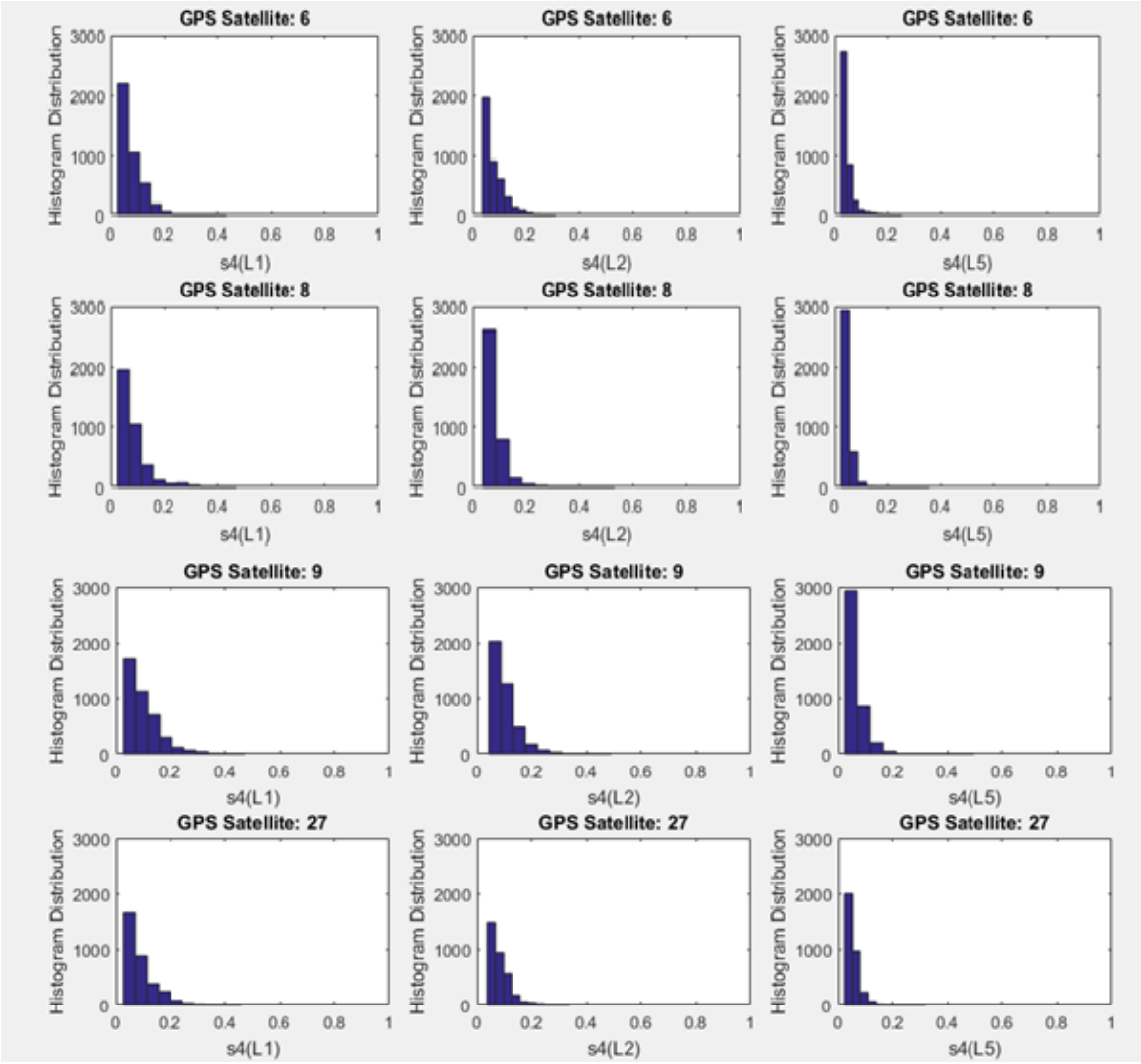

Figure 40: 11-day period and histogram distribution of GPS satellites 6 and 8 (top) and 9 and 27 (bottom) L1, L2, L5 over 11-day period

GLONASS satellites 2 and 3 scintillation distributions across G1 and G2 are shown in **Figure 41**. Like data set 1, scintillation across GLONASS satellites in data set 3 show characteristic differences between G1 and G2. For example, G1 scintillates less than G2 for GLONASS satellite number 3. However, for GLONASS satellite 2 G1 scintillates less than G2 at the start of the distribution, but as the distribution continues G2 scintillates less than G1. As previously mentioned, the discrepancies in scintillation could've been caused by FDMA, since signal transmitted on G1 and G2 frequency bands

are slightly different for all tracked GLONASS satellites or it could've been caused by similarities in signal intensities across G1 and G2, shown in data set 2.

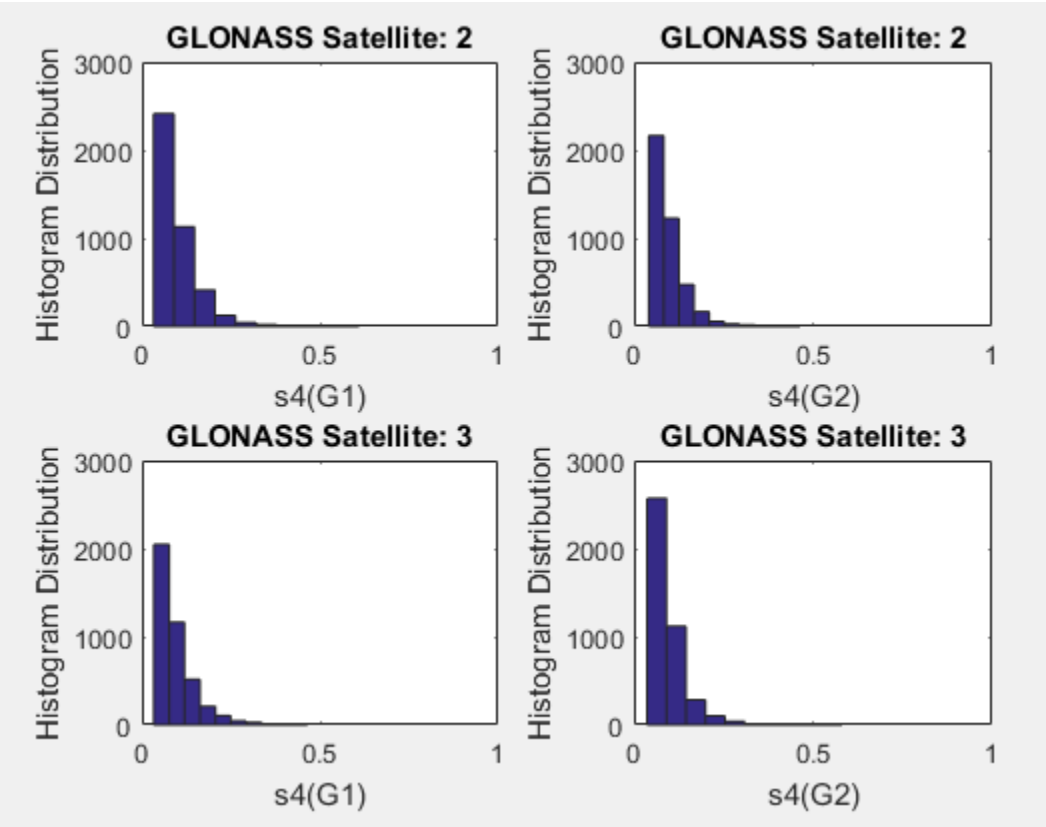

Figure 41: Histogram distributions for GLONASS satellites 2 and 3 G1, G2 over 11-day period

Galileo satellites 11, 12, 24, and 26 scintillation histogram distributions are shown in **Figure 42**. For both satellites 11 and 12, E5B scintillates less than both E1 and E5A. E5A also scintillates less than E1. For Galileo satellites 24 and 26 E5B scintillates less than E1 and E5A. For satellite 24, E5A scintillates less than E1 and for satellite 26 E1 scintillates less than E5A. E1 and E5A may follow the same characteristics as GLONASS G1 and G2. Since E1 and E5A have similar signal strength this could've caused the discrepancies in the amplitude scintillation.

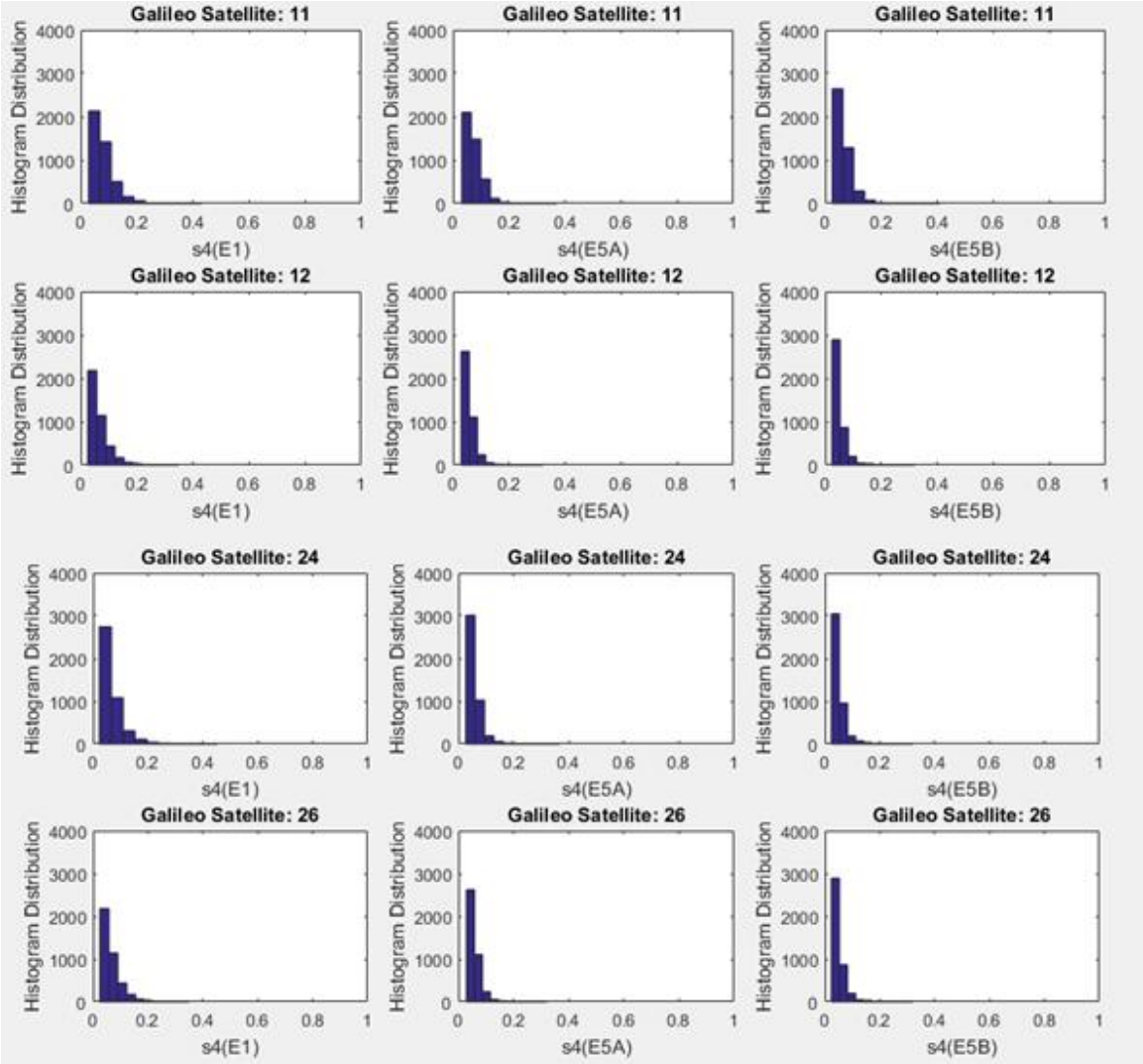

Figure 42: Histogram distributions for Galileo satellites 11 and 12 (top) and Galileo 24 and 26 (bottom) E1, E5A, and E5B over 11-day period

4.4.2 Statistical and Cross Correlation Analysis

Statistical Distribution

A statistical analysis is done across GPS L1, L2, L5, GLONASS G1, G2, and Galileo E1, E5A, E5B bands to measure the probability of phase and amplitude scintillation occurring at specific ranges. For amplitude scintillation, the range is taken by 0.1 increments from 0 to 1 and for phase scintillation the range is taken by 10 degree increments from 0 to 100 degrees. The purpose of these measurements is to compare the

probability distribution at mid-latitude to previous statistical work done at high and low latitudes, presented in **Figure 43**.

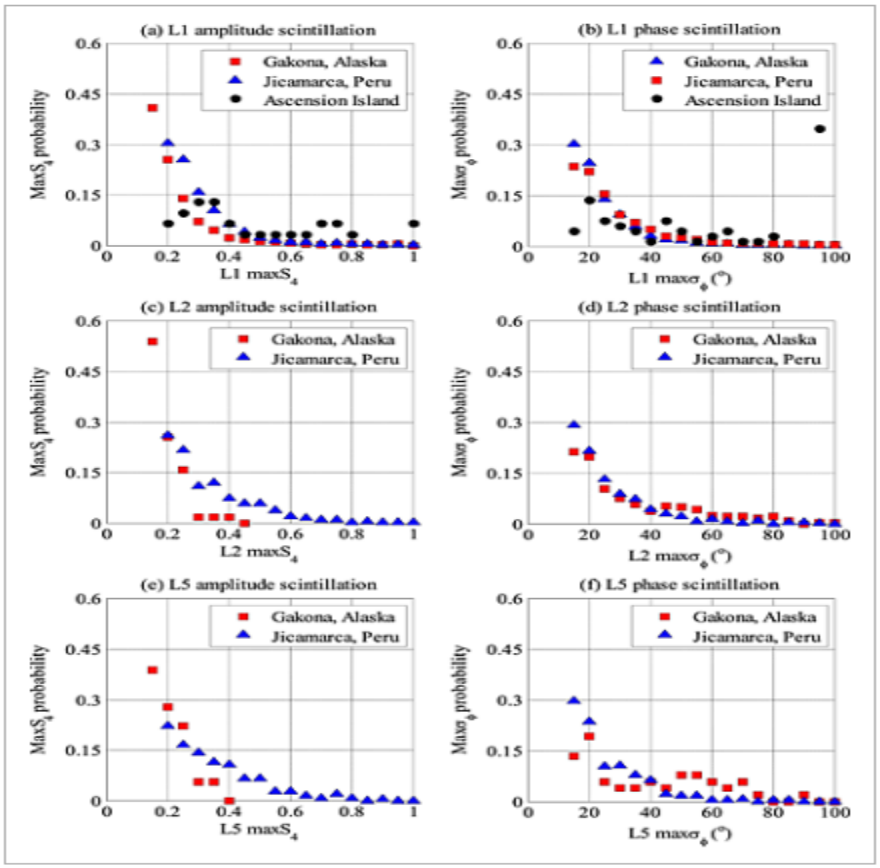

Figure 43: Statistical analysis done at equatorial and high latitude regions [29]

Figure 43 are probability distribution graphs of both amplitude and phase scintillation from data collected at three different regions, which include Gakona, Alaska at high latitude (62.3019 degrees north, 145.3019 degrees west), Jicamaraca, Peru at low latitude (11.9516 degrees south, 76.8743 degrees west), and Ascension, Island at low latitude (7.9467 degrees south, 14.3559 degrees west) [29]. **Figure 43** demonstrates that at low latitude regions the probability of severe amplitude scintillation occurring is higher at low latitude regions than high latitude regions and the probability of severe phase scintillation occurring at high latitude regions is higher than low latitude regions [29].

The research also showed that scintillation across L2 and L5 are more severe than L1 in both high latitude and low latitude regions [29].

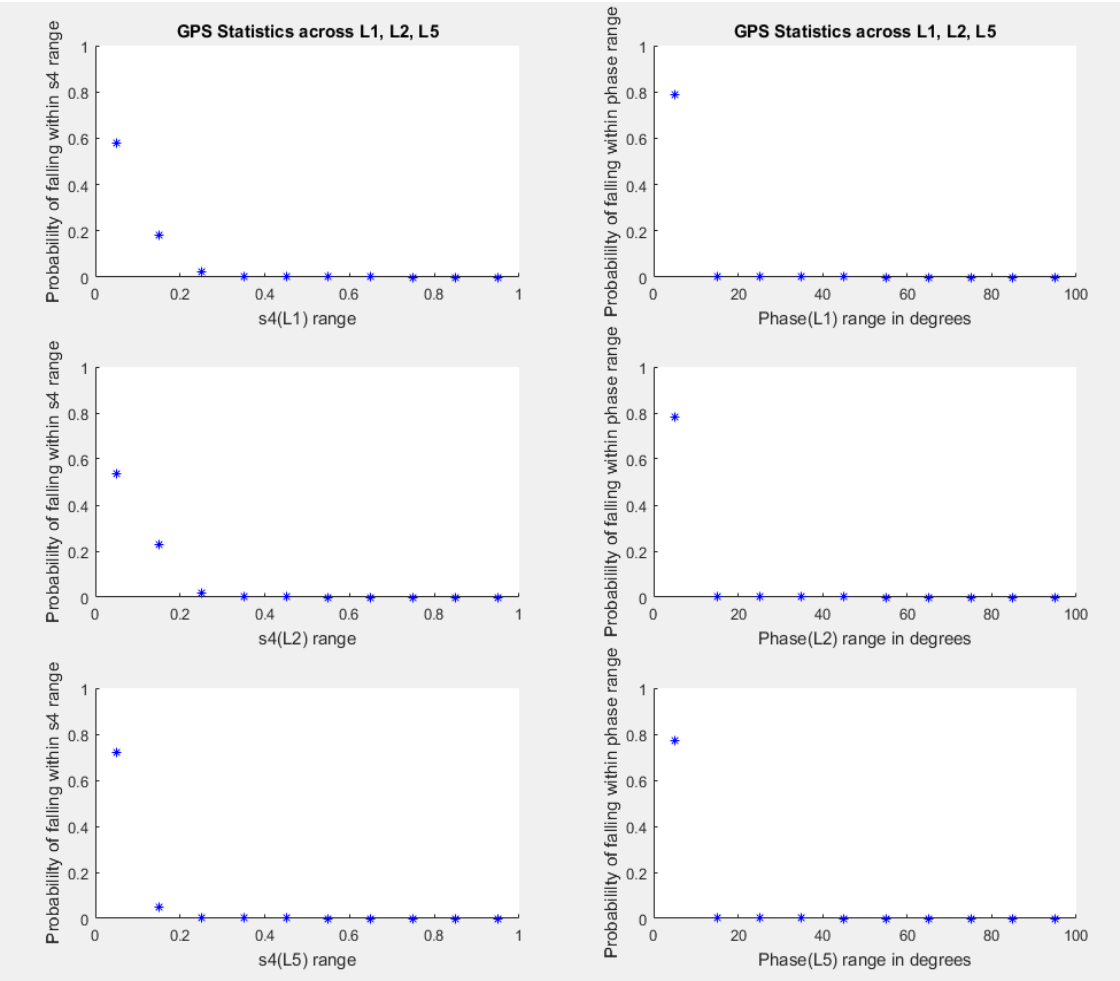

Figure 44: Probability distribution of amplitude and phase scintillation across GPS L1, L2, L5 at mid-latitude for 11 – day period

As shown in **Figure 44**, L5 has the highest probability of 72% of falling within the lowest scintillation region from 0 to 0.1. L1 and L2 have lower probabilities of 57.94% and 53.6% of falling within the lowest scintillation range. Compared to the amplitude scintillation probability distributions from high and low latitude regions in **Figure 43**, it is clear that at mid-latitudes the majority of amplitude scintillation events fall within the lowest range of 0 to 0.1 and are less severe. The phase probability

distribution is very similar at mid-latitude across L1, L2, and L5. The probability of falling within the lowest phase scintillation region from 0 to 10 degrees is 78% for L1, 78% for L2, and 77% for L5. Unlike the phase scintillation of GPS satellites, GLONASS phase scintillation has a higher rate of 3% of falling within 10 to 20 degrees. Compared to phase scintillation probability distributions at high and low latitude regions, the probability of phase scintillation occurring above 10 degrees at mid-latitude is rare and doesn't occur as often as high and low latitude regions, which is shown in **Figure 43**. Compared to high and low latitude regions, phase scintillation is significantly less severe at mid-latitude regions.

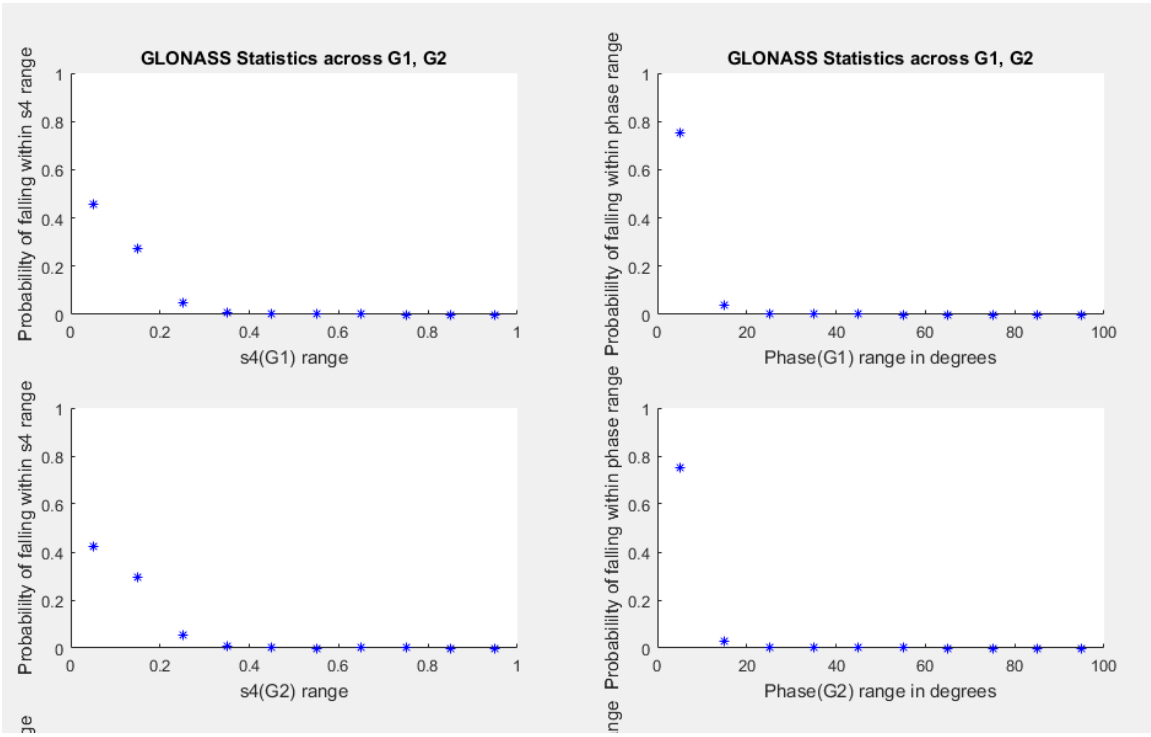

Figure 45: Probability distribution of amplitude and phase scintillation across GLONASS G1 and G2 at mid-latitude for 11 – day period

Figure 45 is the probability distribution for GLONASS satellites across frequency bands G1 and G2. G1 has a 45% probability of falling within the lowest scintillation range from 0 to 0.1, while G2 has a 42% probability of falling within the lowest

scintillation range. Over the 11-day period, G1 is more likely to scintillate less than G2. However, compared to the statistics of GPS L1 and L2, GLONASS G1 and G2 are more likely have higher rates of severe scintillation. The phase scintillation across G1 and G2 have a probability of 75% of falling within the lowest phase scintillation range from 0 to 10 degrees. Like the phase scintillation probability of L1 and L2, GLONASS G1 and G2 have similar phase scintillation probabilities at mid-latitudes. G1 and G2 phase scintillation characteristics further validate that at mid-latitudes phase scintillation rarely surpasses 10 degrees. As a result, phase scintillation isn't as severe at mid-latitudes, compared to low and high latitude regions shown in **Figure 43**.

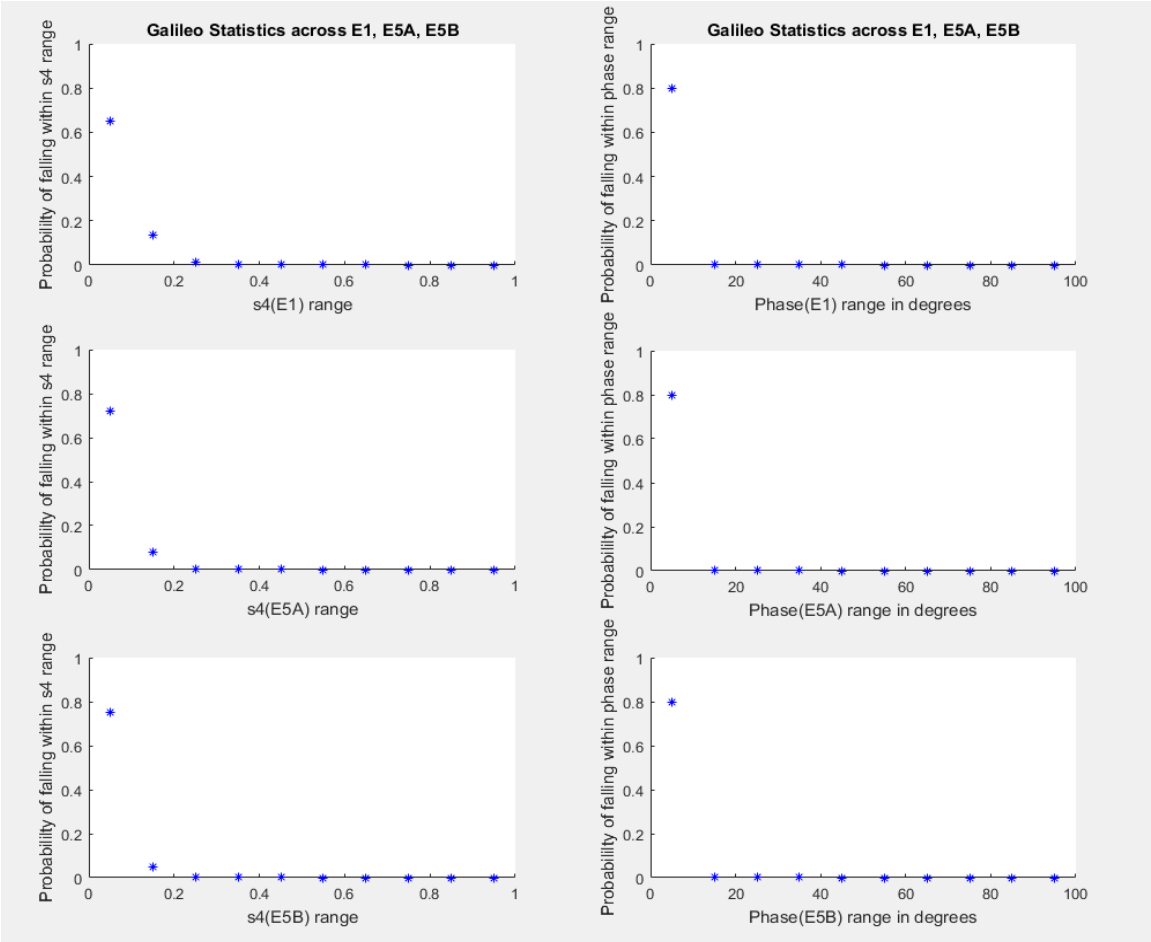

Figure 46: Probability of distribution of amplitude and phase scintillation across E1, E5A, E5B at mid-latitude for 11 – day period

Figure 46 is the probability distribution for Galileo satellites across frequency bands E1, E5A, and E5B. The probability of falling within the lowest scintillation range from 0 to 0.1 is 65% for E1, 71% for E5A, and 74% for E5B. E5B is more likely to scintillate less than both E1 and E5A. E5A is more likely to scintillate less than E1. Like GPS and GLONASS, Galileo phase scintillation have similar probabilities of falling within the lowest phase scintillation range. E1, E5A, and E5B all have a 79% chance of falling within 0 to 10 degrees. This further proves the point that phase scintillation isn't as severe in mid-latitudes, compared to low and high latitudes presented in **Figure 43**.

Frequency Band Cross Correlation of Amplitude and Phase scintillation

Both amplitude and phase scintillation cross correlations across the frequency bands are plotted. For example, for a plot of amplitude scintillation across (L1 vs. L2), if the slope leans towards the L1 axis then the L1 scintillation is more severe than L2. If the slope of the line is close to the value of 1, then this means that the L1 and L2 scintillations are comparable.

Figure 47 are linear fit graphs for GPS satellites 1 and 25 across L1, L2, L5 for both amplitude and phase scintillation. Both amplitude and phase scintillation are plotted with respect to (L1 vs. L2), (L1 vs. L5), and (L2 vs. L5). Linear curves are fitted over the data points and the slopes are listed for each line. For the fitted curves over (L1 vs. L2) and (L1 vs. L5), the slopes are greater than one for both amplitude and phase scintillation. Since the slopes are greater than one, this means that L2 and L5 frequency bands resulted in greater scintillation than L1. The slopes across (L2 vs. L5) are closer to 1, which is an indication of high correlation between both the amplitude and phase scintillation

characteristics across L2 and L5. The results are similar across data taken from high latitude in Gakona, Alaska and low latitude in Jicamarca, Peru.

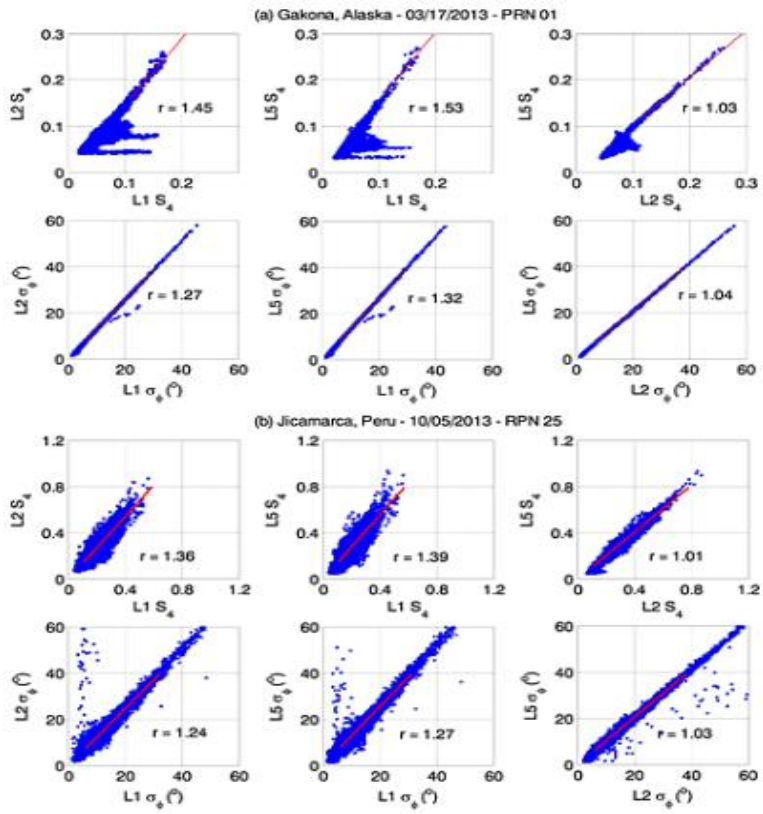

Figure 47: Linear fit curves across GPS L1, L2, L5 amplitude and phase scintillation for satellites 1 and 25 [29]

Figure 48 includes the plots and lists the slopes of the linear fit curves of data collected at mid-latitude over the 11-day period, for both amplitude and phase scintillation, for GPS satellites 1 and 25. The slope values across (L1 vs. L2) are fairly close to one for both amplitude and phase scintillation, which indicates that the scintillation events across L1 and L2 have similar characteristics. This also agrees with the statistics shown in **Figure 44**, which shows that L1 and L2 have similar probabilities of falling within the lowest range of amplitude and phase scintillation. However, L1 does slightly do better than L2, with a 4% greater chance of falling within the lowest

amplitude scintillation range. Since the phase scintillation has a higher correlation than amplitude scintillation, the probability of both L1 and L2 have an equivalent probability of 78% of falling within the lowest phase scintillation range.

(L1 vs. L5) have slopes that lean more towards the L1 axis for amplitude scintillation and slope values closer to one for phase scintillation. The correlation of phase scintillation is higher than amplitude scintillation. The correlation characteristics can be seen in the probability distribution in **Figure 44**, which shows that L5 has a 14% greater chance of falling within the lowest amplitude scintillation range compared to L5. Since the phase scintillation has a high correlation, the probability of falling within the lowest phase range is only 1% difference between L1 and L5.

(L2 vs. L5) have slopes that lean more towards L2 than L5 for amplitude scintillation and have slopes closer to one for phase scintillation. The correlation characteristics can be seen in the probability distribution in **Figure 45**, which shows that L5 has an 18% greater chance of falling within lower amplitude scintillation ranges. Since phase has a greater correlation than amplitude, there is only a 1% difference between L2 and L5 of falling within the lowest phase scintillation range. This further validates the point that L5 has less severe amplitude scintillation, compared to L1 and L2 at mid-latitude.

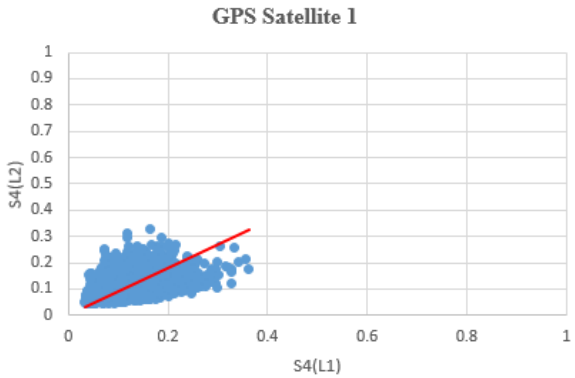

(L1 vs. L2) R = 0.8949

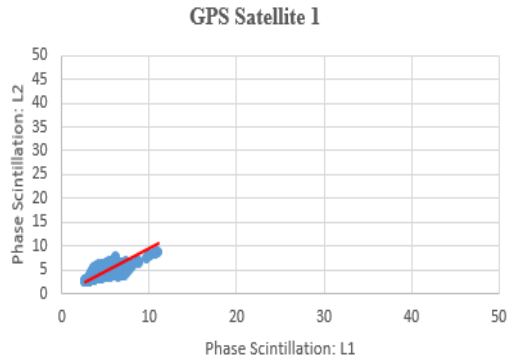

(L1 vs. L2) R = 0.9645

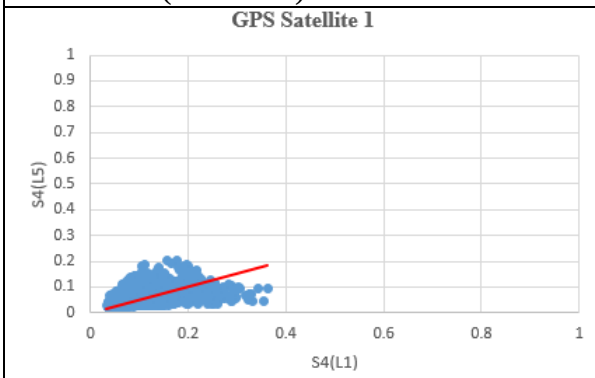

(L1 vs. L5) R = 0.5107

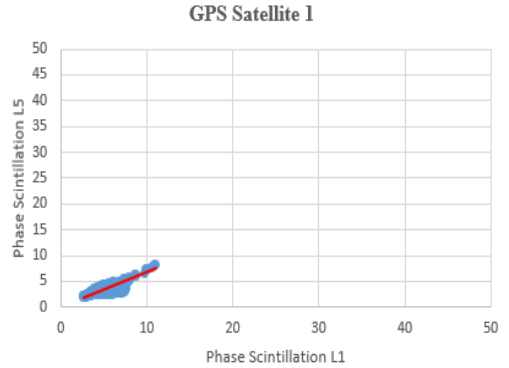

(L1 vs. L5) R = 0.6959

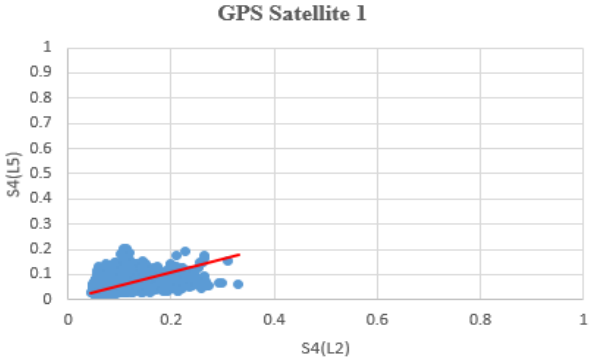

(L2 vs. L5) R = 0.5416

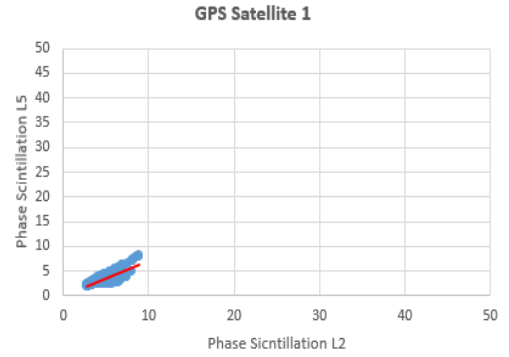

(L2 vs. L5) R = 0.7143

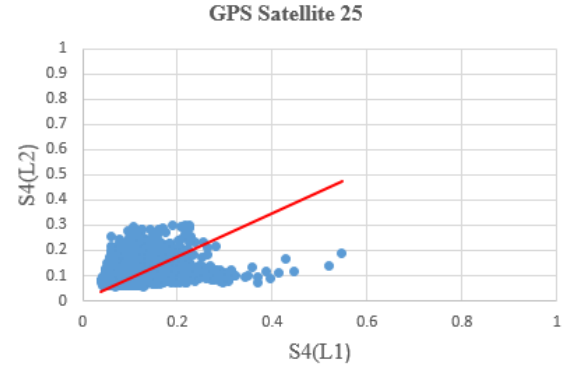

(L1 vs. L2) R = 0.8706

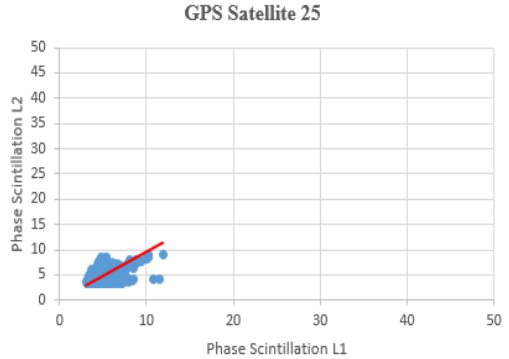

(L1 vs. L2) R = 0.9637

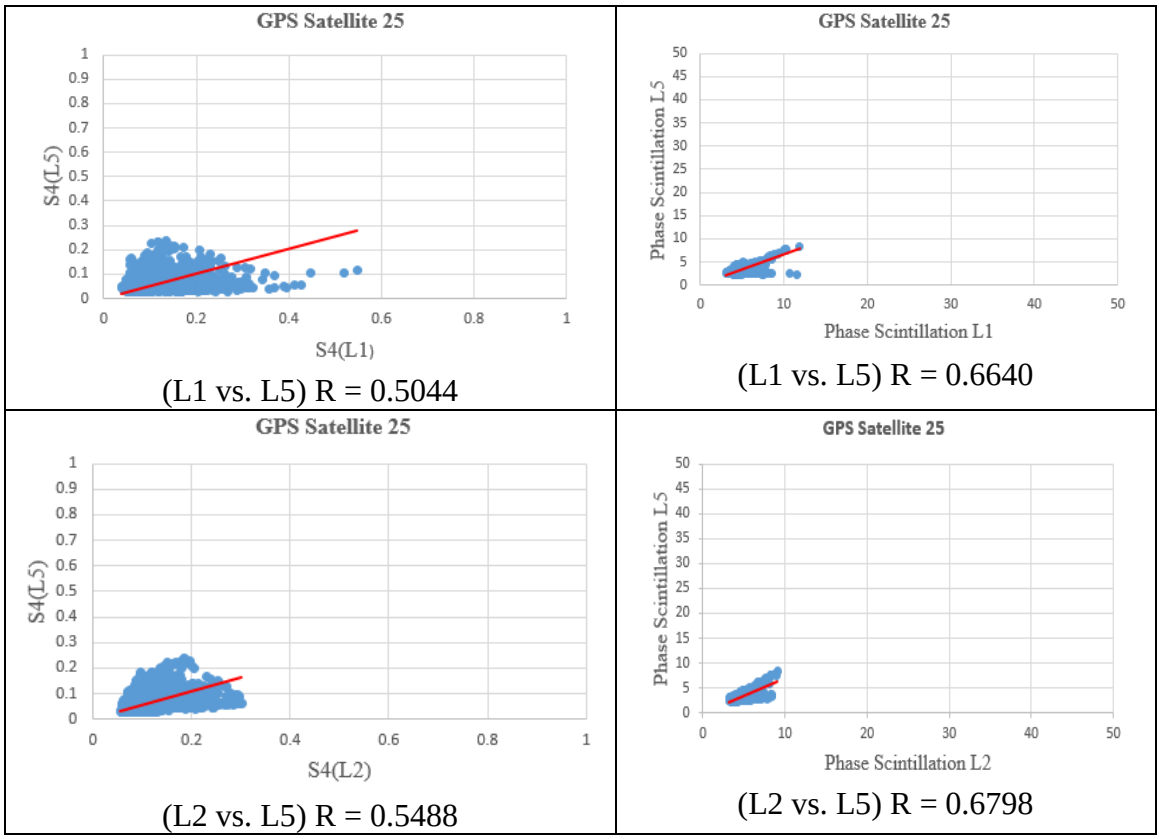

Figure 48: Linear fit curves across GPS L1, L2, L5 amplitude and phase scintillation for satellites 1 and 25 [29]

Figure 49 includes the plots and lists the slopes of the linear fit curves of data collected at mid-latitude over the 11-day period, for both amplitude and phase scintillation for GLONASS satellites 2 and 3. GLONASS (G1 vs. G2) also have slope values that are closer to one for both amplitude and phase scintillation. Since the slopes are closer to one, this implies that the amplitude and phase scintillation across (G1 vs. G2) share similar characteristics. The correlation characteristics can be seen in the statistics shown in **Figure 45**, which shows that G1 and G2 have similar probabilities of falling within the lowest amplitude and phase scintillation range. Unlike the data from the GPS constellation, the phase scintillation across GLONASS (G1 vs. G2) are more severe.

It can be seen from the plot that GLONASS satellite 2 have phase scintillation above 20 degrees and for satellite 3 above 40 degrees.

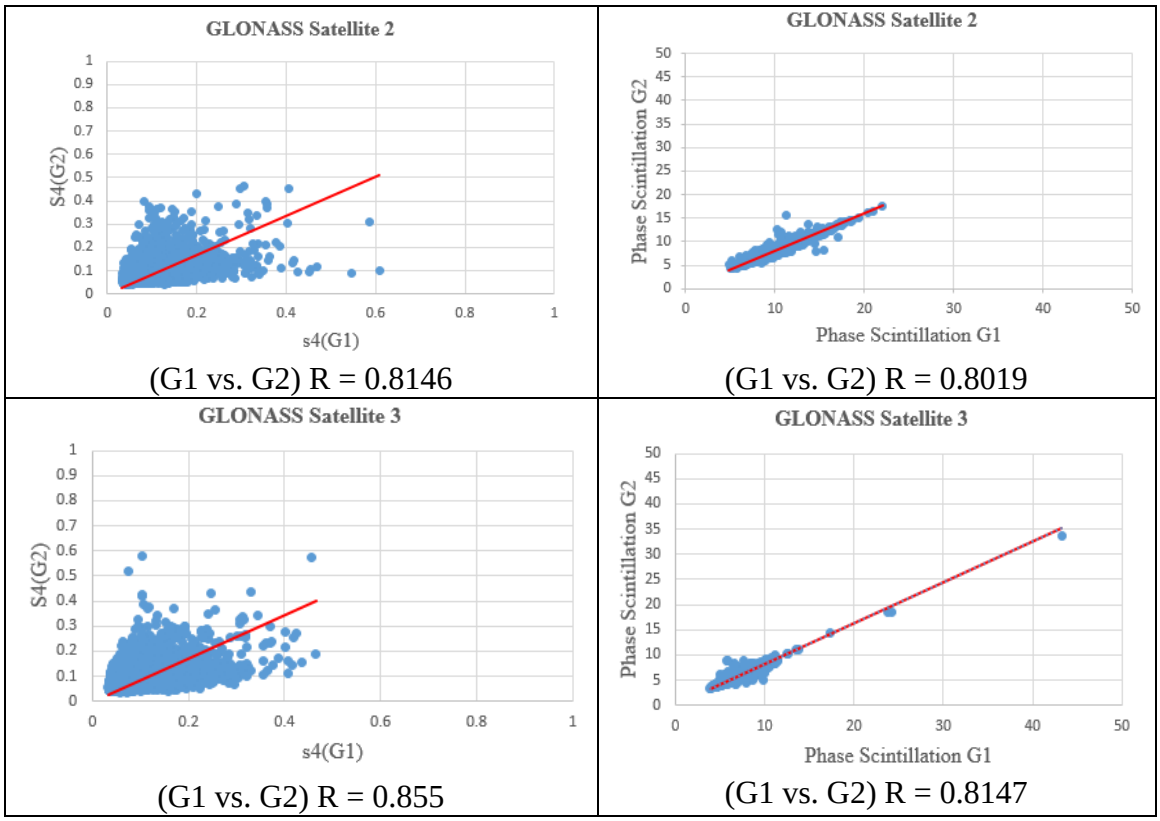

Figure 49: Linear fit curves across GLONASS amplitude and phase scintillation for satellites 2 and 3

Figure 50 includes the plots and lists the slopes of the linear fit curves of data collected at mid-latitude over the 11-day period, for both amplitude and phase scintillation across Galileo satellites 24 and 26. (E1 vs. E5A) have slopes that are fairly close to one for both amplitude and phase. However, the slope across the phase is closer to one than the slope of the amplitude. This means that there is a higher correlation for phase than amplitude. The correlation characteristics can be seen in the statistical distribution shown **Figure 46**, which shows that E5A has a 6% greater chance of falling

within the lowest amplitude scintillation range, compared to E1. For phase both E1 and E5A have a 79% equivalent probability of falling within the lowest phase range.

(E1 vs. E5B) have slopes that lean towards E1 for amplitude and slope values that are closer to one for phase. This indicates that E1 has more severe amplitude scintillation, compared to E5A. For phase scintillation E1 and E5B have higher correlation characteristics, compared to amplitude scintillation. The correlation characteristics can be seen in the statistical distribution in **Figure 46**, which shows that E5B has an 8% greater chance of falling within the lowest amplitude scintillation range than E5B. The statistical analysis also shows that E1 and E5B have an equivalent probability of falling within the lowest phase scintillation range of 79%.

(E5A vs. E5B) plots have slopes that are fairly close to one for both amplitude and phase scintillation. This means that the scintillation characteristics of amplitude and phase are similar across E5A and E5B. However, it can be seen from the correlation characteristics shown in the probability distribution shown in **Figure 46**, that E5B has a 3% greater chance at falling within the lowest amplitude scintillation range, compared to E5A. E5A and E5B have both have equivalent probability of falling within the lowest scintillation range of 79%. This indicates that the phase scintillation has a high correlation across both frequency bands. Overall, these results show that E5B outperforms both E1 and E5A. Like GLONASS, Galileo signals have phase scintillation that can occur above 40 degrees.

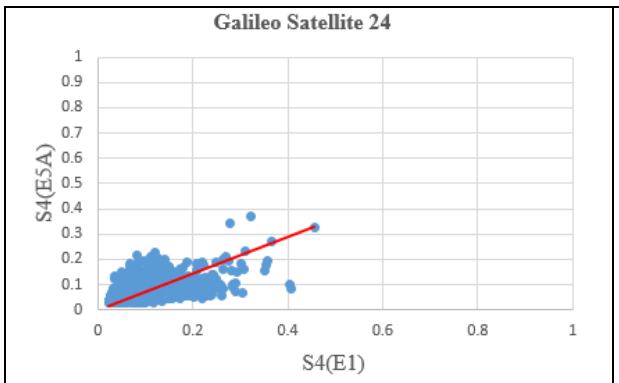

(E1 vs. E5A) R = 0.7243

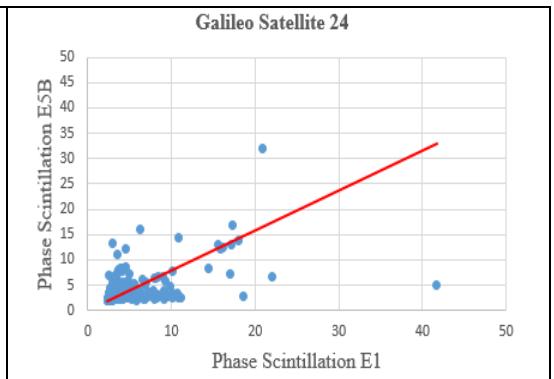

(E1 vs. E5A) R = 0.8734

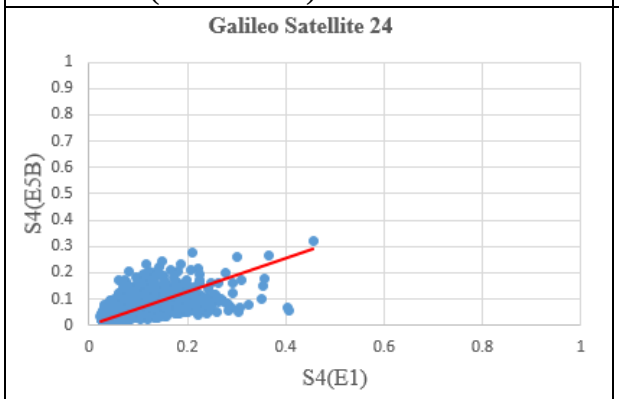

(E1 vs. E5B) R = 0.6384

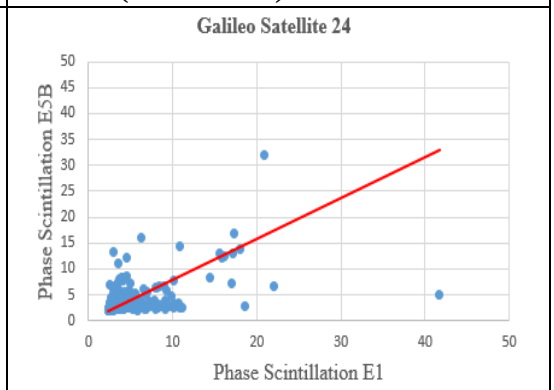

(E1 vs. E5B) R = 0.7879

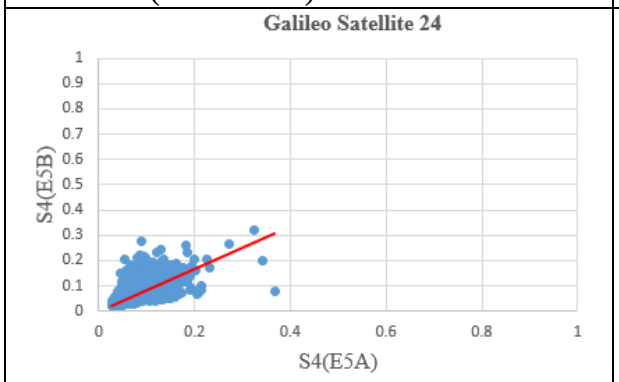

(E5A vs. E5B) R = 0.8391

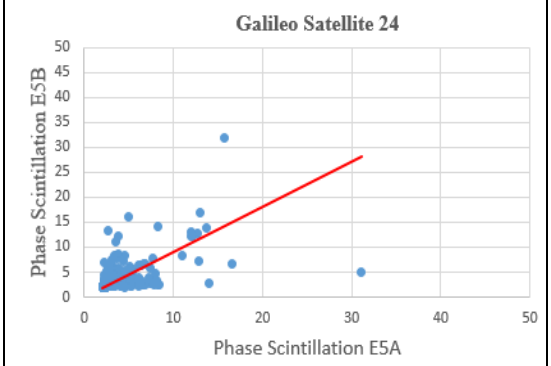

(E5A vs. E5B) R = 0.9031

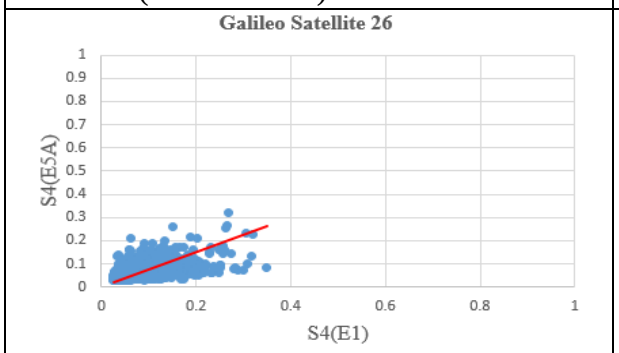

(E1 vs. E5A) R = 0.7843

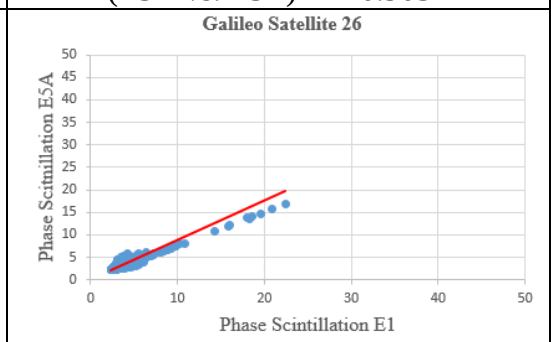

(E1 vs. E5A) R = 0.8809

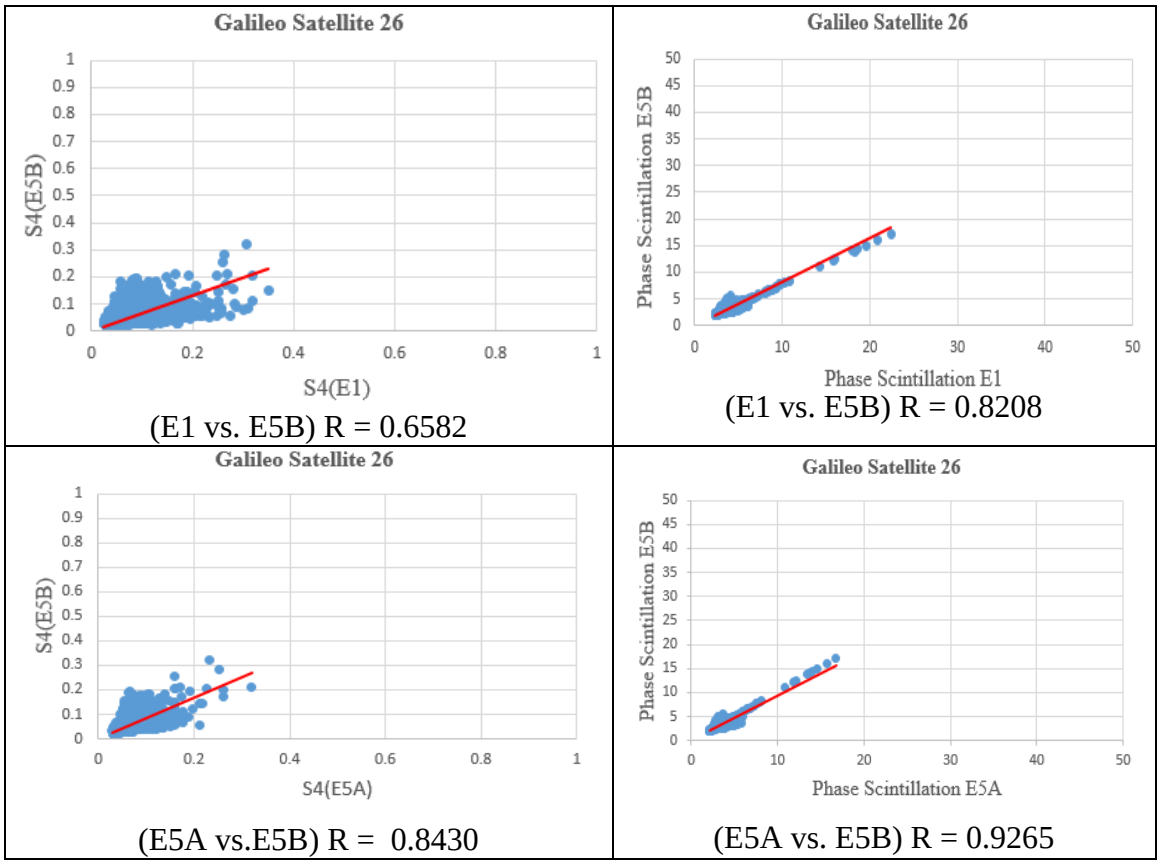

Figure 50: Linear fit curves across Galileo E1, E5A, E5B amplitude and phase scintillation for satellites 24 and 26

4.4.3 Summary

The histogram distributions, statistical distributions, and correlation characteristics for the GPS constellation show that L5 has less severe amplitude scintillation than both L1 and L2, at mid-latitudes. This disagrees with past research done in high and low latitudes, which show that L5 tends to have more severe scintillation than L1 [21], [29]. However, L1 does have slightly less severe amplitude scintillation than L2 at mid-latitudes, which agrees with previous research done at low and high latitudes [21], [22], [29].

The frequency band correlation characteristics and statistical distributions showed that GLONASS G1 and G2 have similar amplitude and phase characteristics at mid-

latitude. The frequency band correlation across both amplitude and phase are close to one, which indicates that the scintillation characteristics are similar. The similarities can also be seen in the statistical analysis, which shows that both G1 and G2 have similar probability distributions. However, G1 does have a slightly greater probability of 3% of falling within the lowest amplitude scintillation range.

The correlation across E1 and E5A is higher for phase than amplitude. Both frequency bands had similar phase scintillation characteristics. E5A has less severe amplitude scintillation than E1. The correlation across E1 and E5B showed higher similarities across phase scintillation than amplitude scintillation. E5B had less severe amplitude scintillation than E1. The correlation of amplitude and phase scintillation across E5A and E5B is high, since the slopes across these frequency bands are also relatively close to the value of one. However, E5B has slightly less severe scintillation than EA. These results are interesting since it was shown previously in data set 2, that E5B has a signal power that is on average roughly 9 dB higher than E5A. This proves that even though a signal has a greater receive power, it doesn't necessarily mean that it will fade less than signals with less receive power. Other factors, such as signal wave length, may play a role on the severity of scintillation.

Based on the results from the probability distribution, the phase scintillation across GPS, GLONASS, and Galileo constellations rarely fall above 10 degrees. Based on the amplitude scintillation probability distributions both GPS and Galileo have a higher probability of having less severe amplitude and phase scintillation compared to GLONASS. At mid-latitude GLONASS tends to have the worst performance, having

lower probability of falling at lower amplitude and phase scintillation ranges. Based on the statistical results, Galileo had the best overall performance. Second to Galileo is GPS.

Chapter 5: GNSS Hardware Signal Simulation of Scintillations Effects

GPS hardware simulators were used to simulate GPS scenarios virtually. The simulators have built in GPS satellite constellations, along with a number of vehicles that can be selected. Hardware simulators can be used to model GPS scenarios for vehicles, such as, cars, planes, and spacecraft. The simulators output a RF signal for an actual GPS receiver. The GPS receiver can therefore process the signal and track the GPS satellites from the simulator. A SPIRENT hardware simulator is used for this study and it incorporates a scintillation model [30] which will be used for some qualitative testing in this study.

The scintillation model built into the simulators replicate low latitude scintillation characteristics for both phase and amplitude [30]. Scintillation index S_4 can be manually entered into the window presented in **Figure 51**. **Figure 51** is the virtual scintillation model built into the SPIRENT simulator. Scintillation index S_4 are entered across latitude regions versus local time. Along with S_4, autocorrelation time can be entered, which dictates how fast scintillation occurs on both the phase and amplitude.

The scintillation model is used to try to mimic the scintillation data collected for the August 16th, 2015 storm. The GPS and GLONASS satellites presented in data set 1 experience, maximum scintillation at 13:18:00 UTC time that range from 0.40 to 0.90. For the simulation test, a scintillation value of 0.50 was entered into the virtual scintillation model from 0 degrees latitude to 70 degrees latitude, along with a

decorrelation time of 1 second, which is the length of time the phase and amplitude change. The scintillation data was collected across GPS frequency bands L1, L2, and L5, to compare the results with mid-latitude scintillation.

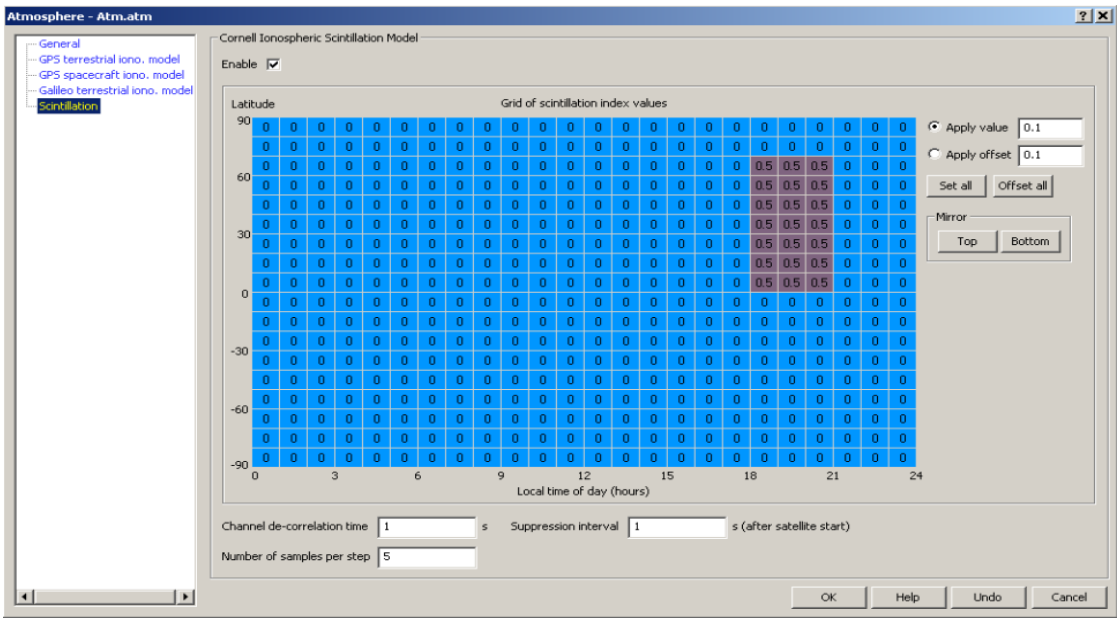

Figure 51: Virtual scintillation window for SPIRENT GPS simulator. As shown in the figure, a scintillation value of 0.50 is inputted from 0 degrees latitude to 70 degrees latitude

A stationary vehicle is selected from the SPRIENT simulator and placed in Blacksburg at coordinates 37.205 degrees latitude north and 80.417 degrees longitude west, at an altitude of 620 meters. The stationary vehicle can be seen in **Figure 52**, which is the ground track window from the SPIRENT GPS simulator. The small white triangle in the stationary vehicle placed in Blacksburg, VA. The green X marks are full fleets of GPS satellite that are built in virtually. Green colored X marks are satellites that are in view of the GPS receiver and are available for tracking.

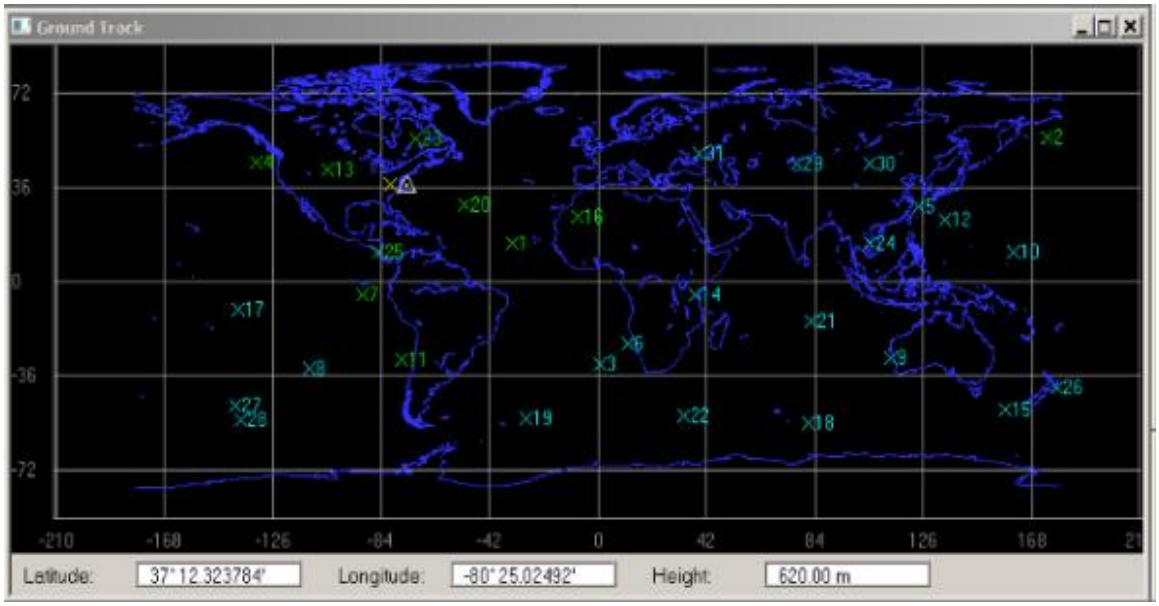

Figure 52: Ground track window from GPS simulator. The white triangle is the stationary vehicle placed in Blacksburg, VA. X marks are GPS satellites that are built in virtually in the GPS simulator

Data from this simulation was collected for about 40 minutes. Data from GPS satellites 1, 4, 7, 20, and 23 are used to observe the performance of frequency bands L1, L2, and L5. **Figure 53** are scintillation graphs of satellite 1, 4, 7, and 20, for frequency bands L1, L2, and L5. For GPS satellite 1, L1 is tracked for about 30 minutes, but L2 and L5 lose lock within the first 3 minutes of tracking. This validates previous research done at low latitudes, which shows that L1 tends to fade less than L2 and L5. However, in the case of satellite 4, both L1 and L5 are tracked for 38 minutes and L2 loses track within the first 6 minutes of tracking and L5 scintillates less than L2 and L1. This disagrees with the idea that lower frequencies tend to do better than higher frequencies and agrees with the analysis done on mid-latitude scintillation for this research, which showed higher signal strengths on L5.

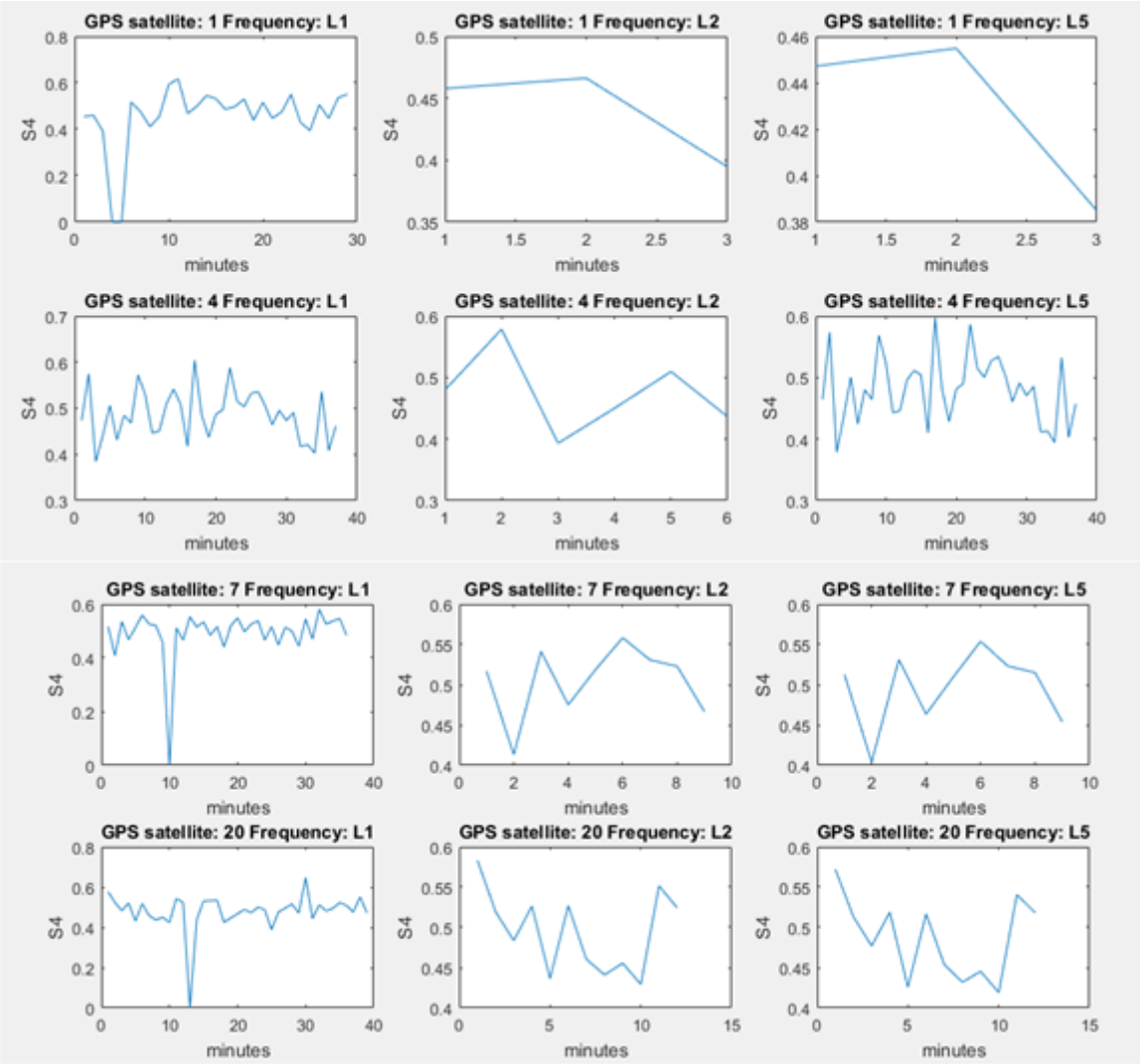

Figure 53: Simulation results for GPS satellite 7 and 20 for frequency bands L1, L2, L5

In **Figure 53**, GPS satellites 7 and 20 L1 are tracked by the receiver for 39 minutes, but it only tracks L2 and L5 for about 8 minutes. This is another case where L1 fades less than both L2 and L5. As a result, L1 would seem more appropriate for tracking compared to L2 and L5. However, it is important to note that this proves that scintillation isn't just dependent on transmit power, frequency or wave lengths, but is also dependent on the structure of electron content in the ionosphere. These observations imply that signals react differently depending on the ionospheric structures the signals travel

through. Even within a simulation environment, discrepancies appear across the frequency bands.

Chapter 6 Conclusion and Future Work

The purpose of this study was to consider if GNSS scintillation could be consequential in mid-latitude regions and compare scintillation at mid-latitude to pervious research done in low latitude, mid-latitude, and high latitude regions. This study was also used to consider which GNSS frequency bands are more favorable at mid-latitudes and how they compare to high and low latitudes. Data sets collected over different time periods were used for this study. However, it is important to note that the data is taken at mid-latitude at only one location, Blacksburg, VA, at coordinates 37.205 degrees latitude north and 80.417 degrees longitude west. As a result, this study is limited and further investigation at other mid-latitude locations needs to be done to further validate the results found in this research.

Shown in data set 1, mid-latitude scintillation could potentially be just as severe as low latitude regions, but for very short durations of time. Data set 1 was collected during a small geomagnetic storm. In data set 1, satellites from the GPS, GLONASS, and Galileo constellation all exhibited high scintillation for a short duration of time. As shown in data set 1, some of these satellites experienced scintillation ranging from 0.8 to 0.9.

Based on all three data sets, GPS L5 had less amplitude and phase scintillation than GPS frequency bands L1, at mid-latitude. Frequency band L5 had less severe scintillation, during the small geomagnetic storm on August the 15th, 2015, which is

analyzed in data set 1. Satellites transmitting on L5 not only scintillated less, but also had better overall carrier to noise ratio density.

As seen from the signal power plots in data set 2, GPS L5 has an average signal power of 106.48 dB, while both L1 and L2 have signal intensities of 100.93 dB and 100.54 dB. On average L5 has roughly 6 dB more signal power than both L1 and L2. Having higher transmit power could be a factor for having less scintillation and higher carrier to noise ratio density.

Histogram, correlation, and statistical distributions done on Data set 3 showed that L5 had less severe amplitude scintillation, compared to L1 and L2. The analysis also showed that L1 had slightly less severe amplitude scintillation than L2. The probability distributions also showed that the phase is fairly similar across all three frequency bands. This further validates the point that phase scintillation isn't as severe at mid-latitudes, compared to amplitude scintillation.

The correlation analysis done on GLONASS satellites show that the slopes of (G1 vs. G2) are above 0.80 for both amplitude and phase scintillation, which means that the scintillation characteristics across both frequency bands are fairly similar. The statistical analysis also shows that G1 and G2 have relatively close probabilities of falling within the lowest amplitude and phase scintillation range.

The probability distribution and cross correlation analysis done on Galileo show that E5A is more likely have less severe amplitude scintillation than E1. The analysis also show that E5B had less severe amplitude scintillation compared to E1. The cross correlation analysis and statistical analysis done on E5A and E5B show that E5B has less severe amplitude scintillation, compared to E5A. However, it is important to note that

E5A and E5B amplitude and phase scintillation have high correlation. Even though E5B on average has a 9 dB higher signal power than E5A, both frequency bands still share similar scintillation characteristics. This proves that transmit power is not the only variable that plays a role on scintillation, but other factors like the ionospheric structure, signal wave lengths, etc. may also be a factor in scintillation.

Aspects of these observations are in line with past observations at low latitudes, but there are some aspects that are different. For mid-latitude, L5 outperforms both L1 and L2. L1 performs slightly better than L2. At low latitude L1 fades less than both L2 and L5 [21], [29]. As a result, further investigation was done using the low latitude scintillation model built into SPIRENT GPS simulators. Based on the data plotted from the simulation shown in **Figure 53**, L2 and L5 tend to fade more than L1 at low latitudes. GPS satellites 1, 7, 20 all lose lock on L2 and L5, but not on L1. In the case of GPS satellite 4, L1 and L5 were both tracked and L2 lost lock. L1 is continuously tracked across all the satellites and is less likely to lose lock compared to L2 and L5. This shows that at low latitudes, L1 outperforms L2 and L5. However, that is not the case at mid-latitudes, where L5 scintillates less than both L1 and L2. For the GPS constellation, the study done at mid-latitude indicates that L5 has the best overall performance.

At mid-latitude the Galileo constellation had less amplitude and phase scintillation than GPS and GLONASS constellations. From the data set 3, the statistics showed that Galileo had the highest probability of falling within the lowest amplitude and phase scintillation range for the duration of 11 days. Galileo has the best overall performance compared to GPS and GLONASS. GPS had the second best overall performance and GLONASS had the worst performance.

The power spectral index values at mid-latitude is comparable to high latitudes. The resemblance can be seen when comparing mid-latitude spectral index plot in **Figure 37** of GPS satellite 9 over 60 minutes, to the high latitude spectral index plot seen in **Figure 9**. It can be seen from both plots that the spectral index values fall within the same range. This could mean that scintillation at mid-latitudes shares similar characteristics as high latitude. The average spectral index value across all the tables from data set 2 of the observed GNSS satellites is -1.764. Since the average value isn't near the value of -2.6 is an indication that scintillation is fairly moderate at mid-latitude**.**

Currently mid-latitude scintillation models do not exist for GNSS hardware simulators. As previously discussed, the scintillation model in SPIRENT simulators is designed from low latitude scintillation due to the fact that low latitude scintillations are more severe and thoroughly studied [19]. One of the future goals of this research is to build a model for mid-latitude scintillation, that is compatible with SPIRENT simulators. Having only low latitude scintillation characteristics doesn't accurately justify conditions that may occur at mid-latitudes or even high latitudes. As a result, future modeling done on GNSS can be made more accurate during strong space weather events.

References

[1] H. Strangeways, Y. Ho, M. Aquino, Z. Elmas, H. Marques, J. Monico and H. Silva, "On determining spectral parameters, tracking jitter, and GPS positioning improvement by scintillation mitigation", *Radio Sci.*, vol. 46, no. 6, 2011.

[2] A. Eltrass, W. Scales, P. Erickson, J. Ruohoniemi and J. Baker, "Investigation of the role of plasma wave cascading processes in the formation of midlatitude irregularities utilizing GPS and radar observations", *Radio Sci.*, vol. 51, no. 6, pp. 836-851, 2016.

[3]"GPS | An Introduction to GNSS | NovAtel", *Novatel.com*, 2016. [Online]. Available: http://www.novatel.com/an-introduction-to-gnss/chapter-3-satellite-systems/gps/. [Accessed: 17- Sep- 2016].

[4]"GLONASS | An Introduction to GNSS | NovAtel", *Novatel.com*, 2016. [Online]. Available: http://www.novatel.com/an-introduction-to-gnss/chapter-3-satellite-systems/glonass/. [Accessed: 17- Sep- 2016].

[5]"Galileo | An Introduction to GNSS | NovAtel", *Novatel.com*, 2016. [Online]. Available: http://www.novatel.com/an-introduction-to-gnss/chapter-3-satellite-systems/galileo/. [Accessed: 17- Sep- 2016].

[6] M. Kelley, *The earth's ionosphere*. Amsterdam: Academic Press, 2009.

[7] "VT Superdarn Home : Virginia Tech Superdarn". *Vt.superdarn.org*. N.p., 2016. Web. 12 Aug. 2016.

[8] K. Deshpande, G. Bust, C. Clauer, H. Kim, J. Macon, T. Humphreys, J. Bhatti, S. Musko, G. Crowley and A. Weatherwax, "Initial GPS scintillation results from CASES receiver at South Pole, Antarctica", *Radio Science*, vol. 47, no. 5, p. n/a-n/a, 2012.

[9] Paul M. Kitner. *Global Positioning Theory and Design*. Cornell University, 2006. Print

[10]"BeiDou Navigation Satellite System", *Wikipedia*, 2016. [Online]. Available: https://en.wikipedia.org/wiki/BeiDou_Navigation_Satellite_System. [Accessed: 17

Sep- 2016].

[11]"Galileoâ€™s dozen: 12 satellites now in orbit", *European Space Agency*, 2016. [Online]. Available: http://www.esa.int/Our_Activities/Navigation/Galileo/Launching_Galileo/Galileo_s_dozen_12_satellites_now_in_orbit. [Accessed: 10- Aug- 2016].

[12]"Galileo (satellite navigation)", *Wikipedia*, 2016. [Online]. Available: https://en.wikipedia.org/wiki/Galileo_(satellite_navigation). [Accessed: 17- Sep- 2016].

[13]"Step 1 - Satellites | An Introduction to GNSS | NovAtel", *Novatel.com*, 2016. [Online]. Available: http://www.novatel.com/an-introduction-to-gnss/chapter-2-basic-gnss-concepts/step-1-satellites/. [Accessed: 18- Oct- 2016].

[14]"Quality Assurance - A PDH Online Course", *Pdhonline.com*, 2016. [Online]. Available: http://www.pdhonline.com/courses/l116/l116content.htm. [Accessed: 09- Aug- 2016].

[15] J. Papon, M. Cohen, B. Cotts and N. Haque, *Ionospheric Morphology*, 1st ed. Stanford University, 2016, pp. 2-4,12-14.

[16] J. Seybold, *Introduction to RF propagation*. Hoboken, N.J.: Wiley, 2005.

[17] http://radiojove.gsfc.nasa.gov/education/educ/radio/tran-rec/exerc/iono.htm

[18]"Ionospheric Delay - Navipedia", *Navipedia.net*, 2016. [Online]. Available: http://www.navipedia.net/index.php/Ionospheric_Delay. [Accessed: 17- Sep- 2016].

[19] T. E. Humphreys, M. L. Psiaki and P. M. Kintner, "Modeling the Effects of Ionospheric Scintillation on GPS Carrier Phase Tracking," in *IEEE Transactions on Aerospace and Electronic Systems*, vol. 46, no. 4, pp. 1624-1637, Oct. 2010. doi: 10.1109/TAES.2010.5595583.

[20] Kintner, P. M., B. M. Ledvina, and E. R. de Paula (2007), *"*GPS and ionospheric scintillations*"*, Space Weather, 5, S09003, doi:10.1029/2006SW000260.

[21] S. Delay, C. Carrano, K. Groves and P. Doherty, "A Statistical Analysis of GPS

L1, L2, and L5 Tracking Performance During Ionospheric Scintillation", *ResearchGate*, 2015. [Online]. Available: https://www.researchgate.net/publication/277332590_A_Statistical_Analysis_of_GPS_L1_L2_and_L5_Tracking_Performance_During_Ionospheric_Scintillation. [Accessed: 10- Aug- 2016].

[22] C. Carrano, K. Groves, W. McNeil and P. Doherty, "Scintillation characteristics across the GPS frequency band", *ResearchGate*, 2012. [Online]. Available: https://www.researchgate.net/publication/289112169_Scintillation_characteristics_across_the_GPS_frequency_band. [Accessed: 11- Aug- 2016].

[23] *GPStation-6 GNSS Ionospheric Scintillation and TEC Monitor (GISTM) Receiver User Manual*, 2nd ed. Novatel Inc, 2016, pp. 62, 66.

[24]"NovAtel Connect | GNSS/GPS Receiver Software | High-Precision GPS Devices | High-Precision GNSS Devices | Products | NovAtel", *Novatel.com*, 2016. [Online]. Available: http://www.novatel.com/products/firmware-options/novatel-connect/#overview. [Accessed: 18- Oct- 2016].

[25]"Planetary K-index", *Swpc.noaa.gov*, 2016. [Online]. Available: http://www.swpc.noaa.gov/products/planetary-k-index. [Accessed: 09- Aug- 2016].

[26]"Index of /aisr/GPSTEC/drewstuff/MATLAB", *Naic.edu*, 2016. [Online]. Available: http://www.naic.edu/aisr/GPSTEC/drewstuff/MATLAB/. [Accessed: 18- Oct- 2016].

[27] "GPS signals", *En.wikipedia.org*, 2016. [Online]. Available: https://en.wikipedia.org/wiki/GPS_signals. [Accessed: 30- Oct- 2016].

[28]"AGI - software to model, analyze and visualize space, defense and intelligence systems", *Agi.com*, 2016. [Online]. Available: https://www.agi.com/products/stk/. [Accessed: 19- Oct- 2016].

[29] Y. Jiao and Y. Morton, "Comparison of the effect of high-latitude and equatorial ionospheric scintillation on GPS signals during the maximum of solar cycle 24", *Radio Science*, vol. 50, no. 9, pp. 886-903, 2015

[30]"GPSL - Cornell University", *Gps.ece.cornell.edu*, 2016. [Online]. Available: https://gps.ece.cornell.edu/tools.php. [Accessed: 19- Sep- 2016].

Appendix

Appendix A: Coding Methods

Script 1: Script used to increment over the header of the .CSV file

```
P1 = fopen(filename);%open file
i = 1;
while(i <= 19)%while loop to iterate through the header
    h1 = fgetl(P1);
    i = i + 1;
end
```

Script 2: Script used to store rows of data in the .CSV file

```
lines = fgetl(P);%get line from .CSV file
[GpsT(count,1) PRN(count,1) y3 freq(count,1) Az(count,1) El(count,1)
CNR(count,1) y8 y9 y10 Scint(count,1) y12 y13 y14 y15 y16
Sig1(count,1)] =
strread(lines,'%f%f%f%f%f%f%f%f%f%f%f%f%f%f%f%f%f%f','delimiter',',');%re
ad line from .CSV file and store data in variables
```

Script 3: Script used to store high rate data in the .CSV file

```
fileID = fopen('GPS9.csv');%open .CSV file
textscan(fileID, '%[^\n\r]',5, 'ReturnOnError', false);%scan every
single column of data in .CSV file
data =
textscan(fileID,'%f%f%f%f%f%*[^\n]','Delimiter',',','EmptyValue',-
Inf);%store all data as cells in variable data
fclose(fileID); %close .CSV file
```